AUGMENTATION OF GPS WITH GLONASS AND PSEUDOLITE SIGNALS FOR CARRIER PHASE BASED KINEMATIC POSITIONING

LIWEN DAI

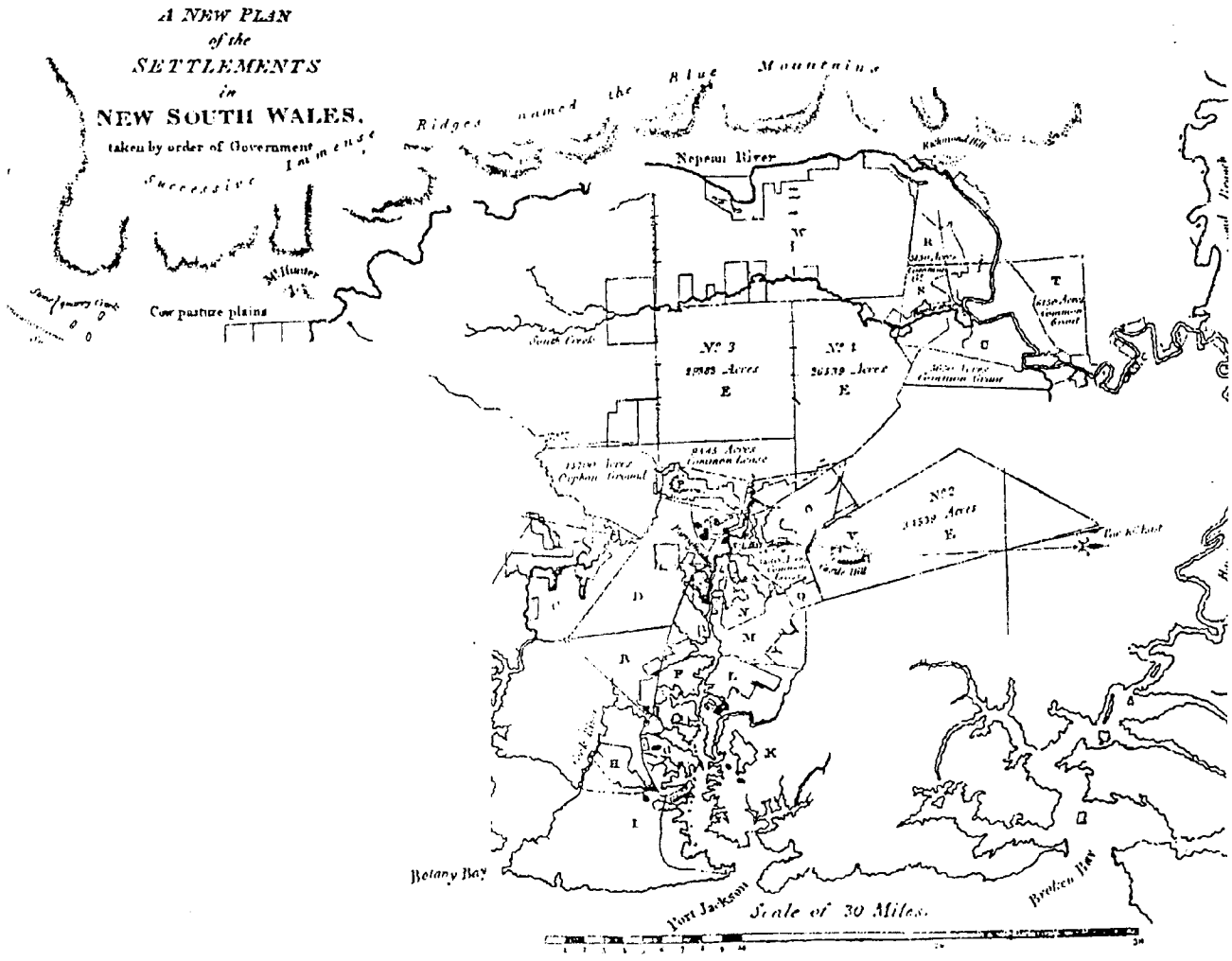

UNISURV S-72, 2002

Reports from

SCHOOL OF SURVEYING
AND SPATIAL INFORMATION SYSTEMS

THE UNIVERSITY OF NEW SOUTH WALES UNSW SYDNEY NSW 2052 AUSTRALIA

UNISURV REPORT S-72, 2002

AUGMENTATION OF GPS WITH GLONASS AND PSEUDOLITE SIGNALS FOR CARRIER PHASE BASED KINEMATIC POSITIONING

LIWEN DAI

Received: October 2002
Accepted: November 2002

SCHOOL OF SURVEYING AND SPATIAL INFORMATION SYSTEMS
(formerly GEOMATIC ENGINEERING)
UNIVERSITY OF NEW SOUTH WALES
UNSW SYDNEY NSW 2052
AUSTRALIA

UNISURV REPORTS

Series Editor: Dr. J. M. Rüeger

National Library of Australia

Card No. and ISBN 0 - 7334 - 1975 - 5

FOREWORD

Carrier phase-based GPS positioning is now an indispensable tool for a wide range of precise applications in navigation, surveying and geodesy. Research into high precision GPS-based positioning has been undertaken at the University of New South Wales (UNSW) since the mid-1980s. This project describes the following augmentations of GPS carrier phase-based positioning: (1) by measurements from the Glonass system (the Russian Federation's satellite navigation system that complements the USA's GPS), (2) from GPS/Glonass multiple-reference station networks, and (3) from ground-based pseudo-satellite ("pseudolite") signals. This thesis describes the mathematical bases for these various augmentations.

The availability of integrated GPS-Glonass receivers offers special challenges for the development of precise positioning algorithms, not the least being that the signals to the different Glonass satellites are of different frequency, making the standard GPS data processing strategies inappropriate. An integrated procedure for combined GPS and Glonass data processing, in combination with a three-step function model procedure, a real-time estimated stochastic model, and a fault detection and adaptive procedure, has been developed. This is a remarkable result, although its usefulness is somewhat undermined by the current critical state of the Glonass constellation. (It is hoped that there will be a revitalised Glonass system by the end of this decade.)

To extend the inter-receiver distances for relative positioning, a network-based methodology for GPS/Glonass reference receiver networks has been investigated. In this thesis Liwen Dai has compared the various network-based methodologies, and the fundamental common bases for all the multiple-reference station techniques currently available have been identified. Several real-time ambiguity resolution scenarios for GPS and Glonass reference station networks were proposed that would improve the efficiency of the network data processing.

Pseudolites are an exciting technology whose potential can be explored for a wide range of positioning and navigation applications, either as a significant augmentation of space-based systems, or as an independent system for indoor positioning. The modelling issues for GPS and pseudolite integration, including non-linearity, pseudolite location errors, tropospheric delays, multipath and noise, have been investigated. Three different pseudolite configurations, including integrated GPS and pseudolite, pseudolite-only, and pseudolite-based 'inverted' positioning, have been investigated, and optimal geometric designs for the various positioning scenarios have been proposed. The research reported in this thesis now forms the basis of further pseudolite studies within the Satellite Navigation and Positioning (SNAP) group at UNSW, some supported by Australian Research Council grants.

During his research, Liwen Dai was supported by an International Postgraduate Research Scholarship at UNSW.

Professor Chris Rizos
November 2002

ABSTRACT

Carrier phase-based GPS positioning is now an indispensable tool for a wide range of precise applications in navigation, surveying and geodesy. Despite the impressive achievements of GPS precise positioning techniques, users have been looking forward to the prospect of more GNSS (Global Navigation Satellite System) signals for improved system availability, integrity, reliability, greater redundancy and better accuracy. Augmentation of GPS carrier phase-based positioning by measurements from the Glonass system, from GPS/Glonass multiple-reference station networks and from ground-based pseudo-satellite signals has been the focus of this study.

The development of integrated GPS-Glonass receivers offers special challenges for the development of precise positioning algorithms, not the least being that the signals to the different Glonass satellites are of different frequency, making the standard GPS data processing strategies inappropriate. An integrated procedure for combined GPS and Glonass data processing, in combination with a three-step function model procedure, a real-time estimated stochastic model, and a fault detection and adaptive procedure, has been developed.

To extend the inter-receiver distances, a network-based methodology for GPS/Glonass reference receiver networks has been investigated. The various network-based methodologies have been compared, and the fundamental common bases for all the multiple-reference station techniques have been identified. Two real-time ambiguity resolution scenarios for GPS and Glonass reference station networks are proposed. Temporally correlated bias models are used to recover ambiguities, whilst the spatially correlated bias models are used to predict residual ionospheric and tropospheric delays for use in wide-lane and narrow-lane ambiguity resolution for a newly risen satellite or after a long data gap.

Pseudolites are an exciting technology whose potential can be explored for a wide range of positioning and navigation applications, either as a significant augmentation of

space-based systems, or as an independent system for indoor positioning. The modelling issues for GPS and pseudolite integration, including non-linearity, pseudolite location errors, tropospheric delays, multipath and noise, have been investigated. Formulas for the effects of non-linearity, and orbital errors and tropospheric delay have been derived. Three different pseudolite configurations, including integrated GPS and pseudolite, pseudolite-only, and pseudolite-based 'inverted' positioning, have been investigated, and optimal geometric designs for the various positioning scenarios are proposed.

ACKNOWLEDGEMENTS

As I complete this thesis I would like to express my sincere gratitude to those who have enabled this study to be accomplished.

I am grateful to my supervisors Prof. Chris Rizos and Dr. Shaowei Han, and co-supervisor Dr. Jinling Wang, for their encouragement, valuable advice, and patient guidance throughout the course of this study.

I also wish to thank members of the Satellite Navigation and Positioning (SNAP) group, Dr. Toshiaki Tsujii, Dr. Joel Barnes, Dr. Horng-yue Chen, Dr. Linlin Ge, Dr. Craig Roberts, Mr. Volker Janssen, Dr. Chalermchon Satirapod, Mr. Michael Moore, Mr. Clement Ogaja, Mr. Jun Zhang and Ms. Ying He, for assistance in GPS data collection and much valued discussion. A special thanks to Dr. Horng-yue Chen and Mr. Jun Zhang, in particular, for their tremendous assistance.

I am indebted to Prof. Jingnan Liu, of Wuhan University, who helped me take my first steps to study abroad, and who continued to give me a lot of advice on GPS research. The support of the members of the Wuhan University GPS research group is also acknowledged.

I would also like to acknowledge the support provided to me by The University of New South Wales through the granting of an International Postgraduate Research Scholarship and an Engineering Faculty Postgraduate Research Scholarship, and funding support from the Australian Research Council for the various projects in which I participated.

Last, but not least, my final and deepest appreciation to my family, especially my wife, Lei Liu, and my daughter, Annie, for their love, encouragement and understanding during my studies.

TABLE OF CONTENTS

Chapter 1

INTRODUCTION

1.1 GPS Background

The NAVSTAR Global Positioning System (GPS) is a satellite-based radio-positioning and time-transfer system designed, financed, deployed, and operated by the U.S. Department of Defense in order to satisfy the requirements for the military forces to accurately determine their position, velocity, and time (PVT) in a common reference system, anywhere on or near the Earth on a continuous basis. GPS has also demonstrated a significant benefit to the civilian community who are using GPS for a rapidly expanding wide range of applications. The number of civilian users is considerably greater than that of the military users.

Development work on GPS commenced within the Department of Defense (DoD) in 1973, and full operational capability was declared in July 1995. The GPS system consists of three segments, namely the *control segment*, the *space segment* (satellites, signals, etc.) and the *user segment* (receivers, etc.). The *space segment* comprises the nominal 21+3 satellites transmitting the GPS signals. With the full constellation (there are currently more than 24 functioning satellites), the space segment provides global coverage with typically between four to eight simultaneously observable satellites above a 15° elevation at any time of the day. The *control segment* consists of a master control station and five monitoring stations situated across the globe, and three ground control stations, which collectively carry out the task of satellite tracking, orbit determination and clock analyses, and telemetry and control necessary for the daily maintenance of the space segment. The *user segment* includes the entire spectrum of the applications equipment, augmentations and computational techniques that provide the users with PVT results.

GPS employs the ECEF (earth-centred, earth-fixed) World Geodetic System 1984 (WGS84), defined and maintained by the U.S. National Imagery and Mapping Agency (NIMA) (formerly the Defense Mapping Agency), as the global geodetic datum. It is the datum to which all GPS point positioning information is referred by virtue of being the reference system of the broadcast ephemeris. GPS time is referenced to the Universal Coordinated Time-UTC (U.S. Navy Observation, USNO) without any leap seconds. The major integer shift between the GPS time and UTC (USNO) time scales is the leap seconds (13 seconds as at March 2002).

The GPS ranging signals are broadcast at two L-band frequencies: a signal at 1575.42MHz (L1) and a second signal at 1227.6MHz (L2). Modulated onto the L1 carrier wave are two pseudo-random noise (PRN) ranging code: the 1-millisecond-long C/A-code with a chipping rate of about 1.023MHz, and a week-long segment of the P-code with a chipping rate of 10.23MHz. Also modulated on the carrier wave is the "navigation message" which contains, amongst other information, the broadcast ephemeris data describing the (predicted) position of the satellite and the (predicted) satellite clock correction terms. The L2 carrier wave is modulated by the P-code and the "navigation message", but no C/A-code. The C/A code is used by the Standard Positioning Service (SPS), while P-code ranging is the basis of the Precise Positioning Service (PPS). The U. S. DoD has encrypted the P-code under a policy known as "Anti-Spoofing" (AS). Hence, the PPS is only available to the military of the United States and its allies, for users equipped with PPS receivers. In addition, the GPS operators have the capability to intentionally degrade the accuracy of the C/A code by desynchronising the satellite clock (δ – process), and/or by incorporating small errors (ε – process) in the broadcast ephemeris. This degradation was known as "Selective Availability" (SA), and was introduced on 25 March 1990. After SA was deactivated by presidential order on 2 May 2000, the accuracy of the SPS increased from about 100m horizontal and 156m height (at the 95% confidence level), to less than 10 metres (Rizos & Satirapod, 2001).

Plans for GPS modernization were first announced in 1998 by then Vice President Al Gore. The modernization plans call for two new civil signals: a C/A-coded signal (or similar) on L2 (at 1227.6MHz), and a third civil signal, which is to be located at 1176.45MHz. The civilian signal on L1 remains unchanged. These new civilian signals, in combination with the L1 signal currently available, will greatly enhance the accuracy, reliability, and robustness of civilian GPS receiver solutions, resulting in significantly improved system capabilities.

1.2 Carrier Phase-Based Positioning Techniques

Carrier phase-based GPS positioning is now an indispensable tool for a wide range of precise applications in navigation, surveying and geodesy. To address such a variety of applications, many implementations of precise GPS techniques have been developed. Almost all techniques involve 'relative' positioning, in which one GPS receiver/antenna's coordinates are determined with the aid of measurements also made at a stationary base or reference receiver. In essence, all of these techniques may be categorised according to a small number of attributes. Is the technique implemented in the post-processed or real-time mode? Does the scenario involve static or kinematic positioning? Is the inter-receiver distance (or baseline length) comparatively short (say <10km) or very long (e.g. >1000km)? Is a single base station involved or a network of reference receivers? and so on. Each of these attributes also dictates the data processing strategies that should be employed to ensure accurate and reliable positioning results.

Carrier phase-based differential GPS (DGPS) techniques involve the crucial mathematical operation of 'ambiguity resolution'. Several ambiguity search procedures for OTF-AR (On-The-Fly-Ambiguity-Resolution) have been suggested during the 1990s, including the FARA, FASF, Cholesky, Hatch, and U-D decomposition methods (Frei & Beutler, 1990; Hatch, 1990; Landau and Euler, 1992; Chen 1993; Abidin, 1993). However, the most optimal procedure uses the LAMBDA transformation in combination with the U-D decomposition search procedure (Teunissen, 1994). Although these are all search techniques in the estimated ambiguity domain, when combined with search procedures in the measurement and coordinate domain, single-

epoch OTF-AR is possible (Han, 1997). Although new search algorithms are still being researched at universities, computation speed or efficiency is no longer the critical problem in the ambiguity resolution process. The most significant contributions will be in increasing the reliability of AR, as well as minimising the 'time-to-AR'. This requires careful attention to issues such as optimal functional and stochastic data modelling, statistical testing, quality assurance (QA), and AR validation procedures. Even though such research is still underway, several commercial products have been released. For example, the Ashtech Z-Extreme claims 'instant' RTK ('time-to-AR' of 2 seconds, or at the very least a few seconds of data) under conditions when tracking six or more GPS satellites (on both the L1 and L2 carrier waves), the receiver-satellite geometry is favourable (Dilution of Precision less than 5), and the baseline length is shorter than 7km. Even if instant AR is not possible, e.g. due to longer baselines, it is claimed that the reliability of AR has been significantly improved. This trend to the introduction of either an improvement in the reliability of OTF-AR (in order to accommodate different scenarios), even sacrificing a very short 'time-to-AR', or ever more restrictive conditions for instant AR, is expected to continue.

The future of precise GPS carrier phase-based positioning is fundamentally dependent on a number of factors, including developments in receiver hardware, carrier phase data processing algorithms, operational procedures, the Internet and mobile communications. However, it could be argued that several more important factors include the *augmentation* of GPS by Glonass, the development of the Galileo system (and its subsequent integration with GPS), the modernization of GPS (to transmit a second and third civilian frequency), the deployment of GPS (and Glonass) reference station networks, implementation of the WAAS system, and the integration of GPS with pseudolites and inertial navigation systems/sensors (Rizos, 2001). All of these will significantly improve the reliability, integrity, and accuracy of the positioning results.

1.3 GPS Augmentation for Carrier Phase-Based Positioning

Augmentation refers to those enhancements to the system, the algorithms or the hardware, designed to improve the performance of GPS in some way. The

improvement(s) may be measurable in terms of some global performance variables such as accuracy, reliability, availability, integrity, or continuity. On the other hand, some enhancements may be introduced in order to make GPS a more attractive technology for addressing some specific applications constrained by signal visibility, as in urban canyons and deep open-cut mines. With respect to the former, there are different regional implementations of certain types of GPS augmentation. For example, within the U.S.A. a complex augmentation system designed for civil aviation is the Wide Area Augmentation System (WAAS) (Enge & Ven Dierendonck, 1996). A similar system in Europe is referred to as the European Geostationary Navigation Overlay Service (EGNOS) (Derambure et al. 1999), and in Japan, it is the Multi-Functional Transport Satellite (MT-SAT) system. The European Union has recently approved plans for the development of its own navigation system known as "Galileo", to be deployed by 2008 (Lucas et al., 2001). In this section, some representative examples of GPS augmentation for carrier phase-based positioning, such as signals from the Russian Federation's Glonass, by the use of GPS/Glonass multiple-reference station network techniques, and via ground-based pseudo-satellite (pseudolites) are briefly discussed.

1.3.1 Introduction to Glonass

The Russian Federation's Global Navigation Satellite System (Glonass) is similar, in many respects to GPS (Hofmann et al. 1994, Rizos, 1996). Glonass provides precise three-dimensional position, velocity and time (PVT) information continuously, in all weather, and on a worldwide basis, for the Russian military and civilian community. It is at present the only satellite-based positioning system which is a direct competitor to GPS, or can be viewed as an independent 'signals-in-space' augmentation of GPS. The first Glonass satellite was launched in 1982, but it wasn't until early 1996 that the system reached its complete constellation of 24 satellites in orbit. However, over the last five or so years there has been a steadily growing number of satellite failures. As of March 2002, there are only eight operational satellites. The Russian Space Forces does plan to replace the existing satellites with the new Glonass-M generation satellites (which are expected to offer improved reliability and longer lifespan), and have committed to reaching full operational capability again by 2008.

Glonass has three segments: the *space segment*, the *ground control segment* and the *user segment*, all designed to transmit, manage and receive the Glonass signals. The Glonass *space segment* comprises 24 satellites located in three approximately circular orbital planes separated by 120°, and inclined by about 64.8° to the equatorial plane. Each satellite orbits the Earth at an altitude of about 19100km, with a period of approximately 11h 15m. With tasks similar to the GPS control segment, the Glonass *ground control segment* consists of the ground control centre, the time standards, and the telemetry and tracking stations. The tracking measurements are processed by the Ground Control Centre located in Moscow, and information is uploaded via the telemetry stations to the satellites (to be then transmitted in the form of satellite ephemerides, clock corrections and almanac information). The ephemerides are predicted every 24 hours and each satellite transmits a new set of ephemeris data every 30 minutes. The almanac is updated approximately daily. The Glonass *user segment* consists of different Glonass receivers, which have a similar architecture to the GPS receivers. In the global commercial market, there are several combined GPS and Glonass receivers, for example the Ashtech GG24 (L1) and Z18 (L1/L2), the 3S Navigation R100 (L1/L2), the JPS Legacy (L1/L2), and the MAN NR124 (L1). These integrated GPS and Glonass receivers can make measurements on both the GPS and Glonass satellite signals (on L1, and sometimes on L2 also) to satisfy a broad range of positioning and timing applications.

The Glonass ephemerides are computed in the ECEF (earth-centred, earth-fixed) Parametry Zelmy (English translation "Parameters of the Earth") geodetic reference frame of 1990, which is known as PZ90 (defined and maintained by the Russian Topographic Service of the Russian Federation Ministry of Defense). The Glonass time system, like GPS, has its own time reference known as Glonass time, which is coordinated with UTC (Moscow) (GLONASS ICD, 1997).

Like GPS, each Glonass satellite transmits signals in two frequency bands, namely the L1 and L2. Again, as is the case with GPS, both carriers are modulated with P-codes, and the L1 additionally is modulated by a C/A code. In contrast to GPS satellites,

however, each Glonass satellite in the same field of view transits its navigation signals at a different frequency, which is defined as 1602 + 0.5625n (MHz) in the L1 band, and 1246 + 0.4375n (MHz) in L2 band, where n =0, 1, ... 24 are frequency channel numbers (Leick, 1995; Parkinson et al., 1996).

A combined GPS+ Glonass receiver can, in principle, track signals from a 48-satellite constellation, twice as many as the GPS-only constellation and therefore significantly improving *availability*. For example, simulation studies have shown that with a 45° obstruction to half the sky (as would be caused by a tall building), five or more GPS satellites are only available for about 33% of the day, and four or more satellites for about 85% of the day (Dai, 1998). However, there is 100% availability of five or more satellites when both GPS and Glonass satellites are considered.

The satellite navigation and positioning community is looking forward to the prospect of more signals-in-space, to satisfy the requirement for improved system availability, integrity, reliability, greater redundancy and better accuracy. For example, in "urban canyon" environments satellite signal availability is severely restricted, and the ability to track both GPS and Glonass satellite signals would mean that the chances that valid positioning can be carried out (based on the availability of four or more satellites) are increased. However, Glonass space assets have continued to decline over the last five or so years, and as of March 2002, eight satellites (of the nominal 24-satellite constellation) are listed as being operational. Although Glonass has the potential to rival GPS in coverage and accuracy, this potential is unlikely to be realised in the medium term. Hence, in the context of many positioning applications, Glonass can be viewed as a GPS augmentation.

1.3.2 GPS and Glonass Multiple-Reference Station Networks

Since the mid-1990s, university researchers have been investigating the use of multiple-reference stations for improved static and kinematic positioning in support of a range of non-geodetic applications (Rizos, 2001). The use of a network of reference receivers (instead of the traditional single base station) permits the baseline lengths (between

reference receivers, as well as between reference and user receivers) to be longer than in the single reference receiver scenario (Gao et al., 1997, Han & Rizos, 1996; Raquet, 1997; Wanninger, 1995; Wubbena et al., 1996). Only recently has there been a commercial implementation of such a positioning methodology in the Trimble Virtual Reference Station (VRS) product. In such "medium-range" (defined here as baselines several tens of kilometres in length) carrier phase-based positioning baseline length dependent biases must be mitigated if 'on-the-fly' ambiguity resolution algorithms must be used. The most important of baseline length dependent biases are those due to satellite orbit errors, and residual ionospheric and tropospheric biases.
If the distances between reference receivers can be tens of kilometres, without compromising the level of performance expected from current short-range (<10km) positioning techniques, then a large area (e.g. a metropolitan city) can be 'serviced' by a smaller number of GPS reference receivers than would be the case if the constraint of sub-10km baseline lengths was enforced.

Network-based carrier phase positioning techniques require that the data from the reference receiver network be used to generate some form of 'correction terms' to the double-differenced carrier phase data (and pseudo-range double-differences as well) formed between a user receiver and one (or more) 'real' or 'virtual' reference receiver. This is not unlike the concept of Wide Area DGPS (WADGPS), except that it involves carrier phase measurements rather than pseudo-range measurements (Rizos, 2001).

Current implementations of reference receiver networks typically have inter-station distances of between 50-100km, the approximate spacing that allows good spatial modelling of the atmospheric biases. Such a multiple-reference receiver system can support real-time kinematic (RTK) operations – the reference receiver data, and the correction messages generated from the real-time processing of the reference network data, are transmitted to the user via some form of wireless or mobile phone infrastructure.

It should be emphasised that the current network-based RTK has been implemented using a dial-up mobile phone service. Such a means of delivery of RTK data via the

digital GSM phone service could be expensive, as call charges mount with increasing connect time. It is hoped that the arrival of the so-called "2.5 G" system (e.g. the General Packet Radio Service – GPRS) will lead to reduced call charges, as GPRS call charges are a function of data 'volume' rather than connect time. As the quantity of data involved is comparatively modest, RTK services via GPRS should be significantly cheaper than the current GSM-based services. In fact, it may be economical to handle all intra-network communications via GPRS, obviating the need for dedicated fixed telephone lines between the reference receivers and the central processing facility.

It is possible to implement the reference network-based approach for static and kinematic positioning in either the post-processed mode (e.g., via a Web-based processing "engine"), or in the real-time mode.

1.3.3 Pseudolites

Global Navigation Satellite Systems (GNSS) such as GPS and Glonass consist of satellites orbiting the Earth at an altitude of about 20000km. The L-band signals from the satellites are very weak when they reach ground-based receivers, and thus can be easily obstructed by buildings, walls, trees and terrain. Therefore the performance of space-borne positioning systems is severely degraded under poor operational environments, such as in urban canyons, deep open-cut mines, etc., and in the worst situations the satellite ranging signals may be completely lost. These shortcomings of GNSS can be addressed by the inclusion of additional measurements from "pseudo-satellites" (or pseudolites).

As only 37 C/A PRN codes are reserved for the GPS satellites, and there are 1024 possible C/A codes, these unassigned codes can be used by other transmitters. Other satellites could also transmit GPS-like signals. Different PRN codes would be assigned to these satellites, and as far as the user hardware is concerned, they would be indistinguishable from the GPS satellite signals. A specialised development that could benefit precise positioning applications is the pseudolite. A GPS pseudo-satellite can be considered as a satellite-on-the-ground that transmits GPS-like ranging signals (Elrod &

Van Dierendonck, 1996). The use of pseudolites can be tracked back as early as the 1970's. Even before the launch of the GPS satellites, pseudolites had been used to test the initial GPS user equipment (Harrington & Dolloff, 1976). In DGPS applications, a pseudolite can be used to provide not only an additional ranging signal, but can also function as a differential data link. During the last decade investigations into pseudolites have intensified in aviation for precision approach and landing, as well as for other general positioning and navigation applications

Pseudolites are a complementary technology that offers opportunities to address a range of robust positioning and navigation applications. It can be expected that such augmentation of GPS will improve the performance of the positioning system because the availability and geometry of positioning solutions can be significantly strengthened. On the other hand, a pseudolite-only positioning system is possible, which can replace the GNSS constellation where the use of space-borne satellite signals is not feasible, such as underground and indoors (Kee et al., 2000).

In principle, pseudolites can transmit their ranging signals on different frequencies, just as the Glonass satellites do. Zimmerman et al. (2000) proposed a design of a pseudolite which uses up to five frequencies (two in the 900MHz ISM band, two in the 2.4GHz ISM band, and the GPS L1 frequency). An advantage of such multi-frequency pseudolite systems is that the integer carrier phase ambiguities can be resolved instantaneously, due to redundant measurements and the extra wide-lane observables that can be constructed from the different frequencies. Currently the majority of the pseudolites transmit GPS-like signals at the frequencies of L1 (1575.42MHz), and possibly on L2 (1227.6MHz). With such a configuration, and after the appropriate modification of the receiver firmware, standard GPS receivers could be used to track pseudolite signals. Pseudolites can be even designed to be capable of both receiving and transmitting ranging signals at the GPS L1/L2, or other frequencies. This type of pseudolite can 'exchange' signals, which can be used to self-determine the geometry of a pseudolite array. These pseudolites are referred to as *transceivers* (Lemaster & Rock, 1999). It is also possible to synchronise the pseudolite ranging signals to the GPS signals. This kind of pseudolites is called a *Synchrolite* (Cobb, 1997).

1.4 Motivation

Although RTK systems represent the 'state-of-the-art' in GPS commercial-off-the-shelf (COTS) technology, able to deliver centimetre-level accuracy in real-time using a pair of GPS receivers, there are several constraints to their use. If enough GPS satellites were continuously tracked and loss-of-signal-lock never occurred, the integer ambiguities determined at the beginning of a survey would be valid for the whole period that GPS was being used. However, the GPS satellite signals can be shaded (for example, due to buildings in urban canyon environments, or when the receiver passes under a bridge or through a tunnel). In the worst cases the number of visible satellites may not be sufficient to even carry out positioning. When ambiguity values are 'lost', they must be redetermined. This process can take from a few seconds (in the case of 'instant' AR systems) up to a few minutes with present GPS COTS systems. The more satellites available, the less 'time-to-ambiguity resolution'. During this "re-initialisation" period while AR is being carried out, centimetre accuracy positioning is not possible. Such constraints may be so restrictive that they may hinder the widespread adoption of carrier phase-based GPS techniques for both engineering surveys (a traditional application of precise GPS techniques), as well as for new applications such as navigation in support of vehicle guidance/control. These constraints can be addressed through various augmentation schemes, such as the combination of GPS with Glonass, GPS with pseudolites, as well as the integration of GPS and inertial navigation systems/sensors.

On the other hand, real-time high precision GPS surveying and navigation techniques have been constrained to 'short-range' due to the presence of distance-dependent errors in the between-receiver observables. However, the adoption of GPS carrier phase-based positioning techniques has been growing rapidly for precise marine and airborne applications. There is a significant challenge when the GPS reference receiver(s) cannot be set up near the survey area, such as out on the continental shelf areas, and in remote and inaccessible land areas such as Antarctica, Australia's outback, Central Asia, Siberia, Greenland, etc. The distance from the fixed reference receiver(s) to the mobile user receiver(s) may range from tens to many hundreds of kilometres, yet the accuracy

requirement may be at the decimetre level or higher. Once Wide Area DGPS systems or GPS (and Glonass) multiple-reference station networks are established, and the appropriate data is transmitted, GPS carrier phase-based medium-range (or even long-range) kinematic positioning techniques may allow a user to precisely position a moving receiver.

1.5 Research Objectives

The main research objectives in this thesis are: (1) to develop an integrated procedure for GPS and Glonass carrier phase data processing; (2) to compare the interpolation methods of various multiple-reference station techniques; (3) to develop data processing algorithms suitable for real-time GPS/Glonass ambiguity resolution between reference stations that account for cycle slips in the data, new satellites rising or long data gaps; and (4) to integrate GPS and pseudolite technologies and investigate potential pseudolite-related applications.

The development of integrated GPS-Glonass receivers which measure carrier phase offers special challenges, not the least being that the signals to the different Glonass satellites are of a different frequency, making the standard GPS data processing strategies based on double-differencing inappropriate. However, the extra satellites that can be tracked should make precise positioning a more robust procedure. During the last few years several research groups have been working to develop integrated GPS and Glonass data processing techniques. A three-step-procedure functional model, which permits an optimally integrated processing of GPS and Glonass data, and takes advantage of features of the different DD combinations, has been developed. An integrated method, with improvements to the real-time stochastic model, a fault detection and adaptive procedure, is proposed for use with this functional model.

One core issue for multi-reference station techniques is how to interpolate the distance-dependent biases generated from the reference receiver network for the user's location? Over the past few years, several methods for implementing a GPS multiple-reference station technique have been developed. These methods have been analysed in detail in

this study, and the basic modelling formulation has been identified. All methods use n-1 coefficients and n-1 independent 'correction terms' generated from a n reference receiver network to form a linear combination that mitigates spatially correlated errors at user stations. The formulas for the coefficient determination for each method have been derived.

Two scenarios for real-time ambiguity resolution appropriate for GPS/Glonass reference station networks are proposed. The first scenario is concerned with the modelling of temporally correlated biases to aid the correct 'recovery' of ambiguities. Three methods have been proposed for modelling temporally correlated biases: the random-constant stochastic method, the linear function fitting method and a method based on Kalman filtering. On an epoch-by-epoch and satellite-by-satellite basis, these systematic errors (or biases) can be estimated using previous measurements with fixed ambiguities, and precisely predicted for subsequent measurement epochs. The second scenario is concerned with the modelling of spatially correlated biases such as the residual ionospheric and tropospheric delay, in order to aid the resolution of the wide-lane and narrow-lane ambiguities for a newly risen satellite, or after a long data gap.

A specialised augmentation that could benefit carrier phase-based positioning is the use of pseudolites. Pseudolites are a promising technology that could, in principle, be used for a wide range of positioning and navigation applications, either as a substantial augmentation of space-borne systems, or as an independent system for indoor positioning. However, due to the comparatively small separation between pseudolites and receivers/users, there are some challenging modelling issues, such as non-linearity, pseudolite location errors, tropospheric delays, multipath, geometry design and potential pseudolite related applications that need to be addressed.

1.6 Contributions of the Research

GPS augmentation for carrier phase-based positioning by the existing space-borne Glonass system, through the use of multiple GPS/Glonass reference stations, and by

ground-based pseudo-satellite transmitters has been investigated in this study. The major contributions of this research can be summarised as follows:

- An integrated procedure for combined GPS and Glonass data processing, in combination with a three-step procedure function model, a real-time estimated stochastic model, fault detection and adaptation, has been developed.

- An underlying common formula for all of the interpolation methods employed by multiple-reference station techniques has been identified. The respective formulas for coefficient determination, for each method, have been derived.

- Two real-time ambiguity resolution scenarios for GPS and Glonass reference station networks have been addressed through the development of several modelling strategies. Temporally correlated bias models are used to recover ambiguities, whilst spatially correlated bias models are used to predict residual ionospheric and tropospheric delays to assist ambiguity resolution for a newly risen satellite, or after a long data gap.

- The modelling issues for GPS and pseudolite integration, including non-linearity, pseudolite location errors, tropospheric delays, multipath and noise, have been addressed. Formulas for the effects of non-linearity and, orbital errors and tropospheric delay have been derived from a theoretical point of view.

- Three different pseudolite configurations, including integrated GPS and pseudolite, pseudolite-only, and pseudolite-based 'inverted' positioning, have been investigated. Practical considerations for pseudolite use, from the point of view of geometric optimisation, have been discussed. Optimal geometric designs for various positioning scenarios have been proposed.

1.7 Outline of the Thesis

This thesis consists of seven chapters. The contents of the each chapter are outlined as follows.

Chapter 1 gives some of the GPS background, carrier phase-based positioning techniques and the GPS augmentation by Glonass, multiple-reference station networks, and pseudolites. After the motivation and research objectives on the GPS augmentation are presented, the contributions of this research work are outlined.

Chapter 2 presents an integrated procedure for GPS and Glonass data processing, which consists of a three-step procedure to improve the functional model, the associated real-time stochastic model, and the proposed fault detection and adaptive procedure.

Chapter 3 compares current interpolation methods for multiple-reference station techniques: the Linear Combination Model, the Distance-Based Linear Interpolation Method, the Linear Interpolation Method, the Lower-Order Surface Model, and the Least Squares Collocation Method. The advantages and disadvantages of each of these techniques are discussed. For all of the abovementioned methods, the essential common formula is identified, which uses the n-1 coefficients and the n-1 independent 'correction terms' generated from a n reference receiver network to form a linear combination that mitigates spatially correlated errors at user stations. The formulas for coefficient determination for each method are derived.

Chapter 4 presents two scenarios for real-time ambiguity resolution appropriate for GPS and Glonass reference station networks. The temporal correlation bias model is used to 'recover' GPS and Glonass ambiguities. The model for spatially correlated residual ionospheric and tropospheric delay can aid the resolution of the wide-lane and narrow-lane ambiguities for a newly risen satellite, or after a long data gap. Other associated issues, such as the criterion to fix ambiguities and the different signal frequencies for the Glonass satellites, are also addressed.

Chapter 5 discusses the modelling issues for GPS and pseudolite integration, such as non-linearity, pseudolite location errors, tropospheric delays, multipath and noise. The effects of non-linearity, orbital errors and tropospheric delay are analysed from a theoretical point of view.

Chapter 6 presents the three different pseudolite configurations (integrated GPS and pseudolite, pseudolite-only, and pseudolite-based 'inverted' positioning). The advantages and disadvantages of each configuration are discussed. The feasibility of using pseudolite for such applications as deformation monitoring and navigation services (based on pseudolite installed on stratospheric airships) is investigated. Based on use of the appropriate quality indicators, the impact of the pseudolite-user geometry on the final positioning solutions is analysed. Optimal geometric designs for various positioning scenarios are proposed.

Chapter 7 summarises the research findings, draws conclusions, and makes recommendations for future investigations.

Chapter 2

INTEGRATED PROCEDURE FOR GPS AND GLONASS CARRIER PHASE-BASED POSITIONING

2.1 Introduction

Carrier phase-based real-time kinematic (RTK) GPS positioning has been playing an increasing role in surveying and navigation, and has become an essential tool for precise relative positioning. However, the reliability of ambiguity resolution increases with the number of observations to as many GPS satellites as possible. This constrains the performance of carrier phase-based techniques, making them difficult to address positioning applications in areas where the number of visible satellites is limited. The most obvious way to increase the number of tracking satellites is to somehow integrate the GPS and Glonass systems. Due to the different signal frequencies for the different Glonass satellites, the commonly used double-differencing (DD) procedure for carrier phase data processing cannot be implemented in its standard form (as is done with GPS). To overcome this problem several modelling methods have been proposed in the literature. Three general classes of integrated GPS and Glonass functional models have been developed over the last decade. The first is to introduce the known relative clock parameter, which is estimated using pseudo-range measurements, into the Glonass DD carrier phase observation equations (see, e.g., Pratt et al., 1998; Leick, 1998). The second class of functional models estimate the clock parameters, baseline vectors and ambiguity parameters together using both the carrier phase and pseudo-range observation equations (see, e.g., Zhodzishsky, 1998; Kozlov, 1997; Wang, 1998; Han et al., 1999; Dai et al., 2001g). However, for these two classes of models, the ambiguity resolution and positioning results are seriously affected by the remaining clock biases and the Glonass pseudo-range inter-channel biases. The third class of models involves a

two-stage procedure or an iterative search approach to process DD observables (expressed in metres) without the receiver clock value (see, e.g., Wang, 2000; Habrich et al., 1999). For this class of models, if the ambiguity sets can be fixed correctly, the positioning results are not affected by the clock bias. Unfortunately, in a two-level search approach any wrong single-differenced (SD) Glonass ambiguity value for the Glonass reference satellite can cause systematic model errors that may affect DD ambiguity resolution. The iterative search approach is only suitable for long session static modes of positioning. A detailed review of the variety of mathematical modelling options for integrated GPS and Glonass data processing can be found in Wang et al. (2001). In this chapter, three general classes of integrated GPS and Glonass functional models have been optimally integrated so that: (1) the ambiguity resolution is insensitive to the remaining clock biases and inter-channel biases, and (2) reliable and precise positioning results will not be affected by residual receiver clock biases.

High quality estimation results from the application of the Least Squares estimation technique requires the specification of the optimal functional and associated stochastic model. The stochastic model is dependent on the choice of the functional model. Hence, for a different choice of functional model, the stochastic characteristics of unmodelled errors will be different, and the stochastic model must reflect this. Based on the assumption that the accuracy of the one-way observations depends on signal-to-noise (Gianniou & Groten, 1996), or satellite elevation (Jin, 1995; Han, 1997), some approximate formulas to compute the variance-covariance matrix for DD observables have been proposed. However, constant coefficients for certain types of GPS receivers, which are empirically estimated from observations collected under specific observing conditions, are probably not well suited for other measurement environments. Due to the high temporal correlation of observations, the compensated method was proposed to estimate a scale factor in the stochastic model, using previous data collected over a certain period (Han, 1997). This method could derive a more realistic stochastic model, and hence increase the reliability of the ambiguity resolution and the positioning accuracy. However, it doesn't take into account the observations' spatial correlation, which would need refining of the variance-covariance matrix. The construction of the variance-covariance matrix can be carried out using the residual series over the previous

epochs, when the integer ambiguities are fixed correctly. Based on the estimated variance-covariance matrix of the residuals, and the relationship between the residuals and the observation errors, an improved variance-covariance matrix of the observations can be derived. Hence, the real-time stochastic model derived in this way will not only reflect the stochastic characteristics of the observation errors, but also the remaining biases due to multipath, atmospheric delay, inter-channel biases and orbital errors. This method could be used for different types (SD, DD, in metres or cycle units) of carrier-phase and pseudo-range observation combinations.

The third problem is the definition of the Fault Detection, Identification and Adaptation procedure, which must guard against wrong integer ambiguity determination. This is an increasingly important aspect of instantaneous (or single-epoch) ambiguity resolution for centimetre accuracy, real-time GPS positioning due to the very small number of degrees of freedom in the estimation process.

In this chapter, an integrated data processing procedure for integrated GPS and Glonass positioning, in combination with a three-step functional model, a real-time (estimated) stochastic model, and a fault detection / adaptation procedure, is proposed. The performance of this data processing strategy will be demonstrated via examples of rapid static positioning and kinematic positioning.

2.2 Functional Modelling Strategy

The SD carrier phase observable between receivers can be expressed as (e.g. Leick, 1998):

$$\lambda_1^p \phi_{kl}^p = \rho_{kl}^p + \lambda_1^p N_{kl}^p - c \cdot dt_{kl} - I_{kl}^p / (f_1^p)^2 + T_{kl}^p + \varepsilon_{kl}^p \qquad (2\text{-}1)$$

where the subscripts k and l identify the ground receivers, and superscript p denotes the satellite. ϕ_{kl}^p is the SD carrier phase observable expressed in units of cycles. λ and f_1^p are the wavelength and frequency of the L1 carrier wave respectively. N is the SD

integer ambiguity; dt_{kl} is the difference between the two receiver clock biases in seconds; c is the speed of light. $I_{kl}^{p}/(f_1^{p})^2$ is the SD ionospheric delay, where I is a function of the Total Electron Content; T_{kl}^{p} is the SD tropospheric delay; and ε_{kl}^{p} is the carrier phase observation noise (and any remaining errors).

Equation (2-1) is valid for GPS and Glonass carrier phase measurements. However, L1 GPS signals have the same frequencies for all satellites, while Glonass signals have different frequencies for different satellites.

2.2.1 Double-Differenced Observables

The DD observable in units of metres can be formed as:

$$\lambda_1^{p}\phi_{kl}^{p} - \lambda_1^{q}\phi_{kl}^{p} = \rho_{kl}^{pq} + \lambda_1^{p}\cdot N_{kl}^{p} - \lambda_1^{q}\cdot N_{kl}^{p} + I_{kl}^{p}/(f_1^{p})^2 - I_{kl}^{q}/(f_1^{q})^2 + \varepsilon_{kl}^{pq} \tag{2-2}$$

It could be seen that data processing for integrated GPS and Glonass data sets becomes more complicated because of the different frequencies for the Glonass satellites. The Glonass DD observables have more ionospheric delay than the GPS DD observables. However it could still be ignored if the distance between the two receivers is short enough. Equation (2-2) could then be rewritten as:

$$\lambda_1^{p}\phi_{kl}^{p} - \lambda_1^{q}\phi_{kl}^{p} = \rho_{kl}^{pq} + \lambda_1^{p}\cdot N_{kl}^{pq} - (\lambda_1^{p} - \lambda_1^{q})\cdot N_{kl}^{q} + \varepsilon_{kl}^{pq} \tag{2-3}$$

It is clear that for GPS carrier phase measurements the third term on the right-hand side of Equation (2-3) will disappear. For Glonass carrier phase measurements the third term, or the SD integer ambiguity for the reference satellite, must be estimated before the DD integer ambiguities can be computed. The remaining errors from the third term could cause systematic model errors and may result in wrong DD ambiguity resolution, and hence degraded positioning accuracy.

An alternative approach is to form the DD observable after the SD observables are expressed in units of cycles:

$$\phi_{kl}^{pq} = \left(\frac{f_1^p}{c}\rho_{kl}^p - \frac{f_1^q}{c}\rho_{kl}^q\right) + \left(\frac{f_1^p}{c}T_{kl}^p - \frac{f_1^q}{c}T_{kl}^q\right) + N_{kl}^{pq} - \left(\frac{I_{kl}^p}{c\cdot f_1^p} - \frac{I_{kl}^q}{c\cdot f_1^q}\right) - \left(f_1^p - f_1^q\right)\cdot dt_{kl} + \varepsilon_{kl}^{pq} \tag{2-4}$$

The differenced receiver clock bias cannot be eliminated in Equation (2-4). The second term (ionospheric delay) and the third term (tropospheric delay) will become slightly larger than in the case when the two frequencies are the same. Using GPS and Glonass pseudo-range measurements, the difference between the two receiver clock biases can be estimated, which could then be used to correct the second term for ambiguity resolution purposes. However, this receiver clock bias will significantly degrade the positioning accuracy.

2.2.2 An Integrated Three-Step Procedure

Due to the different frequencies for the different Glonass satellites, the relative receiver clock bias ΔdT cannot cancel in the Glonass DD carrier phase, see Equation (2-4). To overcome this problem, the SD pseudo-range observations should be included. Although the pseudo-range-derived receiver clock parameter is good enough for ambiguity resolution purposes, it still affects the positioning results. Therefore Equation (2-3) is used to determine the baseline parameters after the integer ambiguities are fixed. The third term on the right-hand side of Equation (2-3) will be considered an additional unknown parameter until a cycle slip occurs on the Glonass reference satellite. Hence the data processing procedure can be summarised as follows.

Step 1: The DD GPS pseudo-range observables and the SD Glonass pseudo-range observables are used:

$$P_{kl,GPS}^{pq} = \rho_{kl}^{pq} + \varepsilon_{kl}^{pq} \tag{2-5}$$

$$P^{p}_{kl,GLONASS} = \rho^{p}_{kl} + c \cdot dt_{kl} + \varepsilon^{p}_{kl} \tag{2-6}$$

where $P^{pq}_{kl,GPS}$ and $P^{p}_{kl,GLONASS}$ are the DD GPS pseudo-range observable and the SD Glonass pseudo-range observable respectively. Why are DD GPS pseudo-range observables used rather than SD GPS pseudo-ranges? When the difference of the two receiver clocks is introduced into the GPS SD observation equation, the inter-channel bias between the GPS satellite and the Glonass satellite may be introduced in order to derive equivalent results, making the data processing more complicated. This model was also identified as an optimal functional model by Rapoport (1997).

In this step, the difference in the two receiver clock biases, the initial baseline parameters and their variance-covariance matrix can be derived for the ambiguity resolution process in the next step.

Step 2: DD GPS and Glonass carrier phase observables in units of cycles, e.g. Equation (2-4), will be used for ambiguity resolution. The second term on the right-hand side of Equation (2-4) will disappear for GPS measurements due to the fact that the same frequency is used for the different GPS satellites. However, this term must be corrected using the difference of the two receiver clock biases.

The frequency difference between Glonass signals is smaller than 12.9MHz for L1 observations, and less than 10.1MHz for L2 observations. Hence the difference in the two receiver clock biases can be expected to be less than 10ns (approximately 3 metres), and therefore this term can be corrected at the 0.1 cycle level. For ambiguity resolution purposes, the bias could be ignored without significant impact on the reliability. However, this error cannot be ignored when Equation (2-4) is used to derive the positioning results. Furthermore, this term could not be considered as the same unknown parameter for different epochs.

Step 3: Although the integer ambiguity set could be determined in Step 2 using Equation (2-4), the positioning results will be affected by the receiver clock biases. However, the DD carrier phase observables in units of metres, e.g. Equation (2-3), where the receiver clock biases are removed and the integer ambiguity sets are determined in Step 2, could be used. In this way the third term on the right-hand side of Equation (2-3) could be considered as an additional unknown parameter over different epochs until a cycle slip occurs on the Glonass reference satellite.

This three-step procedure is an integrated way of processing combined GPS and Glonass data, which takes advantage of features of the different DD combinations. It should be mentioned that: (1) the double-differencing operator is applied to the GPS measurements only or the Glonass measurements only, rather than between GPS and Glonass; and, (2) cycle slip detection at the Glonass reference satellite is required, though not repair.

If a mixed double-differencing operator between GPS and Glonass was used, the coefficient of the clock term will increase dramatically to a value between 26.6MHz and 39.5MHz for L1 observations, and from 18.4MHz to 28.5MHz for L2 observations. It is easily seen that the clock error effect on ambiguity resolution in the mixed formulation is more serious than in the separated formulation. The inter-channel bias must be accounted for in some way if the difference between GPS and Glonass measurements is formed. Although inter-channel biases exist for measurements from different Glonass satellites, they could be ignored for most applications. Hence the separated formulation of double-differences is much more reliable than the mixed formulation (Pratt et al., 1998). The slight disadvantage in the separated formulation is the reduced number of the double-differences (reduced by one). As with the case of the carrier phase, the performance of the separated pseudo-range combination is better than the mixed combination.

The second issue is cycle slip detection on the Glonass reference satellite. It should be noted that the third term should be a constant when tracking at both receivers to the Glonass satellite is maintained. However, when a cycle slip occurs on the SD carrier

phase measurement involving the Glonass reference satellite, this term will no longer be a constant. A new unknown parameter must be introduced, or this cycle slip must be repaired. One cycle slip will result in about 1.5mm for the L1 observations, and 2.0mm for the L2 observations, in the worst case. If the Glonass reference satellite can be chosen from the middle of the Glonass frequency range, it should be less than 1.0mm. Cycle slips should be detected by using the SD carrier phase observables (Equation (2-1)), which is very sensitive to the difference of the two receiver clock biases. In practice, only significant cycle slips were detected or were recorded by the receivers, and a new unknown parameter needed to be introduced.

2.3 Real-time Stochastic Model Estimation

High quality results using Least Squares estimation techniques requires the correct selection of both the functional and stochastic models. The stochastic model is dependent on the choice of the functional model. Hence for a different choice of functional model, a different stochastic model may be needed. GPS and Glonass observations are affected by several kinds of errors and biases. When forming the double-differences, the main biases are caused by multipath effects, residual atmospheric errors, orbital errors, and inter-channel biases. Due to insufficient knowledge about these physical phenomena, the above biases cannot be rigorously accounted for through functional modelling. The stochastic model has to therefore model both the observation noise and the unmodelled residual biases.

2.3.1 Empirical Stochastic Model

The well-known elevation dependent stochastic model is often used, which may be represented as an exponential function or an inverse of the sine of the satellite elevation angle (see, e.g., El-Rabbany, 1994; Jin, 1995). However, constant coefficients can only reflect error characteristics of the GPS receiver, rather than the unmodelled residual biases, which most probably are related to the observing environment. In order to

introduce this "environment information", an adaptive stochastic model was proposed by Han (1997), in which a scale factor is introduced, and estimated in real-time:

$$\sigma = s \cdot (a_0 + a_1 \cdot exp(-E/E_0)) \tag{2-7}$$

where σ is the standard deviation of the carrier phase or pseudo-range observations; a_0, a_1 and E_0 are approximated by constants; E is satellite elevation angle, and s is a scale factor which can be estimated from moving 2-5 minute windows of data. This model more or less accounts for the environmental "impact" on the stochastic model. However, the spatial correlation between the DD observables cannot be defined in this way. In other words, the diagonal elements of the *a priori* variance-covariance matrix cannot be accounted for through the use of a scale factor (in place of the appropriate non-diagonal elements). Therefore the construction of a more rigorous stochastic model is still a challenge. A real-time stochastic model for GPS and Glonass integration based on post-fit residuals is proposed as follows.

2.3.2 Real-Time Stochastic Modelling

Based on the fact that the residual series of Least Squares estimation contains sufficient information of the observation noise and biases, a more rigorous stochastic model is derived. The general Least Squares linearised observation equation and the criteria are:

$$V_i = B_i X_i - L_i \tag{2-8}$$

$$V_i^T D_i^{-1} V_i = \text{Minimum} \tag{2-9}$$

where V_i and L_i are the vectors of all the measurements and residuals at epoch i respectively; B_i is the design matrix related to the vector of measurements L_i; X_i is the estimated unknown parameter vector; and D_i is the variance-covariance matrix of the measurements.

Based on the minimum quadratic form of the residuals, the Least Squares estimated parameters $\hat{X}_i$ are:

$$\hat{\mathrm{X}}_{\mathrm{i}} = (B_{\mathrm{i}}^{T} D_i^{-1} B_{\mathrm{i}})^{-1} B_{\mathrm{i}} D_i^{-1} \mathrm{L}_{\mathrm{i}} \tag{2-10}$$

Substituting Equation (2-10) into Equation (2-8), the $n \times 1$ estimated residual vector is:

$$V_i = (B_i (B_{\mathrm{i}}^{T} D_i^{-1} B_{\mathrm{i}})^{-1} B_{\mathrm{i}} D_i^{-1} - E) L_i \tag{2-11}$$

The relationship between the variance-covariance matrices of post-fit residuals and measurements can be derived from Equation (2-11):

$$D_i = Q_{V_i} + B_{\mathrm{i}} (B_{\mathrm{i}}^{T} D_i^{-1} B_{\mathrm{i}})^{-1} B_{\mathrm{i}}^{T} \tag{2-12}$$

where Q_{V_i} is the variance-covariance matrix of the residuals. Due to the similarity of the observation environments, the residuals of the observations show a high degree of temporal and spatial correlation over the short term. In other words, the residual series could be considered as a wide-sense stationary process. The actual variance-covariance matrix of the residuals can then be estimated from the previous residual series, whose ambiguity sets have already been fixed to their correct values, using the following equation:

$$Q_{V_i} = \frac{1}{N} \sum_{k=1}^{N} V_{i-k} V_{i-k}^{T} \tag{2-13}$$

where N is the width of the moving data window. The minimum N should not be less than the number of DD ambiguities. If N is too large, temporal and spatial decorrelation will occur, and the performance of the model will decrease. Testing has shown that the optimal width of the moving window is in the range of 10-30 epochs with 1-second

sampling rate. In practical applications, residuals from the ambiguities-fixed solutions need to be used because the float ambiguity values may absorb some unmodelled errors.

In Equation (2-12), the variance and covariance of the measurements cannot be estimated directly. An iterative procedure becomes necessary. The initial (or default) variance-covariance matrix is determined by using the previous variance-covariance matrix. Based on the previous measurement residuals, the variance-covariance matrix of the measurements can be rigorously estimated in real-time using Equations (2-12) & (2-13). (Normally iterating twice is sufficient.) The default stochastic model should be used at the beginning of the data processing, or for a new satellite, or after a long data gap.

The stochastic model not only reflects the stochastic characteristics of the observation noise, but also the residual biases due to multipath, the atmospheric delays, the inter-channel biases and the orbital error remaining after double-differencing both the carrier phase and pseudo-range observations. With the help of the estimated variance-covariance matrix, the reliability of ambiguity resolution and the accuracy of the real-time kinematic positioning results can be significantly improved.

2.4 Ambiguity Resolution, Validation and Fault Detection

Equations (2-4), (2-5) and (2-6), combining carrier phase and pseudo-range observations, can be used to estimate the real-valued parameter vector that includes baseline components, ambiguities and clock bias, and their variance-covariance matrix. The associated stochastic model is derived from the residual series over the previous epochs using Equations (2-12) and (2-13). In the case of the ambiguity-float solution, estimates $\hat{X}_C$ ($t \times 1$ baseline components and clock parameter) and $\hat{X}_N$ ($m \times 1$ real-valued ambiguity parameters) are obtained using the standard Least Squares procedure with *a posteriori* weight variance factor $\hat{\sigma}_0^2 = \frac{V^T P V_{Float}}{n-t-m}$, where $V^T P V_{Float}$ is the quadratic form of the residuals. Reliable results at this step are dependent on the

appropriateness of the stochastic model of the observations with respect to the functional model. The following rejection regions should be employed in order to check the fidelity of the stochastic and functional models:

$$V^T PV_{Float} \geq \sigma_0^2 \cdot \xi_{\chi^2_{n-t-m};1-\alpha/2} \tag{2-14}$$

$$V^T PV_{Float} \leq \sigma_0^2 \cdot \xi_{\chi^2_{n-t-m};\alpha/2} \tag{2-15}$$

where $\xi_{\chi^2_{n-t-m};\alpha/2}$ and $\xi_{\chi^2_{n-t-m};1-\alpha/2}$ are the lower and upper bounds of the $1-\alpha$ confidence interval for the χ^2 -distribution statistic with *n-t-m* degrees of freedom respectively. This test is used to monitor the pseudo-range observation quality because $V^T PV_{Float}$ is only dependent on the pseudo-range observations if single-epoch data are processed (Han & Rizos, 1997). If the $V^T PV_{Float}$ is rejected by Equation (2-14), the outlier detection procedure should be applied because the outliers may exist in the pseudo-range observations, which are caused by multipath or system biases, or the stochastic model does not reflect the actual accuracy of the observations. If the $V^T PV_{Float}$ is rejected by Equation (2-15), a check should be made to determine whether there are enough redundant observations, or whether the stochastic model does reflect the actual accuracy of the observation.

The LAMBDA procedure is then implemented to search the integer ambiguity set (see, e.g., Teunissen, 1994; Han & Rizos, 1995). The validation criteria test suggested by Han (1997), and the ratio test, are implemented. If both tests are passed, the ambiguity resolution is assumed to be correct. The quadratic form of the residuals $\Omega_{Fix,k}$ corresponding to the ambiguity-fixed solution should be compatible with σ_0^2, represented by the condition:

$$\sigma_0^2 \cdot \xi_{\chi^2_{n-t};\alpha/2} \leq \Omega_{Fix,k} \leq \sigma_0^2 \cdot \xi_{\chi^2_{n-t};1-\alpha/2} \tag{2-16}$$

where $\xi_{\chi^2_{n-t};\alpha/2}$ and $\xi_{\chi^2_{n-t};1-\alpha/2}$ are the lower and upper bounds of the $1-\alpha$ confidence interval for the χ^2 -distribution statistic with *n-t* degrees of freedom respectively. If $\Omega_{Fix,k}$ is rejected, the corresponding integer vector will be rejected. In this case, using the outlier detection procedure, or partial fixing procedure, a satellite with the outlier should be removed so as to attempt to fix the ambiguities again, or the previous fixed ambiguities (without cycle slips) should be introduced in order to generate reliable positioning results.

In order to further ensure that the ambiguity resolution is correct and reliable, additional global information should be used in the case of dual-frequency data. As is well known, the Total Electron Content (TEC) of the path through the ionosphere has a very strong correlation in space and time. The TEC value for the adjacent epoch should therefore be very similar and this information will be considered the basis for a global test. The difference between the double-differenced ionospheric delay on L1 and L2 carrier phase observations of the satellites *p* and *q* is defined as $\nabla\Delta TEC$, which can be represented as:

$$\begin{aligned}\nabla\Delta TEC = {} & \lambda_1^p \phi_{kl,1}^p - \lambda_2^p \phi_{kl,2}^p - \lambda_1^q \phi_{kl,1}^q + \lambda_2^q \phi_{kl,2}^q + (\lambda_1^p - \lambda_1^q)\cdot N_{kl,1}^q - (\lambda_2^p - \lambda_2^q)\cdot N_{kl,2}^q \\ & - \lambda_1^p N_{kl,1}^{pq} + \lambda_2^p N_{kl,2}^{pq}\end{aligned} \tag{2-17}$$

where $N_{kl,1}^q$ and $N_{kl,2}^q$ are single-differenced ambiguities for the reference satellite on L1 and L2 respectively. In Equation (2-17) it is obvious that the Glonass $\nabla\Delta TEC$ values are biased by the single-differenced ambiguity at the Glonass reference satellite. If the double-differenced integer ambiguities are resolved correctly, and no cycle slips occur on the single-differenced carrier phase measurement involving the Glonass reference satellite, the $\nabla\Delta TEC$ sequence should change smoothly. Otherwise, a 'jump' will occur due to wrong ambiguity resolution. The 'jump' can be determined using the difference δTEC_{kl}^{pq}, between $\nabla\Delta TEC$ at the current epoch and its value at the previous epoch for whose ambiguities have been correctly fixed. If wrong ambiguity resolution at the current epoch has occurred, and there are no cycle slips at the Glonass reference satellite, δTEC_{kl}^{pq} can be represented by:

$$\delta TEC_{kl}^{pq} = -\lambda_1^p \delta N_{kl,1}^{pq} + \lambda_2^p \delta N_{kl,2}^{pq} \tag{2-18}$$

where $\delta N_{kl,1}^{pq}$ and $\delta N_{kl,2}^{pq}$ are the magnitudes of the integer biases caused by wrong ambiguity resolution on L1 and L2 respectively. It should be noted that δTEC_{kl}^{pq} is not affected by cycle slips, except those related to the Glonass reference satellite. It should also be pointed out that as far as the accuracy of the final ambiguity-fixed solutions is concerned, the tropospheric delay and the orbit errors have no influence on the accuracy of δTEC_{kl}^{pq}. If single-epoch ambiguity resolution is correct at the current epoch and the previous epoch, δTEC_{kl}^{pq} should be very small. Therefore, the criteria:

$$\delta TEC_{kl}^{pq} < 5.0\,\text{cm} \tag{2-19}$$

is used for fault detection. However, some special integer bias combinations cannot be identified (Han, 1997, Dai, 2000). Obviously, if ambiguity resolution is correct and no cycle slips occur at the Glonass reference satellite, the condition at Equation (2-19) will be satisfied. The critical value depends on the ionospheric change and the magnitude of the multipath. The magnitude of the ionospheric change between epochs depends on the sampling rate or the length of data gap. The critical value is selected as 5cm for the experiments described in this study. It should be emphasised that cycle slips at the Glonass reference satellite have to be considered in the process of fault detection for ambiguity resolution. It is noted that when a cycle slip occurs on the Glonass reference satellite, Equation (2-18) should be modified to:

$$\delta TEC_{kl}^{pq} = (\lambda_1^p - \lambda_1^q)\cdot \delta N_{kl,1}^{q} - (\lambda_2^p - \lambda_2^q)\cdot \delta N_{kl,2}^{q} - \lambda_1^p \delta N_{kl,1}^{pq} + \lambda_2^p \delta N_{kl,2}^{pq} \tag{2-20}$$

where $\delta N_{kl,1}^{q}$ and $\delta N_{kl,2}^{q}$ are the single-differenced cycle slip values at the Glonass reference satellite on L1 and L2 respectively. One cycle slip on L1 (or L2) will result in about 1.5mm (or 2.0mm) bias in δTEC_{kl}^{pq} for the worst case. It is clear that small cycle slips have no significant influence on fault detection. *It should be emphasised that cycle slips do not affect single-epoch ambiguity resolution.*

Before default detection, a two-step procedure has been suggested to check for cycle slips affecting the Glonass reference satellite. The first step is that after the 'best' ambiguities pass the validation criteria, the Glonass satellite without significant cycle slips will be selected as the reference satellite. In this step, the difference in the single-differenced TEC with ambiguities between two epochs can be used to detect cycle slips. In practice, significant cycle slips are easily detected. The second step, if the Glonass reference satellite has been changed, is that the corresponding double-differenced ambiguities will have to be reconstructed. If all the Glonass satellites are suspected of having significant cycle slips, all the Glonass observations will be deleted, and the fault detection procedure will not be applied to the Glonass ambiguities. It should be pointed out that the cycle slips on the single-differenced carrier phase measurement involving the GPS reference satellite have no influence on fault detection. Any ambiguities that cannot satisfy Equation (2-19) should be rejected. In practice, this proposed fault detection procedure could effectively identify incorrect ambiguity resolution.

2.5 Adaptation

Based on the above discussion, an *adaptive* procedure for the functional model should be applied if the Equations (2-14) and (2-15) are accepted, or the Equations (2-16) and (2-19) are rejected (Dai et al., 2002d). If the resolved integer ambiguities are incorrect, in general the wrong integer ambiguities will refer to more than one satellite pair, and it is almost impossible to identify which ambiguities are incorrect. However, the fact that some significant biases are present in the observations can be confirmed. For ambiguity resolution and positioning purposes the minimum number of satellites is 5 for GPS or Glonass, and 6 for combined GPS and Glonass processing. If more satellites are tracked, some of these observations, which are suspected as being contaminated by outliers or biases, can be removed so that: (1) instantaneous ambiguity resolution is possible with a maximum success rate; and (2) the position solution can still be output using the fixed ambiguities from the previous epoch (if ambiguity resolution fails and there are enough satellites without cycle slips). The objective of the adaptive procedure for the functional model based on the outlier detection algorithm is: (1) to judge whether any outlier is present; (2) to determine which observations should be identified as containing outliers;

and (3) to make an acceptable decision about outliers and to estimate the corresponding effect on the final solution if outliers cannot be uniquely identified. All the above are important for a successful outlier detection algorithm. However, the emphasis of this study will be on the former two issues. In this chapter, two outlier detection algorithms are tested.

2.5.1 Outlier Detection Methods

Baarda's data snooping theory assumes that only one outlier is present in the independent observations (Baarda, 1968). Applying a series of one-dimensional tests, that is, testing consecutively all residuals, is the standard data snooping strategy. Baarda's Test belongs to the group of un-studentised tests that assume that the *a priori* variance of unit weight is known. The test statistic is written as:

$$n_i = \frac{V_i}{\delta_0 Q_{vv_{ii}}} \in N(0, 1) \qquad (2\text{-}21)$$

The critical value can be determined from the normal distribution with a significance level of α. If α is assigned 5%, the critical value is 1.96. It should be emphasised that the critical value for this test is independent of the degrees of freedom.

Another outlier detection algorithm based on correlation analysis theory has been proposed by Shi (1998) and Dai et al. (1999). Any observation errors, including outliers, affect the residuals through the reliability matrix in the least-squares adjustment. The correlation coefficient between the column vector of the reliability matrix and the residual vector is considered critical information, which can reflect the relationship between the true error of the correlated observations and the residuals. It replaces the standardised residual for the detection and analysis of the outliers in the correlated double-differenced observations. The correlation coefficient (See appendix) is:

$$\rho_{R_j,V} = \frac{\sum_{i=1}^{n}(r_{ij} - \bar{r}_j)(v_i - \bar{v})}{\sum_{i=1}^{n}(r_{ij} - \bar{r}_j)^2 \sum_{i=1}^{n}(v_i - \bar{v})^2} \tag{2-22}$$

where r_{ij} denotes the elements in the reliability matrix R; and $\bar{v}$ and $\bar{r}_j$ are the average values of the residual vector V and the column vector (R_j) related to the R matrix respectively. According to the correlation analysis theory, the following statistic for the correlation coefficient test (See appendix) can be obtained (Shi, 1998):

$$t_c = \frac{\rho_{R_j,V}}{\sqrt{\frac{1 - \rho_{R_j,V}}{n-2}}} \tag{2-23}$$

where t_c is the critical value associated with the t-distribution, with a given significant level and *n-2* degrees of freedom. If the correlation coefficient is greater than the given critical value, it is significant. It indicates the possibility that the observation(s) relating to the significant correlation coefficient(s) should be considered as having been contaminated by an outlier (or outliers). An observation with the largest correlation coefficient should be removed at each iteration. Hence, multiple outliers can be located through an iterative procedure. After the outliers have been located, the outliers should be substituted back into the observations to test them one by one, so that any mis-flagged outliers can be restored.

2.5.2 Adaptive Procedure

The adaptive procedure using outlier detection algorithm based on correlation analysis theory for GPS/Glonass instantaneous ambiguity resolution and positioning can be summarised as follows:

1. After computing the ambiguity-float solution using the estimated stochastic model from the residuals, test whether the $V^T PV_{Float}$ is less than a detection threshold defined by the a priori σ_0^2 with degree of freedom *n-t-m* and significant level 1-α. If the test is accepted, go to the next step; otherwise go to Step 3. It should be emphasised that if there is less than the necessary number of satellites when some satellites are removed, go to Step 4.

2. Attempt ambiguity resolution, and apply validation and fault detection procedures. If one ambiguity set can pass all the tests, output the ambiguity-fixed solution, keep the corresponding residuals and go to Step 1, to process the next epoch of data.

3. After computing the correlation coefficients between the residuals and the column vectors of the reliability matrix, test whether the maximum correlation coefficient is greater than a detection threshold with degrees of freedom n-2 and significant level 1-α. If true, delete the satellite relating to the maximum correlation coefficient and go to Step 1. Otherwise, go to Step 4.

4. After introducing the previous fixed ambiguity set, and restoring all the deleted satellites, test according to Equation (2-14) using only carrier phase observations. If the test passes, the positioning solution is output. Otherwise, an iterative process, with the satellite relating to the maximum correlation coefficient removed, would be repeated until the test passes, or less than the necessary double-differenced carrier phase observables can be formed. If less than the necessary number of DD carrier phase observables can be formed, the process will be repeated again after some eliminated satellites are restored and the reference satellite is deleted. If all the adaptive procedures still fail, the adaptive procedure is considered to have finally failed. In this case go to Step 1, to process the next epoch of data.

It should be emphasised that if the previous ambiguities, fixed to the wrong values, are introduced in Step 4, the wrong ambiguities can easily pass the test according to Equation (2-16). It will lead to seriously biased positioning solutions. Hence care should

be taken to ensure that the introduced ambiguity sets are indeed the correct ones. In this study, if the ratio value for the ambiguity validation is greater than 3, the ambiguities can only be introduced in the next epoch. If the outliers, such as cycle slips, exist in the observations, it is almost impossible to pass the test in Equation (2-16). On the other hand, in order to obtain a precise positioning solution, the satellite geometry should satisfy at least some minimum condition (PDOP<5, in the following experiment).

The integrated procedure is summarized in Figure 2-1.

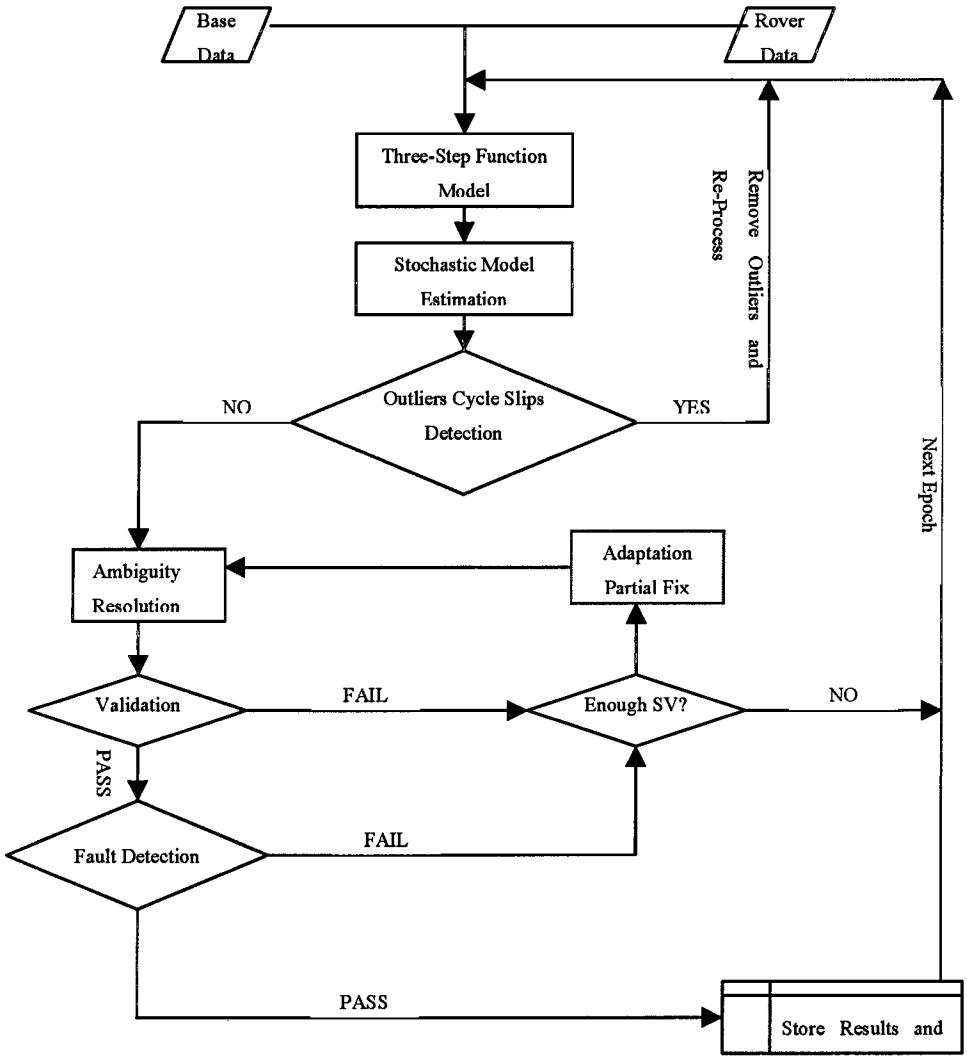

Figure 2-1 Float chart for the integrated procedure

2.6 Experiments

In order to test the performance of the integrated GPS and Glonass data processing procedure, including the three-step procedure to improve the functional model, the real-time stochastic modelling technique, and the proposed fault detection and adaptive procedure, the following static positioning and kinematic positioning experiments were carried out.

2.6.1 Static Data Experiments

The first is a set of static experiments using data with one-second sampling rate from dual-frequency GPS/Glonass JPS receivers and single-frequency GPS/Glonass Ashtech GG24 receivers. The reference GG24 receiver was set up on the Mather Pillar, on the roof of the Geography and Surveying building, at The University of New South Wales. The 'user' GG24 receiver was set up at different sites, which included the same roof nearby to the reference receiver, at Coogee Beach, at Maroubra Beach, and at the La Perouse Beach. The baseline names, baseline lengths, number of satellites, observation span (total number of epochs) are given in Table 2-1. The positioning results can be easily checked from the repeatability of the baseline vectors for the different sessions. In the case of all the data sets the cut-off elevation angle was set to 15° during the processing.

Table 2-1. Details of the test data sets

Name	Length (m)	GPS/GLN satellites	Total Epochs	Receivers	Survey Date DD/MM/YY
A1 Roof - Pillar	12	8-5/7-3	14362	GG24	12/5/99
A2 Coogee - Pillar	2873	9-5/7-4	4012	GG24	11/5/99
A3 Maroubra - Pillar	4053	9-6/5-3	6868	GG24	10/5/99
A4 La Perouse - Pillar	12103	7-5/6-3	9344	JPS	11/8/99

The observations are divided into different sessions, 10 seconds in length for one set of sessions and 1 minute in length for another set of sessions. The data processing results are listed in Table 2-2 for the 10-second sessions and in Table 2-3 for the 1-minute sessions. It is observed that rapid static positioning derives solutions with more than success rate of 98.3% using 10 seconds of data, and with 100% success rate using 1 minute of data for each session.

Table 2-2. Rapid static positioning results using 10 seconds of data for each session

Name	Total sessions	Correct (%)	Reject (%)	Wrong (%)
A1	1406	1396 (99.3%)	10 (0.7%)	0 (0.0%)
A2	401	401 (100.0%)	0 (0.0%)	0 (0.0%)
A3	631	629 (99.7%)	2 (0.3%)	0 (0.0%)
A4	934	934 (100%)	0 (0.0%)	0 (0.0%)

Table 2-3. Rapid static positioning results using 1 minute of data for each session

Name	Total sessions	Correct (%)	Reject (%)	Wrong (%)
A1	233	233 (100.0%)	0 (0.0%)	0 (0.0%)
A2	66	66 (100.0%)	0 (0.0%)	0 (0.0%)
A3	109	109 (100.0%)	0 (0.0%)	0 (0.0%)
A4	155	155 (100.0%)	0 (0.0%)	0 (0.0%)

The rapid static positioning results (1 minute for each session, Baseline A2) were also derived using Equation (2-4), in which the clock biases are considered as unknown parameters, and plotted in Figure 2-2 (grey colour, relative to the GPS-only solution using the whole data). Comparing against the positioning results (black colour, relative to the GPS-only solution using the whole data) derived using Equation (2-3), in which the third term of the SD integer ambiguity for the reference satellite is considered as a unknown parameter, it is clear that the proposed procedure derives positioning solutions with a higher accuracy.

In order to demonstrate the performance of the proposed stochastic model, two different strategies have been applied to the processing of all static data in single-epoch mode. One strategy only applies the empirical stochastic model based on the satellite elevation angle, and the other one applies the proposed adaptive procedure.

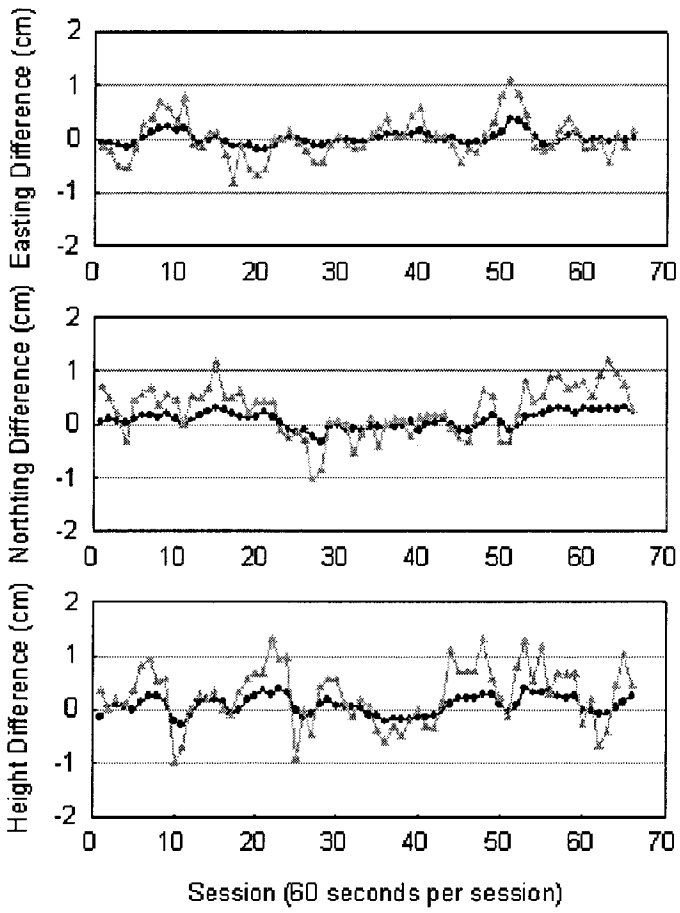

Figure 2-2. Rapid static positioning results for 1 minute sessions

The results are listed in columns 3-5 in Tables 2-4 and 2-5. The third column is the number (and percentage) of epochs for which ambiguity resolution is successful on an epoch-by-epoch basis. The fourth column is the number of epochs (and percentage), which do not pass the validation criteria test. The fifth column is the number of epochs (and percentage) which pass the validation criteria tests, but for which the result is incorrect. In Table 2-5 there are three sub-columns in column 3, where the first sub-

column is the total success rate. Case 1 means the ambiguities can be successfully resolved directly; and Case 2 means that the ambiguities can be resolved successfully or whose correct positioning results can be output after the adaptive procedure is applied.

Table 2-4. Single-epoch solution using the elevation-dependent stochastic model

Name	Total Epochs	Correct (%)	Reject (%)	Wrong (%)
A1	14362	11689(81.4%)	2639(18.4%)	33(0.2%)
A2	4012	3335(83.1%)	677(16.9%)	0(0.0%)
A3	6868	5723(83.3%)	1145(16.7%)	0(0.0%)
A4	9344	9344(100.0%)	0(0.0%)	0(0.0%)

Table 2-5. Single-epoch solution using the integrated procedure

Name	Total Epochs	Correct (%)			Reject (%)	Wrong (%)
		Total	Case 1	Case 2		
A1	14362	14362 (100.0%)	13273 (92.4%)	1089 (7.6%)	0 (0.0%)	0 (0.0%)
A2	4012	4012 (100.0%)	3922 (97.8%)	90 (2.2%)	0 (0.0%)	0 (0.0%)
A3	6868	6821 (99.3%)	6474 (94.3%)	347 (5.1%)	47 (0.7%)	0 (0.0%)
A4	9344	9344 (100.0%)	9344 (100.0%)	0 (0.0%)	0 (0.0%)	0 (0.0%)

It can be seen that using the elevation-dependent empirical stochastic model the success rates for ambiguity resolution range from 81.4% to 100.0%. It should be emphasised that because of the redundant dual-frequency observations, the ambiguities for the GPS/Glonass data from the JPS receivers can be fixed easily to the correct ones in the single-epoch mode even though the baseline length is over 10km. It also shows that quite a large percentage of the epochs (0.2%) at baseline A1 give the wrong ambiguity resolution results. After applying the adaptive procedure and the real-time stochastic

model estimated using the residuals from the previous epochs (in this study, 10 epochs), the success rates of ambiguity resolution range from 99.3% to 100.0%. No wrong ambiguity resolution results or incorrect positioning results, estimated using fixed ambiguities that are introduced from the previous epoch, are accepted. It is also noted that the adaptive procedure is responsible for quite a large percentage of epochs (7.6% for A1, 2.2% for A2, 5.1% for A3) whose ambiguities are resolved correctly or whose positioning results are output correctly. The results indicate that single-epoch ambiguity resolution can achieve up to success rate of 99.3% with redundant GPS and Glonass satellite observations. The conclusion that can be drawn is that the adaptive procedure using the multiple outlier detection algorithm based on correlation analysis theory and the estimated stochastic model from the residuals are, in theory, rigorous and, in practice, very powerful.

The ratio values for the validation criteria are plotted at each epoch in Figure 2-3 for baseline A2. The grey and black dots in Figure 2-3 are ratio values from the elevation-dependent empirical stochastic model and the estimated stochastic model from residuals, respectively. It can be seen that the ratio values using the estimated stochastic model from residuals are much larger than those using the elevation-dependent empirical stochastic model. It is generally believed that the larger the ratio values the more reliable the ambiguity resolution.

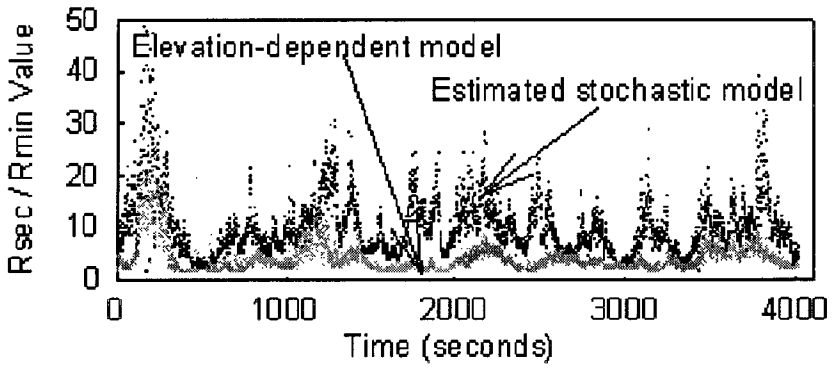

Figure 2-3. Ratio values for different stochastic models

The positioning results are also derived using two different stochastic models for

baseline A2. The differences of the three coordinate components, between the single-epoch solutions and the final baseline solution using whole data set, are plotted in Figure 2-4. The grey and black curves are positioning results using the elevation-dependent empirical stochastic model (grey) and the estimated stochastic model from residuals (black), respectively. Standard deviations are 6.3mm and 4.5mm in East, 7.1mm and 4.8mm in North, and 14.2mm and 11.2mm in Height, for the elevation-dependent and the estimated stochastic model respectively. It can be observaed that a realistic stochastic model can significantly improve the accuracy of the final positioning solutions.

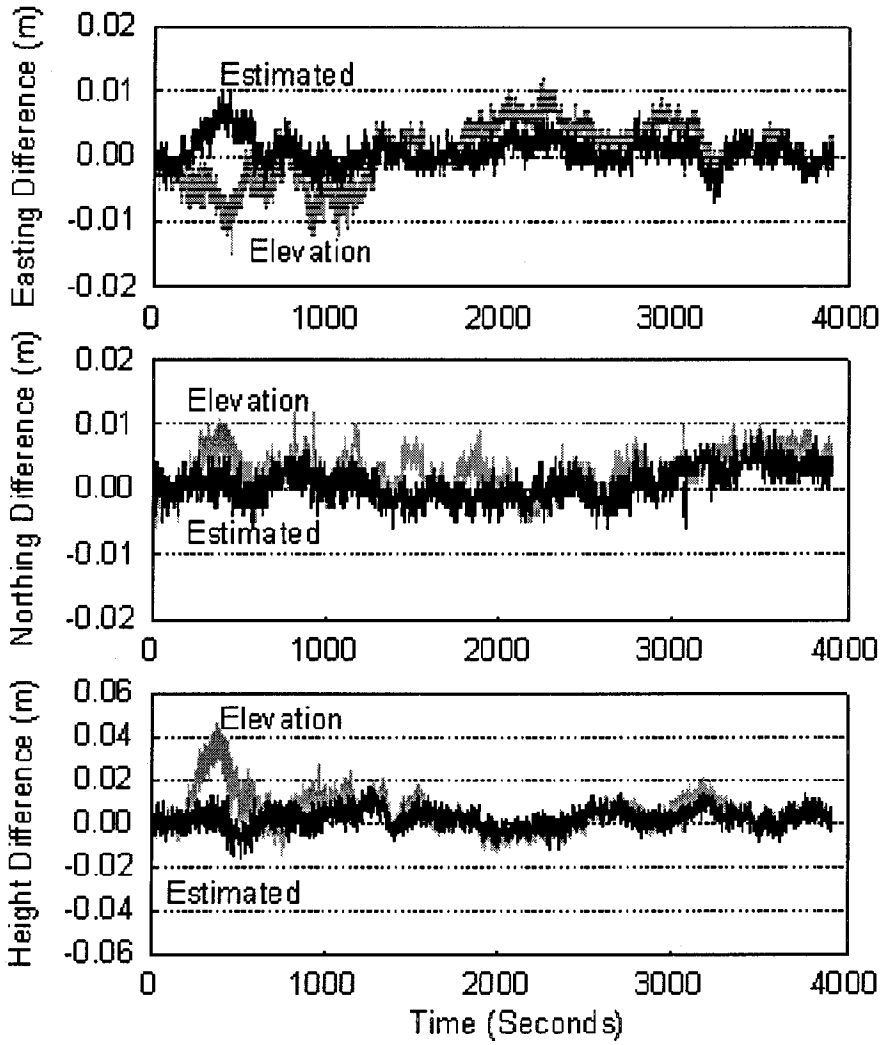

Figure 2-4. Positioning results using the elevation-dependent empirical stochastic model (grey) and the estimated stochastic model from residuals (black)

The TEC test, which makes use of the correlation information between neighbouring epochs, has been applied in data set A4 for further testing of the ambiguity resolution. The TEC value should not change by very much within a short time span. This test is a necessary condition, but not a sufficient condition. If the resolved ambiguity set cannot pass this test (Equation (2-19)), the ambiguity resolution will also be considered to have failed. Figures 2-5 and 2-6 show the double-differenced TEC and the corresponding change in the final positioning solutions for GPS and Glonass satellites respectively. It is observed from Figure 2-6 that the Glonass TEC values have been biased by the single-differenced ambiguity involving the Glonass reference satellite. However, it will have no influence on the TEC change if no cycle slip occurs on the Glonass reference satellite.

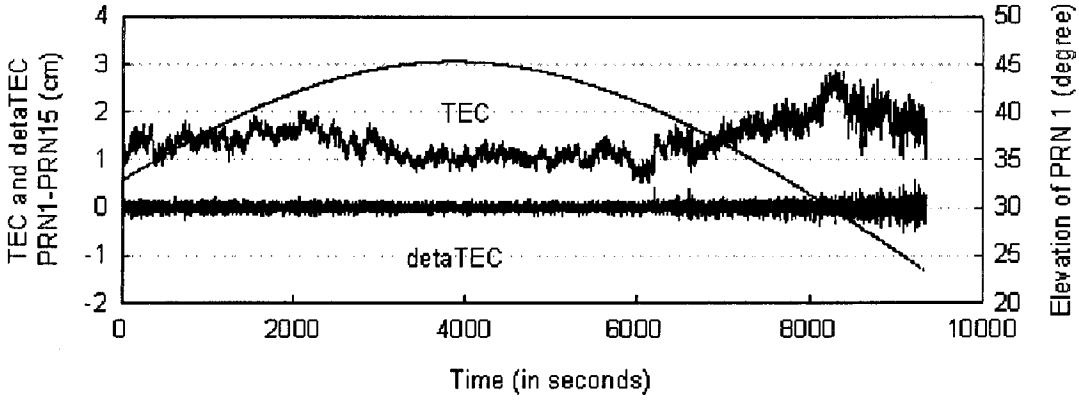

Figure 2-5. $\nabla\Delta TEC$ and δTEC values for GPS PRN 1

(Reference GPS PRN 15, with highest elevation)

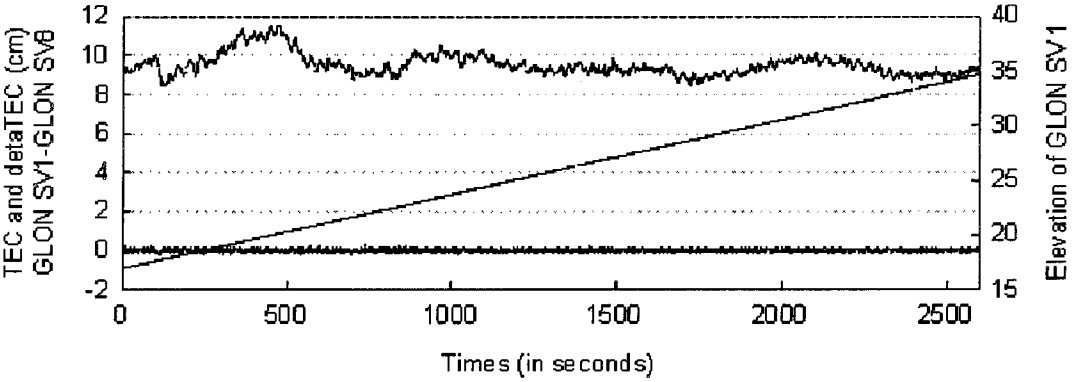

Figure 2-6. $\nabla\Delta TEC$ and δTEC values for Glonass PRN 1

(Reference Glonass PRN 8, with highest elevation)

In order to demonstrate the power of the multiple detection procedure based on correlation analysis theory, the 9th epoch in the A1 data containing 5 GPS satellites and 7 Glonass satellites is analyzed. In this epoch, the ambiguities cannot be fixed correctly. Hence, the previous epoch's fixed ambiguities are introduced. Five (5) simulated outliers are added to the GPS 3 (0.5 cycle), 19 (1 cycle) and 27 (1 cycle) satellites, and the Glonass 38 (1 cycle) and 48 (.2 cycle) satellites. Table 2-6 lists the relevant numerical results of the multiple outlier detection on a step-by-step basis.

Table 2-6. Test results of the multiple outlier detection algorithm with 5 simulated outliers

Iterations		SV 3 **(-0.5)**	SV 19 **(1.0)**	SV 27 **(1.0)**	SV 31	SV 39	SV 40	SV 38 **(1.0)**	SV 42	SV 48 **(0.2)**	SV 52	V^TPV	$\rho_{R,V}$ (1-5%)	Upper Boundary χ^2(1-0.05)
1	V	0.63	-0.64	0.13	0.30	0.56	0.76	-0.16	**0.83**	-0.22	0.40			12.59
	R	0.84	1.67	0.18	0.35	**1.78**	0.94	0.92	0.89	0.24	0.19	1386.5	**0.549**	
	ρ	0.36	**-0.61**	-0.22	0.07	0.21	0.32	-0.31	0.40	-0.37	0.12			**FAIL**
2	V	**0.85**		-0.36	0.55	0.44	0.40	-0.17	0.44	-0.04	0.67			11.07
	R	1.54		0.66	0.87	**1.95**	0.68	1.34	0.65	0.07	0.44	652.09	**0.582**	
	ρ	0.48		-0.43	0.13	0.28	0.34	**-0.59**	0.35	-0.46	0.31			**FAIL**
3	V	0.46		**-0.57**	-0.08	0.05	0.37		0.36	-0.32	-0.12			9.49
	R	1.46		**1.77**	0.25	0.69	1.05		0.88	0.80	0.14	203.72	**0.621**	
	ρ	0.66		**-0.84**	-0.02	0.19	0.41		0.42	-0.35	-0.15			**FAIL**
4	V	**0.37**			-0.13	-0.01	-0.03		-0.07	**-0.37**	0.01			7.82
	R	**1.85**			0.59	0.32	0.17		0.34	1.46	0.01	66.14	**0.669**	
	ρ	**0.87**			-0.28	0.05	0.03		-0.09	-0.76	0.08			**FAIL**
5	V				0.11	-0.03	0.02		-0.02	**-0.19**	0.13			5.99
	R				1.31	1.67	0.18		0.22	**1.69**	0.48	11.45	**0.729**	
	ρ				0.33	-0.79	0.33		0.08	**-0.96**	0.54			**FAIL**
6	V				-0.01	0.00	0.02		-0.02		0.08			3.84
	R				1.12	0.57	1.03		0.63		1.16	0.46	0.805	
	ρ				-0.93	-0.90	0.63		-0.12		0.94			PASS
Estimated Outliers		**-0.48**	**1.00**	**1.11**				**0.99**		**0.29**				

For each iteration, three sub-rows are included. The first sub-row is the residual value (in cycles), the second sub-row is the standardised residual, and the third sub-row is the correlation coefficient between the residual vector and the column vector of the reliability matrix. The 12th, 13th and 14th columns give the quadratic form of the residuals and the corresponding upper boundary value of the $\rho_{R_j,V}$ and the χ^2 -distribution statistic respectively.

From Table 2-6 it is clear that in the first iteration the maximum residual and standardised residual correspond to satellites 42 and 39. However, in reality they have no simulated outlier! It should also be noted that the maximum standardised residual is less than 2. The outliers cannot be located through the standard data snooping and τ test procedures. Fortunately the outliers can be located using the correlation coefficient test with the application of the iterative process. At each iteration, the satellite containing the biggest outlier will be removed until the χ^2 -distribution test can pass or the maximum $\rho_{R_j,V}$ is less than the critical value with the significance level 1-α and degrees of freedom n-2. At last, the identified outliers values are estimated and given in the last rows. The conclusion can be drawn that the outlier detection procedure based on the correlation analysis theory can indeed locate multiple outliers. It is especially powerful when only one outlier occurs. The applied algorithm for multiple outlier detection can work well not only for independent observations, but also for highly correlated observations.

2.6.2 Kinematic Experiments

This kinematic experiment was carried out on 29 April 1999 using two GG24 single-frequency receivers and three dual-frequency Leica SR399 receivers. One GG24 receiver and one Leica SR399 were set up at the reference site. The other GG24 receiver and the two Leica GPS receivers were mounted on a car. The trajectory of the rover receivers is shown in Figure 2-7. (The reason for using three rover receivers is as a mutual check on whether the derived positioning results are correct.) The experiment started on the roadside of the M4 Motorway, Sydney, which is nearby to the reference

site. After the first 40 minutes in static mode, the car moved along the Motorway and the Great Western Highway, finishing the experiment in static mode again for 15 minutes. This concluded a single loop. A total of two loops were completed with 1Hz data rate. The number of observed satellites is plotted in Figure 2-8.

In this kinematic experiment the processed results are shown in Table 2-7. The constant distance (about 60cm) between the two Leica receivers and one GG24 receiver was used to check whether or not the kinematic positioning results were correct. If the distance differences between the Leica rover receivers and the GG24 rover receiver exceeded some specified tolerance value (10cm in this experiment), the ambiguities are considered to have been fixed to the wrong values.

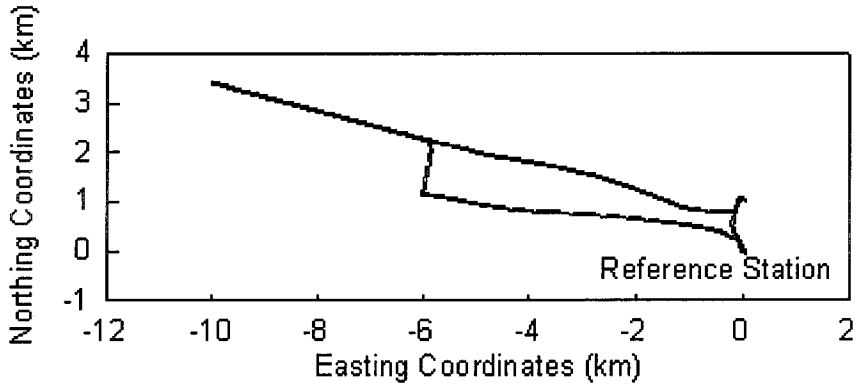

Figure 2-7. Trajectory of the rover receivers relative to the reference station

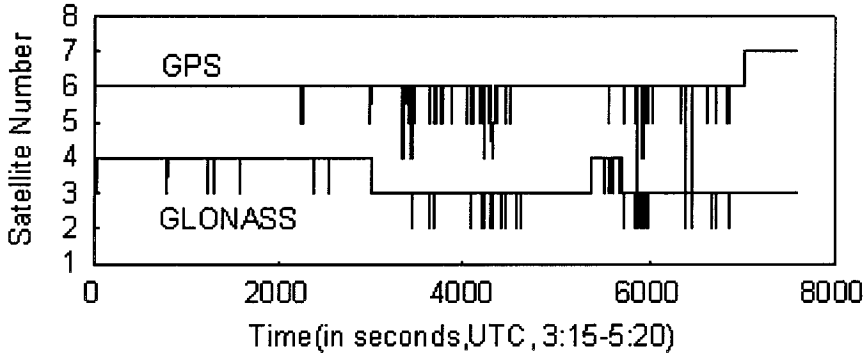

Figure 2-8. Number of observed satellites in this experiment

From Table 2-7 it can be seen that using the elevation-dependent empirical stochastic model the success rate for ambiguity resolution is only 62.4% for the GG24 receivers, and 87.7% and 87.8% for the Leica receivers. It should be noted that due to there being only six (or fewer) common visible satellites for most of the time the success rate for the dual-frequency Leica receivers is low. The percentage of rejected epochs is 33%, 12.3% and 12.2% respectively. It also shows that quite a large percentage of epochs (4.6%) in B3 from the GG24 receiver gave incorrect ambiguity resolution results.

Table 2-8 lists the processing results after applying the proposed adaptive procedure and real-time stochastic model. The success rates of single-epoch ambiguity resolution (and hence correct positioning results) can be significantly improved to 98.2%, 99.3% and 99.9%. No wrong ambiguity resolution results or incorrect positioning results, estimated by using fixed ambiguities that are introduced from the previous epoch, are accepted. It can also be seen that the adaptive procedure contributes quite a large percentage of epochs (4.4% for B1, 5.2% for B2, 19.7% for B3) whose ambiguities are fixed correctly. The results indicate that single-epoch ambiguity resolution (or correct positioning results) can achieve up to a success rate of 99.3%. The results also indicate that the proposed adaptive procedure has the ability to detect outliers even in correlated observations.

Table 2-7. kinematic positioning results using a single epoch of data (elevation-dependent empirical stochastic model)

Baseline Name	Total Epochs	Correct (%)	Reject (%)	Wrong (%)
B1 Leica 1-Leica Ref.	5767	5762 (87.8%)	705 (12.2%)	0 (0.0%)
B2 Leica 2-Leica Ref.	5720	5019 (87.7%)	701 (12.3%)	0 (0.0%)
B3 GG24-GG24 Ref.	7572	4721 (62.4%)	2501 (33.0%)	350 (4.6%)

Table 2-8. Single-epoch solution using the proposed integrated procedure

Name	Total Epochs	Correct (%)			Reject (%)	Wrong (%)
		Total	Case 1	Case 2		
B1 Leica 1-Leica Ref.	5767	5760 (99.9%)	5510 (95.5%)	259 (4.4%)	7 (0.1%)	0 (0.0%)
B2 Leica 2-Leica Ref.	5720	5682 (99.3%)	5383 (94.1%)	299 (5.2%)	38 (0.7%)	0 (0.0%)
B3 GG24-GG24 Ref.	7572	7436 (98.2%)	5945 (78.5%)	1491 (19.7%)	136 (1.8%)	0 (0.0%)

2.7 Concluding Remarks

An integrated procedure for GPS and Glonass data processing that consist of a three-step procedure to improve the functional model, a real-time stochastic model estimated using residuals from previous epochs, and a fault detection and adaptation procedure, has been proposed in this chapter. The proposed functional model improves the performance because the ambiguity resolution process is insensitive to the residual clock biases and the inter-channel biases, and hence reliable and precise positioning results are obtained. The real-time stochastic model can significantly improve the ambiguity resolution success rates, as well as the accuracy of the final solutions. A fault detection and adaptive procedure have been developed and tested. The outlier detection algorithm is based on correlation analysis, and can locate rapidly and reliably outliers, even in the case of highly correlated observations. It is especially powerful in the case of only one outlier with small degrees of freedom. It can improve significantly the ambiguity resolution success rate and the number of valid kinematic positioning solution epochs.

The results of a number of tests indicate that using the integrated procedure results in a success rate of 99.3% for single-epoch solutions. This is a significant improvement on

the success rate of 81.4% using standard procedures. The single-epoch success rate of 98.3% for kinematic positioning using dual-frequency GPS-only receivers and single-frequency GPS/Glonass receivers is a significant increase from 62.4%, over baseline lengths greater than 10km.

This algorithm has been designed for real-time applications. Although the data has been post-processed, all computations were carried out in a simulated real-time processing mode.

The integrated procedure for GPS and Glonass data processing is typically suitable for short baselines because distance-dependent biases in the between-receiver can be neglected. If the orbit errors, ionospheric and tropospheric bias corrections (e.g. generated from regional reference station networks) can be applied to the user data, the proposed data processing procedure can be extended to medium-range and long-range positioning. This research will be investigated further in the next chapter.

Chapter 3

OMPARISON STUDY ON GPS AND GLONASS MULTIPLE REFERENCE STATION TECHNIQUES

3.1 Introduction

High precision GPS and Glonass surveying and navigation techniques have been constrained to 'short range' due to the presence of distance-dependent biases in the between-receiver single-differenced observables. Over the past few years the concept of using reference station *networks* for kinematic GPS positioning (including in real-time) has been promoted strongly by several investigator groups. The basic idea is that, with the pre-determined coordinates of reference stations and fixed GPS carrier phase ambiguities, the so-called 'correction terms' for the atmospheric biases and orbit errors can be generated to support 'medium-range' carrier phase-based positioning. See, for example, Gao et al. (1997), Han & Rizos (1996); Raquet (1997); Wanninger (1995, 1997); Wubbena et al. (1996). A detailed review and comparison of the various multi-reference receiver approaches can be found in Fotopoulos & Cannon (2001) and Dai et al. (2001e).

After the double-differenced ambiguities associated with the reference station receivers have been fixed to their correct values (for more details concerning this issue see, e.g. Gao et al., 1997; Schaer et al., 1999; Rizos, 2000; Colombo et al., 1999; Chen et al., 2000; Chen, 2000; Dai et al., 2001b), the double-differenced GPS/Glonass residuals can be generated. The spatially correlated errors to be interpolated could be the pseudo-range and carrier phase residuals for the L1, L2 frequencies, or other linear combinations.

One core issue for multi-reference receiver techniques is how to interpolate the distance-dependent biases generated from the reference station network for the user's location? Over the past few years, in order to interpolate (or model) the distance-dependent residual biases, several interpolation methods have been proposed. They include the Linear Combination Model (Han & Rizos, 1996; 1998), the Distance-based linear Interpolation Method (Gao et al., 1997; 1998), the Linear Interpolation Method (Wanniger, 1995; Wübbena et al., 1996), the Low-order Surface Model (Wübbena et al., 1996; Fotopoulos & Cannon, 2000), and the Least Squares Collocation Method (Raquet, 1997; Marel, 1998). It should be emphasised that the Virtual Reference Station (VRS) method is merely an *implementation* of the multiple-reference receiver approach, and all of the aforementioned interpolation methods can be applied.

In this chapter, the aforementioned interpolation methods are compared in detail. The advantages and disadvantages of each of these techniques are discussed. An underlying common formula for all of the interpolation methods has been identified. Their performance will be demonstrated through case study examples of GPS (and Glonass) reference station networks.

3.2 Existing Interpolation Methods

3.2.1 Linear Combination Model (LCM)

A linear combination of single-differenced observations was proposed by Han & Rizos (1996, 1998) to model the spatially correlated biases (i.e. orbit bias $\Delta\rho_{orb,i}$, residual ionospheric bias $\Delta d_{ion,i}$ and residual tropospheric bias $\Delta d_{trop,i}$), and to mitigate multipath $\Delta d^{\phi}_{mp,i}$ and noise $\varepsilon_{\sum_{i=1}^{n}\alpha_i\cdot\Delta\phi_i}$:

$$\sum_{i=1}^{n}\alpha_i\cdot\Delta\phi_i=\sum_{i=1}^{n}\alpha_i\cdot\Delta\rho_i+\sum_{i=1}^{n}\alpha_i\cdot\Delta d\rho_i-c\cdot\sum_{i=1}^{n}\alpha_i\cdot\Delta dT_i+\lambda\cdot\sum_{i=1}^{n}\alpha_i\cdot\Delta N_i-\sum_{i=1}^{n}\alpha_i\cdot\Delta d_{ioni}+\sum_{i=1}^{n}\alpha_i\cdot\Delta d_{tropi}$$
$$+\sum_{i=1}^{n}\alpha_i\cdot\Delta d_{mpi}^{\phi}+\varepsilon_{\sum_{i=1}^{n}\alpha_i\cdot\Delta\phi_i} \qquad (3\text{-}1)$$

where n is the number of the reference station, i indicates the i^{th} reference station, and u the user station. A set of parameters α_i is estimated, satisfying the following conditions:

$$\sum_{i=1}^{n}\alpha_i=1 \qquad (3\text{-}2)$$

$$\sum_{i=1}^{n}\alpha_i(\hat{X}_u-\hat{X}_i)=0 \qquad (3\text{-}3)$$

$$\sum_{i=1}^{n}\alpha_i^2=Min \qquad (3\text{-}4)$$

where $\hat{X}_u$ and $\hat{X}_i$ are horizontal coordinate vectors for the user station and the i^{th} reference station respectively.

Based on Equations (3-1) to (3-4), effect of orbit errors can be eliminated, and ionospheric biases, tropospheric biases, multipath and measurement noise can be significantly mitigated. As a result, the double-differenced observables can be formed after ambiguities in the reference station network have been fixed to their correct integer values:

$$\nabla\Delta\phi_{u,n}-[\alpha_1\cdot V_{1,n}+\ldots+\alpha_i\cdot V_{i,n}+\ldots+\alpha_{n-1}\cdot V_{n-1,n}=\nabla\Delta\rho_{u,n}+\lambda\nabla\Delta N_{u,n}+\varepsilon_{\sum_{i=1}^{n}\alpha_i\nabla\Delta\phi_i} \qquad (3\text{-}5)$$

where $V_{i,n}$ (called 'correction terms') is the residual vector generated from the double-differenced measurements between reference station n and i:

$$V_{i,n} = \nabla\Delta\phi_{i,n} - \nabla\Delta\rho_{i,n} - \lambda\nabla\Delta N_{i,n} \text{ (i=1,...,n-1)} \tag{3-6}$$

3.2.2 Distance-based linear Interpolation Method (DIM)

A distance-based linear interpolation algorithm for ionospheric correction estimation has been suggested by Gao et al. (1997), described by the following equations:

$$\nabla\Delta\hat{I}_u = \sum_{j=1}^{n-1} \frac{w_i}{w} \nabla\Delta\hat{I}_i \tag{3-7}$$

$$w_i = \frac{1}{d_i} \tag{3-8}$$

$$w = \sum_{j=1}^{n-1} w_i \tag{3-9}$$

where n is the number of reference stations in the network, and d_i is the distance between the i^{th} reference station and the user station. $\nabla\Delta\hat{I}_i$ is the double-differenced ionospheric delay at the i^{th} reference station.

In order to improve interpolation accuracy, two modifications were made by Gao & Li (1998). The first modification is to replace the ground distance with a distance defined on a single-layer ionospheric shell at an altitude of 350km. The second modification is to extend the model to take into account the spatial correction with respect to the elevation angle of the ionospheric delay paths on the ionospheric shell.

3.2.3 Linear Interpolation Method (LIM)

Wanninger (1995) first suggested a regional differential ionospheric model derived from dual-frequency phase data from at least three GPS monitor stations surrounding the user station. Unambiguous double-differenced ionospheric biases can be obtained on a satellite-by-satellite and epoch-by-epoch basis after ambiguities in the reference station

network have been fixed to their correct integer values. Ionospheric corrections for any station in the area can be interpolated by using the known coordinates of the monitoring stations and approximate coordinates of the station(s). Wübbena et al. (1996) extended this method to model the distance-dependent biases such as the residual ionospheric and tropospheric biases, and the orbit errors. Similar methods have been proposed by Wanninger (1999), Schaer (1999), Chen et al. (2000), Vollath et al. (2000), and others.

For a network with three or more stations, the linear model can be described by:

$$\begin{bmatrix} V_{1n} \\ V_{2n} \\ \vdots \\ V_{n-1,n} \end{bmatrix} = \begin{bmatrix} \Delta X_{1n} & \Delta Y_{1n} \\ \Delta X_{2n} & \Delta Y_{2n} \\ \vdots & \vdots \\ \Delta X_{n-1,n} & \Delta Y_{n-1,n} \end{bmatrix} \cdot \begin{bmatrix} a \\ b \end{bmatrix} \tag{3-10}$$

where ΔX and ΔY are the plane coordinate differences referred to the master reference station. Parameters a and b are the coefficients for ΔX and ΔY (the so-called 'network coefficients' according to Wübbena et al., 1996). In the case of more than three reference stations, the coefficients a and b can be estimated by a Least Squares adjustment on an epoch-by-epoch, satellite-by-satellite basis. Then the GPS user within the coverage of the network can apply the following 2D linear model to interpolate the distance-dependent biases:

$$V_{un} = a \cdot \Delta X_{un} + b.\Delta Y_{un} \tag{3-11}$$

3.2.4 Low-order Surface Model (LSM)

The distance-dependent biases exhibit a high degree of spatial correlation across reference station networks. Low-order surfaces can be used to 'fit' the distance-dependent biases (Wübbena et al., 1996; Fotopoulos, 2000). The fitted surfaces are known as trend or regression surfaces, and they model the major trend of the distance-dependent biases. The coefficients of the low-order surfaces can be estimated via a Least Squares adjustment using data from the reference station network. The variables

of the fitting function could be two (i.e. the horizontal coordinates), or three (horizontal coordinates and height). The fitting orders could be one, two or higher. Some fitting functions are:

$$V = a \cdot \Delta X + b.\Delta Y + c \tag{3-12}$$

$$V = a \cdot \Delta X + b.\Delta Y + c \cdot \Delta X^2 + d.\Delta Y^2 + e \cdot \Delta X \Delta Y + f \tag{3-13}$$

$$V = a \cdot \Delta X + b.\Delta Y + c \cdot \Delta H + d \tag{3-14}$$

$$V = a \cdot \Delta X + b.\Delta Y + c \cdot \Delta H + d.\Delta H^2 + e \tag{3-15}$$

Schaer et al. (1999) have proposed that Equation (3-12) be used to model residual ionospheric refraction on a satellite-by-satellite and epoch-by-epoch basis after double-differencing, and that Equation (3-14) could be used to estimate the tropospheric zenith delay. Equations (3-14) and (3-15) can be derived by applying partial derivative principles (Varner & Cannon, 1997; Varner, 2000). After the fitted coefficients are computed, they can be used to predict the biases for the user station(s).

3.2.5 Least Squares Collocation (LSC)

Least Squares Collocation has been used for many years to interpolate gravity at any given location using only measurements at some discrete locations (Tscherning, 1974; 2001; Schwartz, 1978). The following is the basic interpolation equation:

$$\hat{U} = C_{vu} \cdot C_v^{-1} \cdot V \tag{3-16}$$

where C_v is the covariance matrix of the measurement vector V, and C_{uv} is the cross-covariance between the ineterpolated vector $\hat{U}$ and the measurements vector V. If these covariance matrices are computed correctly, and the measurements satisfy the conditions of zero mean and a normal distribution, Equation (3-16) gives the optimal

estimator (Raquet & Lachapelle, 2001). Least Squares Collocation is also well suited to interpolating the distance-dependent biases in a network. Raquet (1997) proposed the NetAdjust method, which in essence is equivalent to Least Squares Collocation.

The challenge for this method is to calculate the covariance matrices C_v and C_{uv}. The following covariance function was proposed (Raquet, 1998):

$$C_{ab}^{x} = \mu^2(\varepsilon) \cdot \left[\delta_{c_z}^2(P_a, P_0) + \delta_{c_z}^2(P_b, P_0) - \delta_{c_z}^2(P_a, P_b)\right] \tag{3-17}$$

where the computation of the double-differenced covariance matrices can be decomposed into two mathematical functions. First, a correlated variance function which maps the zenith variance of the correlated errors over the network area is computed:

$$\delta_{c_z}^2(P_n, P_m) = k_1 d + k_2 d^2 \tag{3-18}$$

where $\delta_{c_z}^2(P_n, P_m)$ is the differential zenith variance of the correlated errors for points p_n and p_m in the network. This function is based on the two-dimensional distance d between the reference stations. k_1 and k_2 are constant coefficients (k_1 = 1.1204e-4 and k_2 = 4.8766e-7 for L1 phase in their paper). Secondly, a mapping function is needed to map the zenith correlated and uncorrelated errors to the elevation of the satellite at each epoch:

$$\mu(\varepsilon) = \frac{1}{\sin\varepsilon} + \mu_k(.53 - \frac{\varepsilon}{180})^3 \tag{3-19}$$

where $\mu(\varepsilon)$ is a dimensionless scale factor which, when multiplied by the zenith variance obtained from Equation (3-18), gives the correlated variance for the specified satellite elevation ε, and μ_k is a constant coefficient (μ_k = 3.9393 for L1 phase in their paper). Tests have shown that the estimated corrections are not sensitive to the choice of

the covariance function. However, estimated variances are sensitive to the covariance function used (Raquet & Lachapelle, 2001).

Based on the principles of Least Squares Collocation, a practical interpolator for ionospheric biases (or tropospheric biases) is presented (Marel, 1998; Odijk et al., 2000):

$$I_{1u}^{1s} = \begin{bmatrix} C_{u1}^{s} & C_{u2}^{s} & \cdots & C_{un}^{s} \end{bmatrix} \cdot \begin{bmatrix} C_0 & C_{12}^{s} & \cdots & C_{1n}^{s} \\ C_{21}^{s} & C_0 & \cdots & C_{2n}^{s} \\ \vdots & \vdots & \ddots & \vdots \\ C_{n1}^{s} & C_{n1}^{s} & \cdots & C_0 \end{bmatrix}^{-1} \cdot \begin{bmatrix} \hat{I}_{12}^{1s} \\ \hat{I}_{13}^{1s} \\ \vdots \\ \hat{I}_{1n}^{1s} = 0 \end{bmatrix} \tag{3-20}$$

The spatial covariance function C_{kl}^{s} is linearly dependent on the distance between the stations, or rather, their ionospheric pierce points:

$$C_{kl}^{s} = l_{\max} - l_{ks}^{s} \tag{3-21}$$

In this covariance function C_{kl}^{s} is the linear distance between the ionospheric points of stations k and l with respect to satellite s, with $l_{\max} > l_{kl}^{s}$, where $l_{\max}$ (300km was used in their paper) is a distance which is larger than the longest distance between the ionospheric points of the stations in the network. Therefore, the larger the distance between the points, the smaller the correlation.

3.3 Comparison of Interpolation Methods

3.3.1 General Formula

On an epoch-by-epoch and satellite-by-satellite basis, all of the abovementioned methods use a n-1 independent error vector generated from a n reference station network to interpolate (or estimate) the distance-dependent biases for the user station location. One significant characteristic shared by all of the methods is that it is

necessary to first compute the n-1 coefficients, and then to form a n-1 linear combination with the n-1 error vector generated by the reference station network:

$$\hat{V}_u = \vec{\alpha} \cdot \vec{V} = \alpha_1 V_{1n} + \alpha_2 V_{2n} + \cdots + \alpha_{n-1} V_{n-1,n} \tag{3-22}$$

It should be emphasised that all the coefficients can be calculated without using any actual measurements, and are constant if the user receiver is not in motion. The coefficients depend on the geometry between the user station and the reference station network (and the GPS satellite geometry). They refer to one master reference station and one reference satellite.

The formulas for the determination of the coefficients, and a discussion on the advantages and disadvantages of each interpolation method, are presented below.

3.3.2 Coefficient Determination

Linear Combination Model

Equations (3-2) and (3-3) can be re-written as:

$$\begin{bmatrix} 1 & 1 & \cdots & 1 & 1 \\ \Delta X_{1n} & \Delta X_{2n} & \cdots & \Delta Y_{n-1n} & 0 \\ \Delta Y_{1n} & \Delta Y_{2n} & \cdots & \Delta Y_{n-1n} & 0 \end{bmatrix} \cdot \begin{bmatrix} \alpha_1 \\ \alpha_2 \\ \vdots \\ \alpha_n \end{bmatrix} = \begin{bmatrix} 1 \\ \Delta X_{un} \\ \Delta Y_{un} \end{bmatrix} \tag{3-23}$$

If three or more reference stations are available, the n coefficient vector α can be determined using the Least Squares condition adjustment based on Equation (3-4):

$$\vec{\alpha} = B^T (BB^T)^{-1} W \tag{3-24}$$

where

$$B=\begin{bmatrix} 1 & 1 & \cdots & 1 & 1 \\ \Delta X_{1n} & \Delta X_{2n} & \cdots & \Delta Y_{n-1n} & 0 \\ \Delta Y_{1n} & \Delta Y_{2n} & \cdots & \Delta Y_{n-1n} & 0 \end{bmatrix},\ \vec{\alpha}=\begin{bmatrix} \alpha_1 \\ \alpha_2 \\ \vdots \\ \alpha_n \end{bmatrix},\ W=\begin{bmatrix} 1 \\ \Delta X_{un} \\ \Delta Y_{un} \end{bmatrix} \tag{3-25}$$

In this method, although a total of n coefficients can be derived from Equation (3-24), only n-1 coefficients are used to interpolate the distance-dependent biases. Coefficient α_n is related to the master reference station.

The linear combination model is formed from the single-differenced functional equation for baselines from the user receiver to two or more reference stations. The advantage of this model is the elimination of the orbit bias. The residual ionospheric delay and the tropospheric delay can also be reduced to the same degree that the epoch-by-epoch and satellite-by-satellite ionosphere and the troposphere models are able to. Multipath and measurement noises can be reduced if the user receiver is located within the network of reference stations, so that the coefficients are less than one. Otherwise the multipath and noise may be amplified (because the coefficients might be larger than one).

Distance-based linear Interpolation Method

From Equation (3-7), it can be seen that the n-1 coefficients can be determined as follows:

$$\vec{\alpha}=\begin{bmatrix} \frac{w_1}{w} & \frac{w_2}{w} & \cdots & \frac{w_{n-1}}{w} \end{bmatrix} \tag{3-26}$$

In this method it should emphasised that the coefficients always are less than one, even if the user receiver is located outside the network of reference stations.

Although this method was originally proposed by Gao et al. (1997) to interpolate residual ionospheric biases, it can, to a certain degree, mitigate other distance-dependent biases such as tropospheric bias and orbit errors.

Linear Interpolation Method

If three or more reference stations are available, the parameters $\hat{a}$ and $\hat{b}$ can be estimated using Least Squares based on Equation (3-10):

$$\begin{bmatrix} \hat{a} \\ \hat{b} \end{bmatrix} = (A^T A)^{-1} A^T V \tag{3-27}$$

where

$$V = \begin{bmatrix} V_{1n} \\ V_{2n} \\ \vdots \\ V_{n-1,n} \end{bmatrix}, \quad A = \begin{bmatrix} \Delta X_{1n} & \Delta Y_{1n} \\ \Delta X_{2n} & \Delta Y_{2n} \\ \vdots & \vdots \\ \Delta X_{n-1,n} & \Delta Y_{n-1,n} \end{bmatrix} \tag{3-28}$$

After the parameters $\hat{a}$ and $\hat{b}$ have been estimated, the biases at the user location within the coverage of the network can be interpolated using Equation (3-11):

$$\hat{V}_{1u} = \begin{bmatrix} \Delta X_{un} & \Delta Y_{un} \end{bmatrix} \cdot \begin{bmatrix} \hat{a} \\ \hat{b} \end{bmatrix} = \begin{bmatrix} \Delta X_{un} & \Delta Y_{un} \end{bmatrix} \cdot (A^T A)^{-1} A^T V \tag{3-29}$$

From Equation (3-29), it can be seen that the n-1 coefficient vector α can be written as:

$$\vec{\alpha} = \begin{bmatrix} \Delta X_{un} & \Delta Y_{un} \end{bmatrix} \cdot (A^T A)^{-1} A^T \tag{3-30}$$

The coefficients can also be derived using the satellite-by-satellite, epoch-by-epoch ionospheric model, to reduce residual ionosphere and troposphere delay. It can be

shown that if only three reference station are used, the coefficients α_1 and α_2 are exactly the same for the linear combination model as for the linear interpolation method. However, they are different when the number of reference stations is greater than 3 (see Experiments) because the linear combination model eliminates the orbit bias as well. The advantage of this method for real-time implementation is that the implementation is easier because only two coefficients for each satellite pairs are required for transmission to the user.

Low-order Surface Model

The different variables and orders of the fitting surfaces result in a different *n-1* coefficient vector α. However, the computation procedure is the same. Here, an example of a plane-fitting function will be used.

If four or more reference stations are available, the parameters $\hat{a}$, $\hat{b}$ and $\hat{c}$ can be estimated using Least Squares based on Equation (3-12):

$$\begin{bmatrix} \hat{a} \\ \hat{b} \\ \hat{c} \end{bmatrix} = (A^T A)^{-1} A^T V \tag{3-31}$$

where

$$V = \begin{bmatrix} V_{1n} \\ V_{2n} \\ \vdots \\ V_{n-1,n} \end{bmatrix}, \quad A = \begin{bmatrix} \Delta X_{1n} & \Delta Y_{1n} & 1 \\ \Delta X_{2n} & \Delta Y_{2n} & 1 \\ \vdots & \vdots & \vdots \\ \Delta X_{n-1,n} & \Delta Y_{n-1,n} & 1 \end{bmatrix} \tag{3-32}$$

After the parameters $\hat{a}$, $\hat{b}$ and $\hat{c}$ have been estimated, the biases at the user location within the coverage of the network can be interpolated using Equation (3-12):

$$\hat{V}_{1u} = \begin{bmatrix} \Delta X_{un} & \Delta Y_{un} & 1 \end{bmatrix} \cdot \begin{bmatrix} \hat{a} \\ \hat{b} \\ \hat{c} \end{bmatrix}$$
$$= \begin{bmatrix} \Delta X_{un} & \Delta Y_{un} & 1 \end{bmatrix} \cdot (A^T A)^{-1} A^T V \tag{3-33}$$

From Equation (3-33) it can be seen that the *n-1* coefficient vector α can be written as:

$$\vec{\alpha} = \begin{bmatrix} \Delta X_{un} & \Delta Y_{un} & 1 \end{bmatrix} \cdot (A^T A)^{-1} A^T \tag{3-34}$$

For a low-order surface model the required number of reference stations depends on the fitting variable and the fitting order. In general, the minimum number of reference stations is four if the plane-fitting function is used. It is obvious that the linear interpolation method is a special case of the plane-fitting function.

Least Squares Collocation

For the Least Squares Collocation Method the *n*-1 coefficients can be determined using Equation (3-16):

$$\vec{\alpha} = C_{uv} \cdot C_v^{-1} \tag{3-35}$$

The *n* coefficients in the interpolator suggested by Marel (1998) can be determined by:

$$\vec{\alpha} = \begin{bmatrix} C_{u1}^s & C_{u2}^s & \cdots & C_{un}^s \end{bmatrix} \cdot \begin{bmatrix} C_0 & C_{12}^s & C_{1n}^s \\ C_{21}^s & C_0 & C_{2n}^s \\ \vdots & \vdots & \vdots \\ C_{n1}^s & C_{n2}^s & C_{n1}^s \end{bmatrix}^{-1} \tag{36}$$

It should be emphasised that although there are n coefficients in this interpolator, only the first n-1 coefficients are used for interpolation because the n^{th} coefficient is related to the reference satellite and a zero error value has been assigned to this satellite.

This method explicitly attempts to minimise the differenced phase-code biases between any reference station receiver and the user receiver. Note that the accuracy of the Least Squares Collocation Method is dependent upon the accuracy of the covariance matrix (Raquet, 1998). In practice it is very difficult to calculate precise covariance matrices.

3.3.3 Coefficient Comparison in a Simulated Multiple-Reference Network

From the previous discussions it can be seen that all the methods use n-1 coefficients to form a linear combination with the 'correct terms' to mitigate spatially correlated biases at user stations. In fact the coefficients can be considered as weighting for the 'correction terms'. Therefore, the major differences between all the methods are only the coefficients. In order to further analyse the coefficient differences for the different interpolation methods, a simulation study has been carried out. Figure 3-1 shows the configuration of the reference station network used in the simulation. '*Ref. 1*'-'*Ref. 7*' and '*Master Ref.*' indicate the seven reference stations and one master reference station respectively.

Figures 3-2a to 3-2g show the distribution of all the coefficients for the user location within (100km x 100km) and outside (50km) the reference station network, using the seven different interpolation methods respectively. Figures 3-2d and 3-2e refer to the Low-Order Surface Model using the Equations (3-12) and (3-13) respectively. It can be clearly seen from Figures 3-2a, 3-2c and 3-2d that for the linear combination model, the linear interpolation method, and the 1^{st} order surface model, each coefficient distribution lies in one plane whose form is defined by the reference station coordinates. This can be proven using Equations (3-24), (3-30) and (3-34) respectively. Figures 3-2a and 3-2c also show that the corresponding coefficients (α_1 to α_7) are quite similar. Therefore, the performance of the two methods should be similar too. Figure 3-2e

shows that each coefficient form is a 2nd order surface defined by the reference station coordinates. Figures 3-2b, 3-2f and 3-2g show that the closer to the reference station the user location is, the larger (up to 1) the corresponding coefficient. It is interesting that the *every* coefficient trend is almost the same for the Least Squares Collocation methods suggested by Raquet (1998) and Marel (1998), even though their derived formulas are quite different.

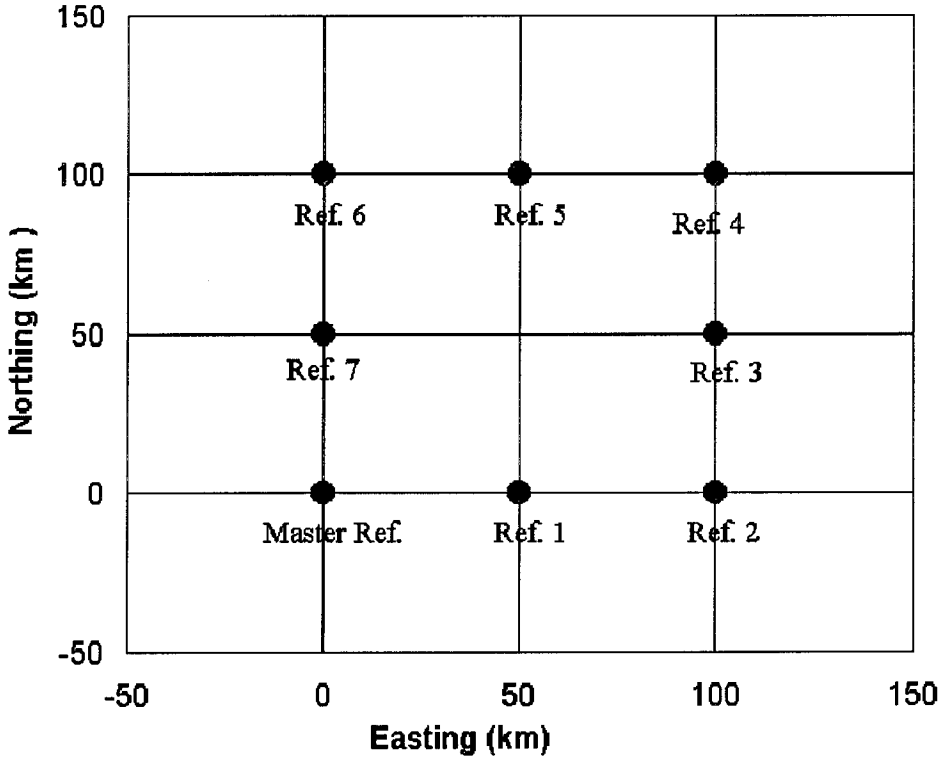

Figure 3-1. Configuration of the simulated reference station network

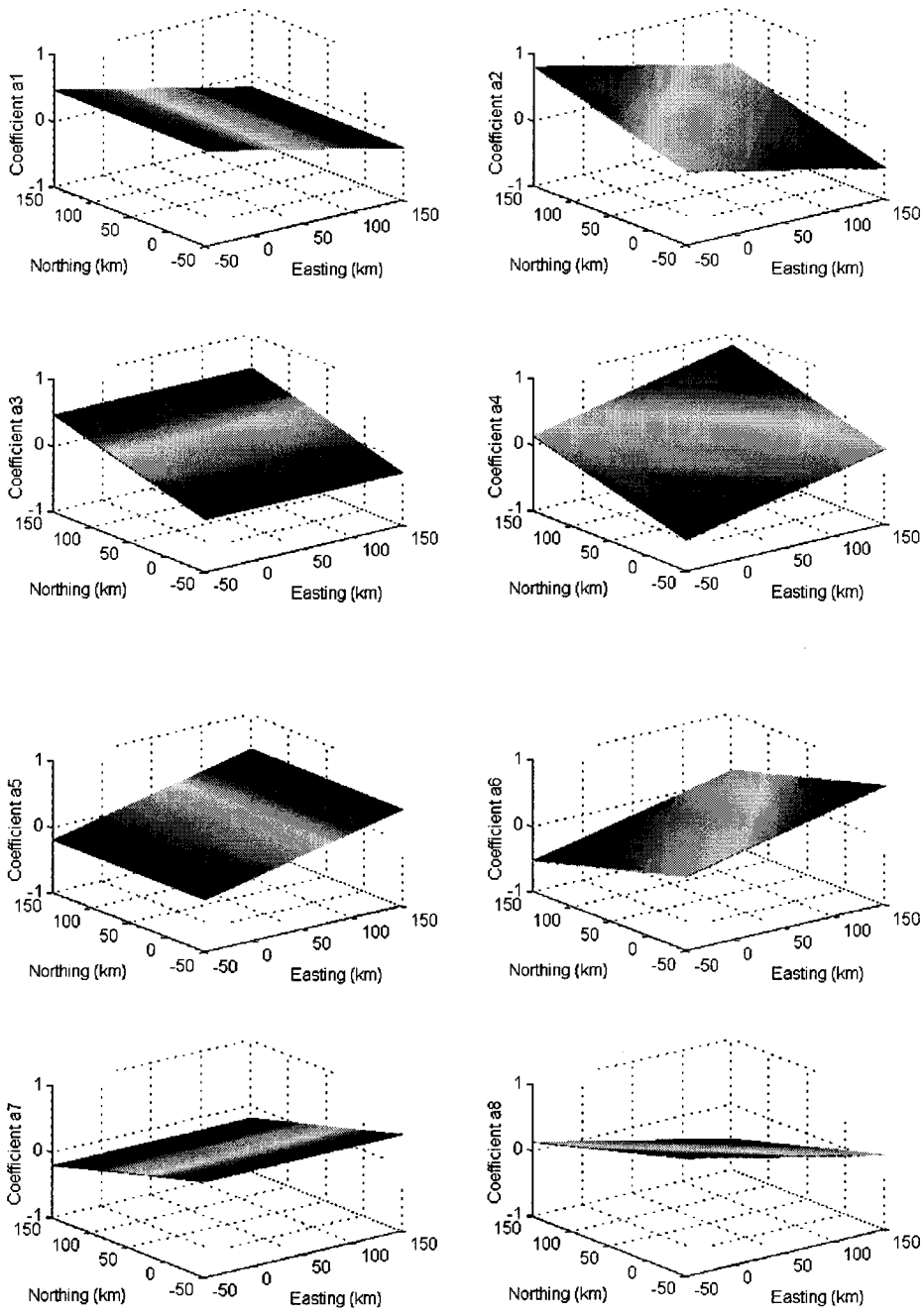

Figure 3-2a. Coefficients generated by the Linear Combination Model

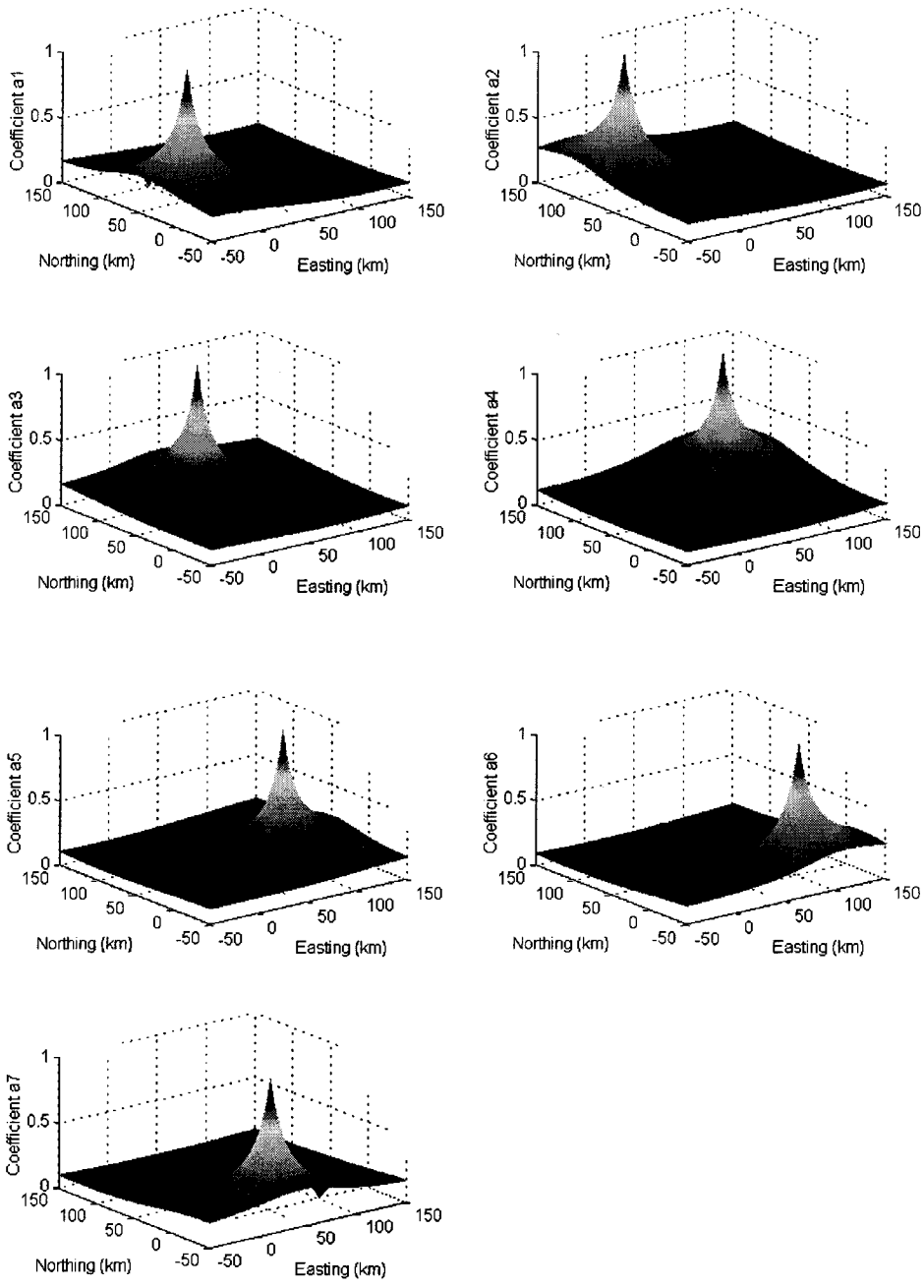

Figure 3-2b. Coefficients generated by the Distance-based linear Interpolation Method

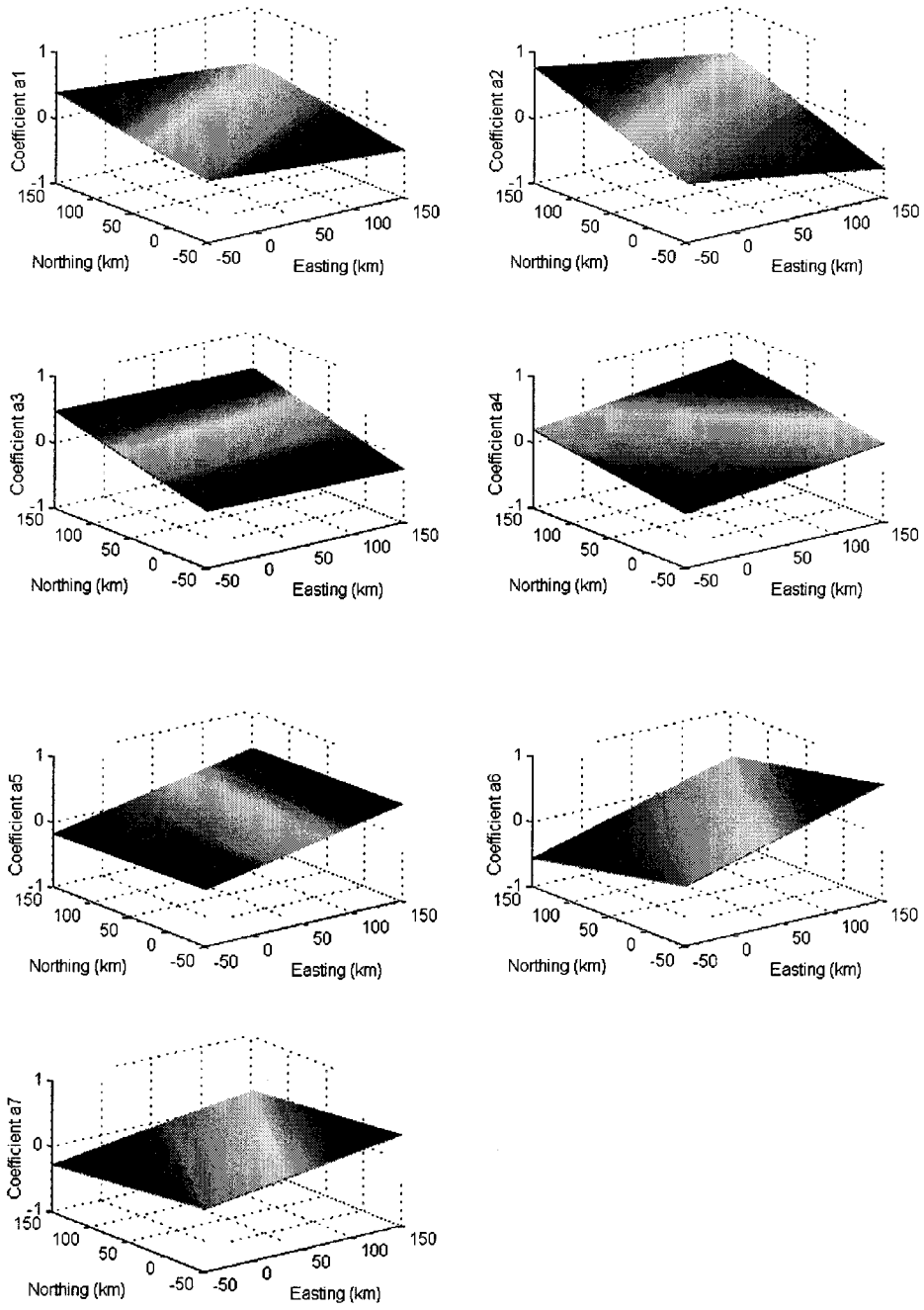

Figure 3-2c. Coefficients generated by the Linear Interpolation Method

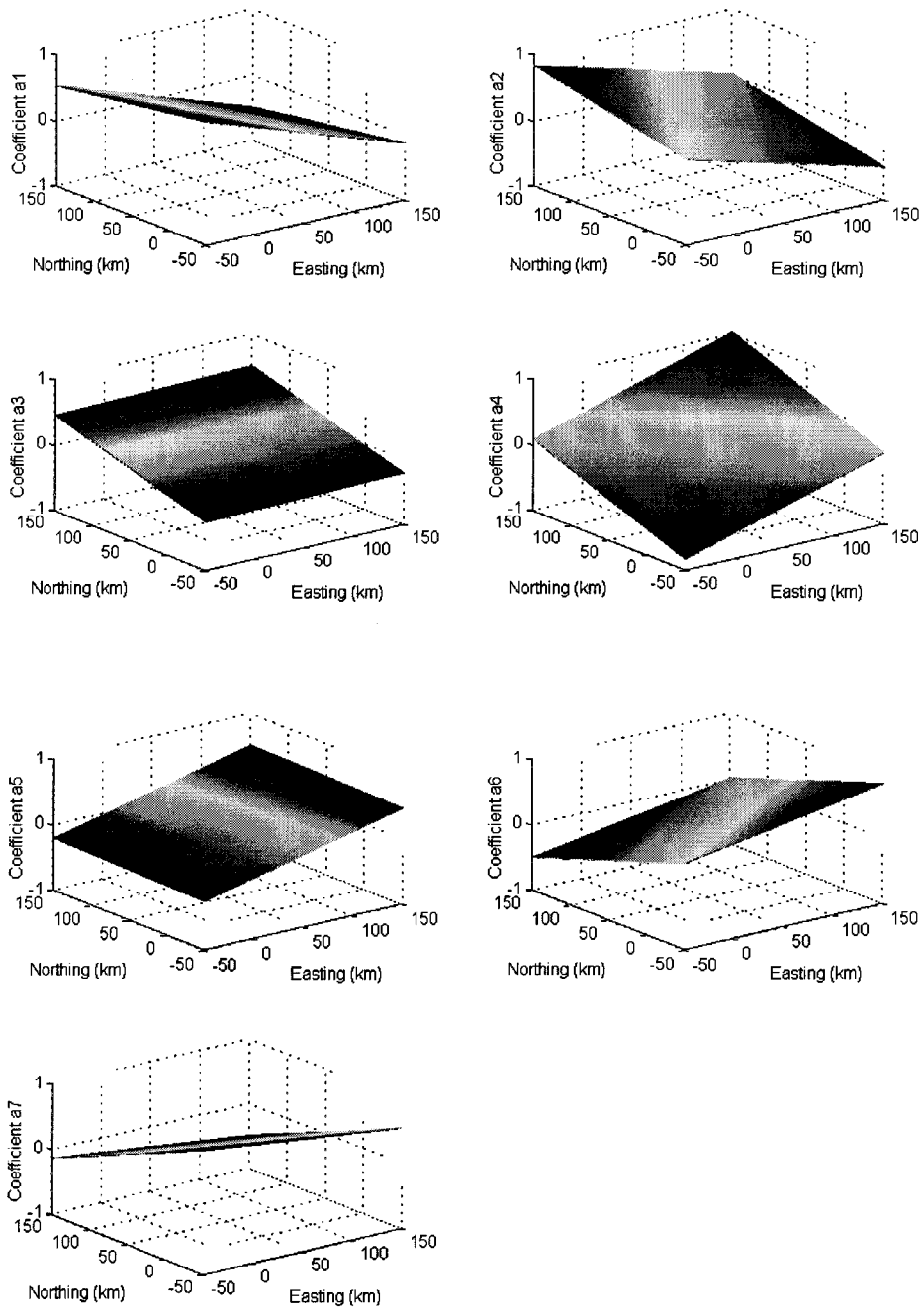

Figure 3-2d. Coefficients generated by the Low-order Surface Model (1st order)

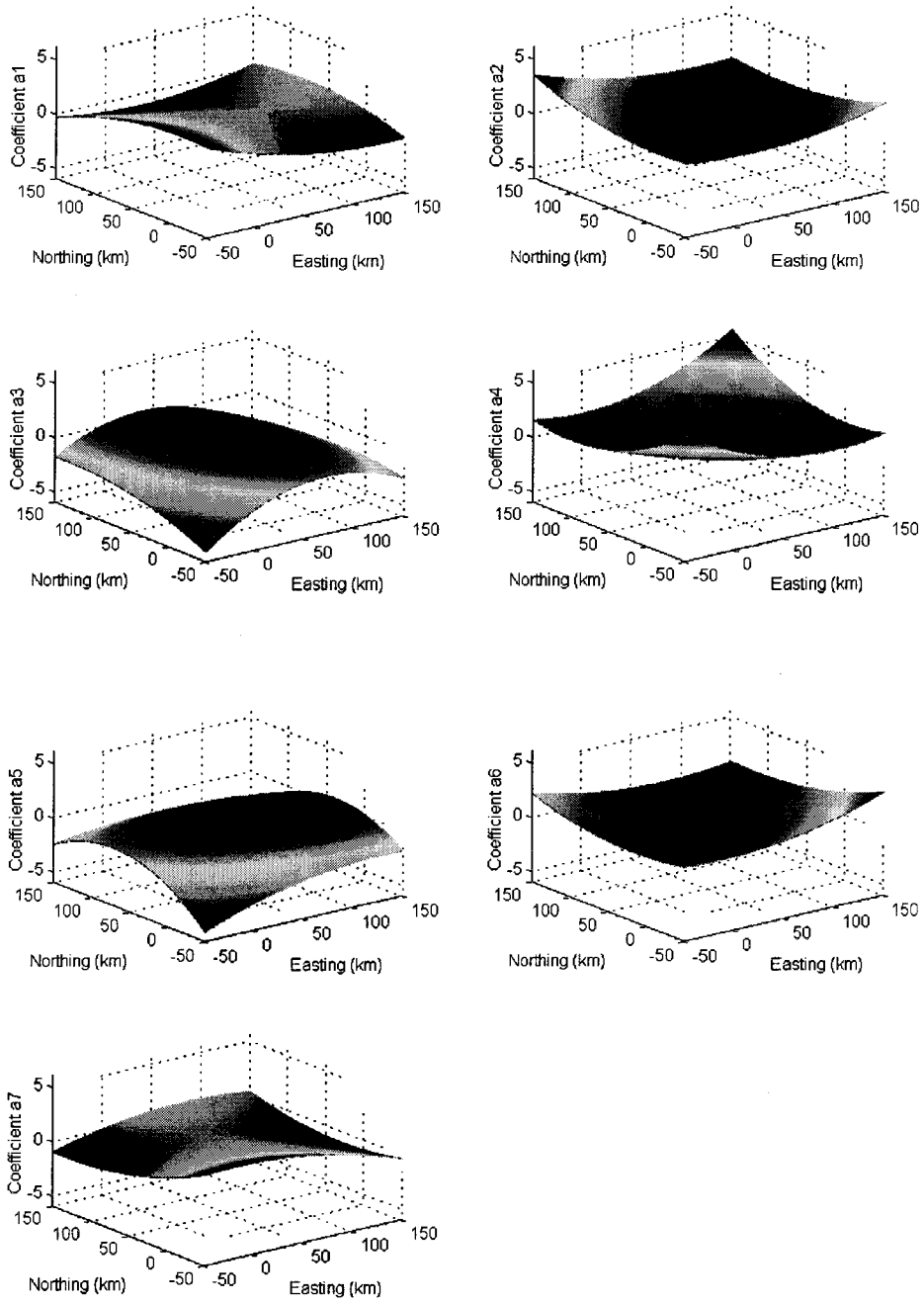

Figure 3-2e. Coefficients generated by the Low-order Surface Model (2nd order)

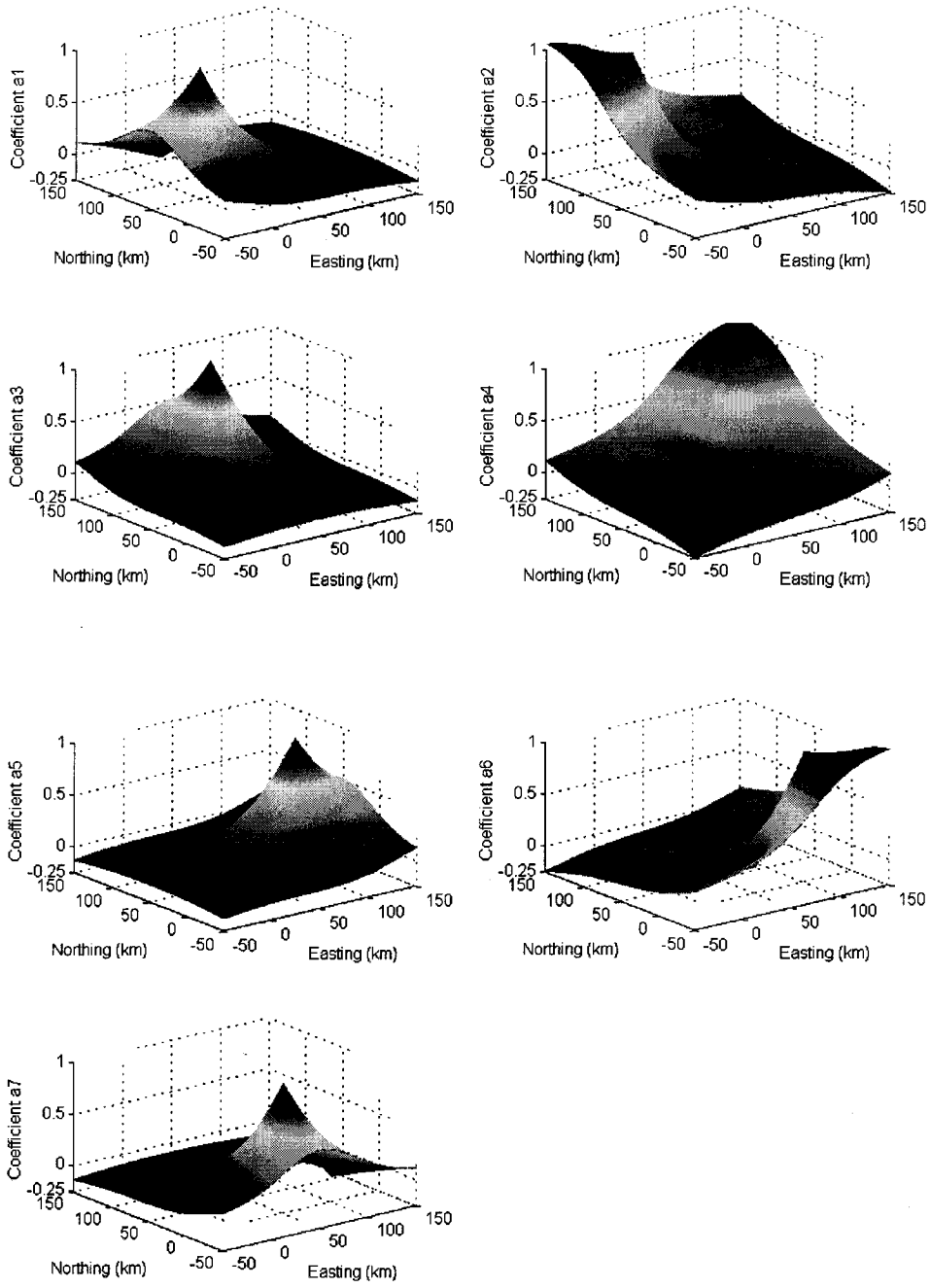

Figure 3-2f. Coefficients generated by the Least Squares Collocation method proposed by Raquet (1998)

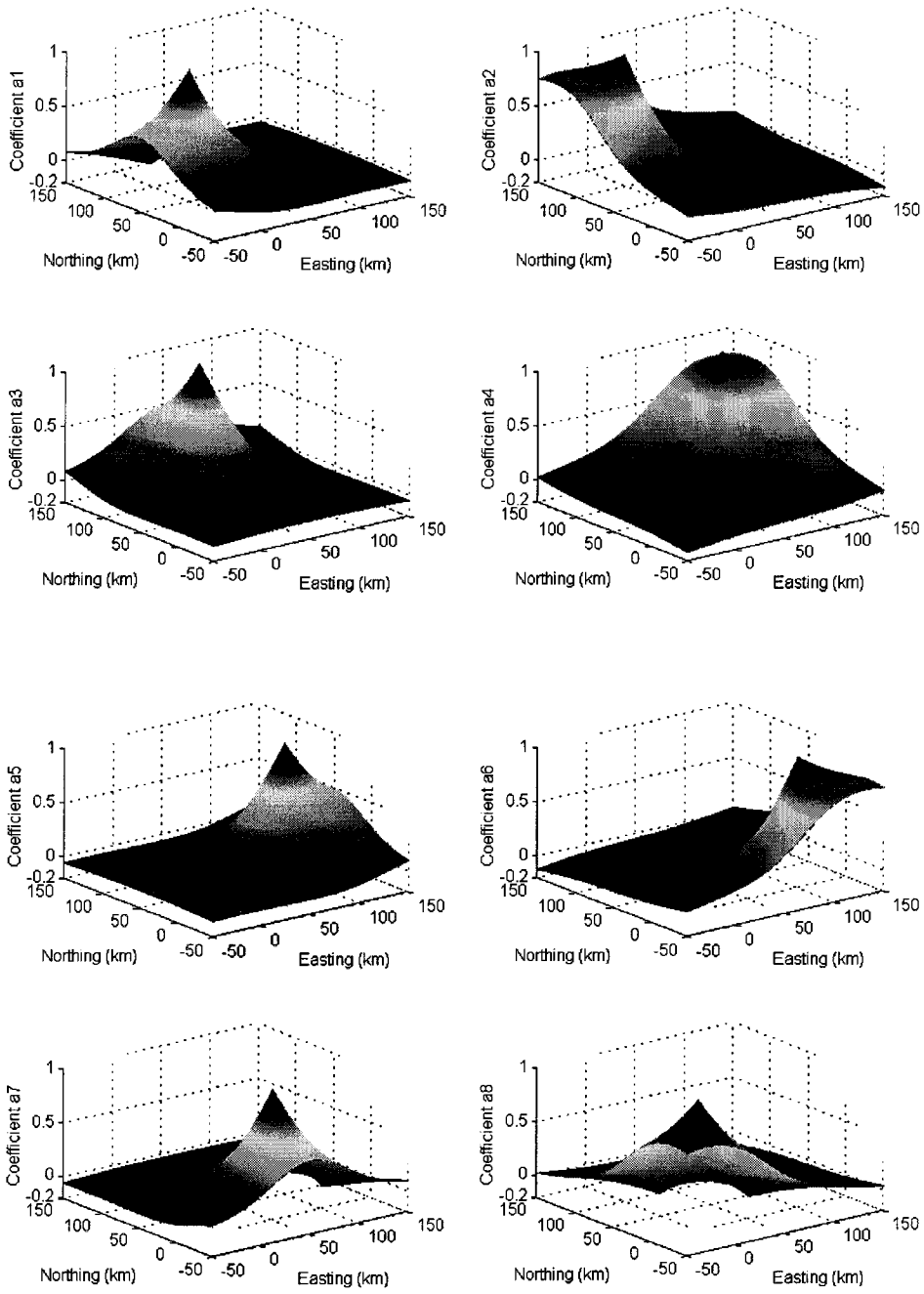

Figure 3-2g. Coefficients generated by the Least Squares Collocation method proposed by Marel (1998)

3.4 Experiments

In order to compare the performance of the different interpolation methods, two experiments were carried out.

3.4.1 Sydney: GPS and Glonass Reference Stations

This experiment was carried out on 15 May 2000, using four dual-frequency integrated GPS/Glonass JPS receivers to simulate a reference station network (Figure 3-3). One of the reference stations was located on the roof of the Geography and Surveying building, at The University of New South Wales (UNSW). The other two reference stations were located at Camden and Richmond. The distances between the reference stations were 55.9km, 48.2km and 49.5km. The user receiver was located at the side of the Motorway No.4, 31.4km, 26.5km and 32.4km away from the UNSW, Richmond and Camden respectively. The station UNSW was selected as the master reference station. The experiment commenced at 8:30AM and concluded at 12:30PM. A total of 3 hours of GPS and Glonass measurements for all the receivers, with one-second sampling rate and a 15° cut-off angle, were collected. During the period, between 5 and 9 GPS, and between 3 and 5 Glonass satellites were tracked.

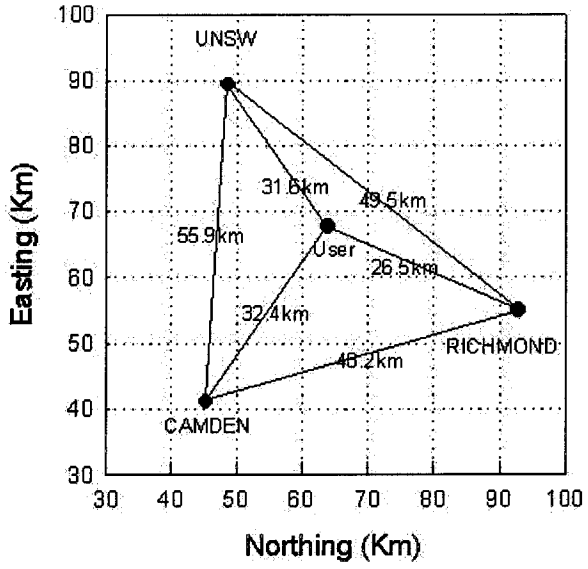

Figure 3-3. Configuration of the Sydney GPS/Glonass multiple-reference receiver network

The reference station ambiguities were correctly determined in the post-processing mode using the recorded GPS and Glonass measurements (see next chapter for details). Table 3-1 shows the coefficients for the different interpolation methods. The last two columns denote the sum and square sum of the *n-1* coefficients. The square sum factor is an indicator of noise for the 'correction terms', hence the smaller the better. The LSC1 and LSC2 refer to the Least Squares Collocation Method suggested by Raquet (1998) and Marel (1998) respectively. It can be seen that the coefficients for LCM and LIM are exactly same, and that the coefficients for LSC1 and LSC2 are very close. However, there is a larger difference for the DIM method.

Table 3-1. Coefficients generated for the different methods

	Ref. Sta.	LCM	DIM	LIM	LSC1	LSC2
α_1	CAMD	0.193	0.450	0.193	0.249	0.256
α_2	RICH	0.448	0.550	0.448	0.421	0.424
α_3	UNSW	0.360				0.337
$\sum_{i=1}^{2}\alpha_i$		0.640	1.000	0.640	0.670	0.680
$\sqrt{\sum_{i=1}^{2}\alpha_i^2}$		0.487	0.711	0.487	0.489	0.495

Figures 3-4a to 3-4d show the L1 and L2 residuals for the baseline UNSW-USER, for satellite pairs PRN39-41 and PRN16-11, with and without the Linear Combination Model. The distance-dependent biases have been reduced significantly after the 'correction terms' from the reference station network were applied. In this experiment there are two data gaps caused by data loss at the user receiver when recording. If the data gap had occurred at the reference station receivers, correction terms can be predicted for up to a few minutes using a Kalman filter or by linear function fitting (see Dai et al., 2002c).

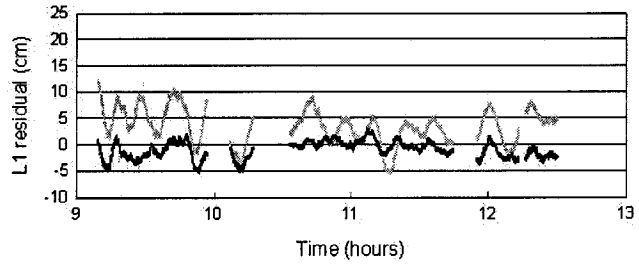

Figure 3-4a. L1 residuals for Glonass satellite pair PRN39-41 with (black) and without (grey) the Linear Combination Model

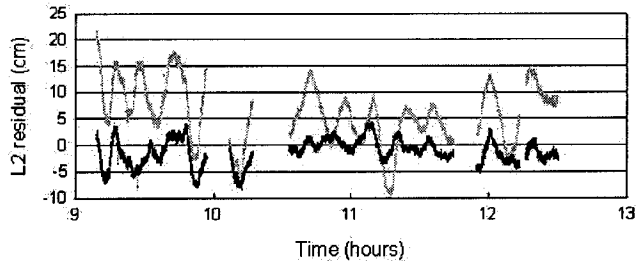

Figure 3-4b. L2 residuals for Glonass satellite pair PRN39-41 with (black) and without (grey) the Linear Combination Model

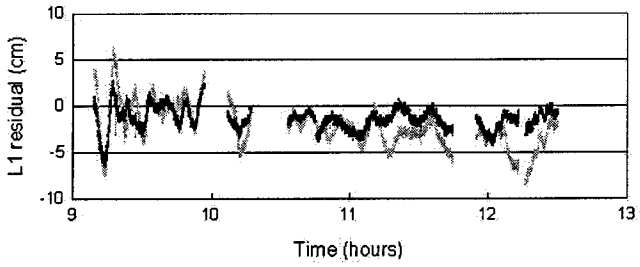

Figure 3-4c. L1 residuals for GPS satellite pair PRN16-11 with (black) and without (grey) the Linear Combination Model

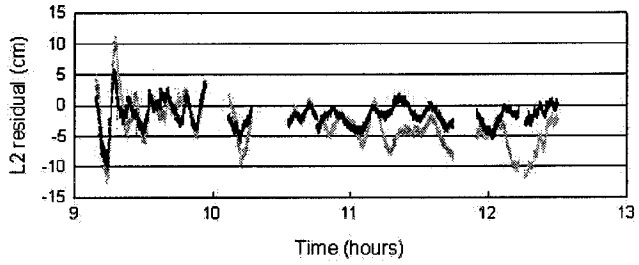

Figure 3-4d. L2 residuals for GPS satellite pair PRN16-11 with (black) and without (grey) the Linear Combination Model

Figure 3-5a shows the original L1 resiudals for all the satellite pairs at the baseline UNSW-USER. It can be seen that the residuals can be up to 20cm for the 31.6km baseline. Figures 3-5b, 3-5c, and 3-5d show the L1 residuals after the correction terms from the reference stations are applied using the LIM, DIM and LSC methods respectively. As the coefficients are the same, or very close, for the LCM and LIM, and the LSC1 and LSC2, the results for these are not plotted. It can be seen that the LCM and LSC methods give almost the same results, but the DIM method gives slightly worse results.

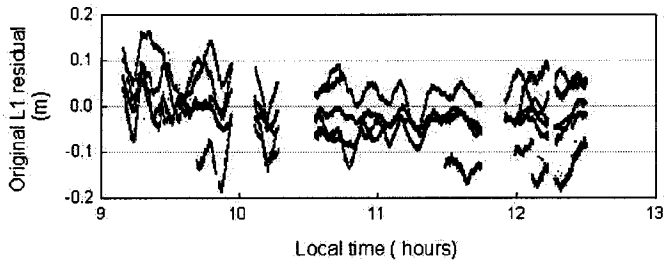

Figure 3-5a. Original double-differenced L1 residuals for all the satellites pairs

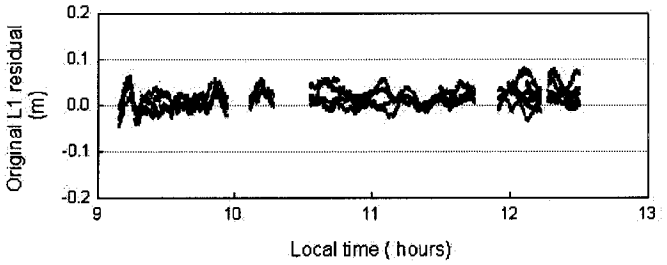

Figure 3-5b. Double-differenced L1 residuals for all the satellites pairs using the Linear Combination Model

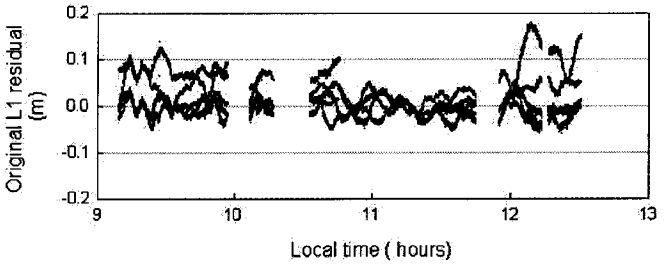

Figure 3-5c. Double-differenced L1 residuals for all the satellites pairs using the Distance-based Linear Interpolation Method

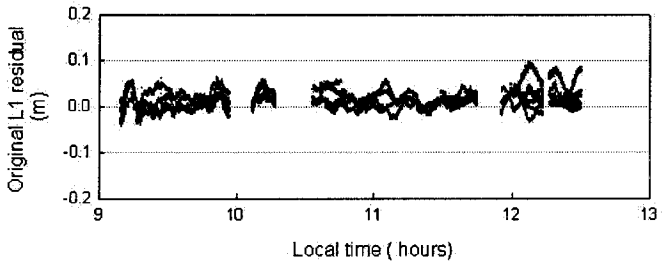

Figure 3-5d. Double-differenced L1 residuals for all the satellites pairs using the Least Squares Collocation Method

Figure 3-6 shows the L1, L2, P1 and P2 RMS statistics for the original residuals (ORG), and after the different interpolation methods (LCM, DIM, LIM, SC1 and LSC2) were applied. The conclusion can be made that all the interpolation methods can significantly mitigate the distance-dependent biases in the L1, L2, P1 and P2 double-differenced measurements.

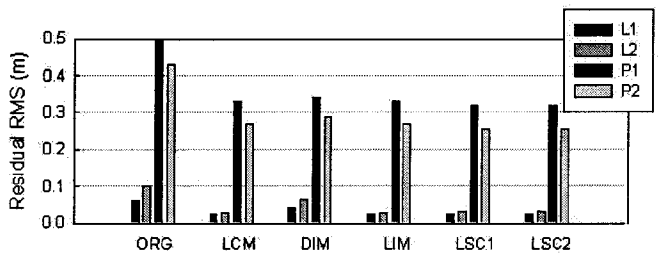

Figure 3-6. L1, L2, P1 and P2 RMS statistics for the different interpolation methods

3.4.2 Taiwan: Multiple-Reference Receiver Test

In order to further investigate the performance of the different interpolation methods, data from permanent GPS stations established for deformation monitoring purposes in the Taiwan region (Figure 3-7) have also been analysed. The data was collected on 31 December 2000, logged at a 30 second sampling rate and a cut-off angle of 15°. Of the six reference stations (S011, S104, S058, I007, FCWS and S01R) S011 was selected as the master reference station and I007 as the user. There were two Leica CRS1000 recevers at stations S011 and I007, and four Trimble SSI receivers at S01R, FCWS, S058 and S104.

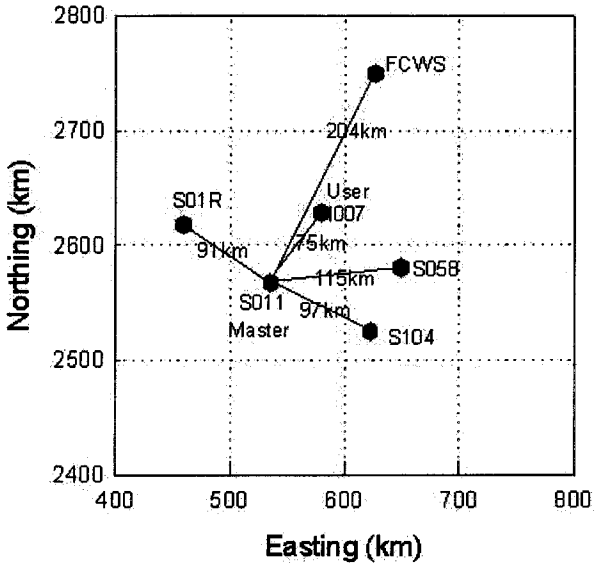

Figure 3-7. Configuration of the Taiwan multiple-reference station test network

The reference station ambiguities were determined using the Bernese software v4.2 in the standard post-processing mode. Due to the high geomagnetic activity in the Taiwan region over recent years, the ambiguities between the reference stations were very difficult to determine correctly. Therefore, a cut-off angle 25° was used in the data processing. Table 3-2 shows the coefficients for the LCM, DIM, LIM, LSM, LSC1 and LSC2 interpolation methods. The coefficients for LSC1 and LSC2 are very similar.

Table 3-2. Coefficients generated for the different methods

	Ref. Sta.	LCM	DIM	LIM	LSM	LSC1	LSC2
α_1	FCWS	0.297	0.209	0.329	0.283	0.316	0.266
α_2	S01R	0.208	0.225	0.004	0.305	0.024	0.163
α_3	S104	0.142	0.244	0.016	0.202	-0.081	0.004
α_4	S058	0.180	0.322	0.114	0.211	0.282	0.330
α_5	S011	0.173					0.344
$\sum_{i=1}^{4}\alpha_i$		0.827	1.000	0.463	1.000	0.540	0.763
$\sqrt{\sum_{i=1}^{4}\alpha_i^2}$		0.429	0.507	0.349	0.508	0.431	0.454

The Figure 3-8a shows the original L1 resiudals for all the satellite pairs. It can be seen that the residuals can be up to 3 metres for the 75km baseline between S011 and I007! It should be emphasised that the distance-dependent biases became quite large and variable between local time 13:00-22:00. This is likely to be due the high solar activity. Figures 3-8b to 3-8g show the L1 residuals after the 'correction terms' from the reference station network have been applied, using the LIM, DIM, LIM, LSM, LSC1 and LSC2 methods respectively. It can be seen that all six methods can significantly reduce the distance-dependent biases, and demonstrate similar interpolation accuracy. Again, the DIM method does give slightly worse results. It is obvious that during high solar activity the accuracy of the interpolation for all the methods is reduced significantly.

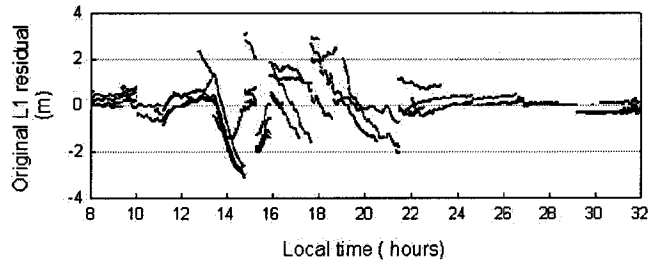

Figure 3-8a. Original double-differenced L1 residuals for all the satellites pairs

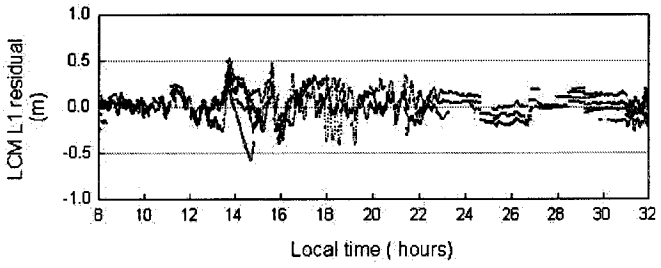

Figure 3-8b. Double-differenced L1 residuals for all the satellites pairs using the Linear Combination Model

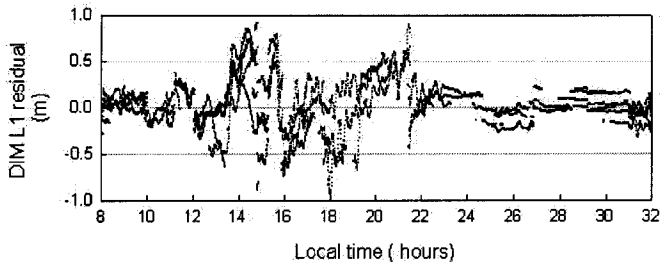

Figure 3-8c. Double-differenced L1 residuals for all the satellites pairs using the Distance-based Linear Interpolation Method

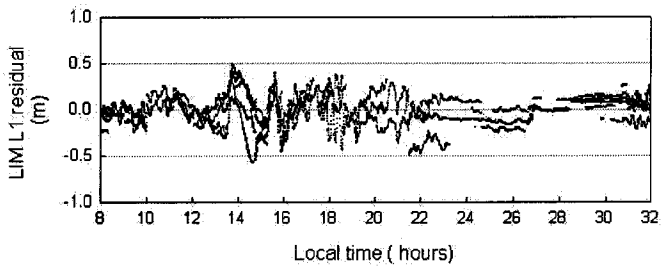

Figure 3-8d. Double-differenced L1 residuals for all the satellites pairs using the Linear Interpolation Method

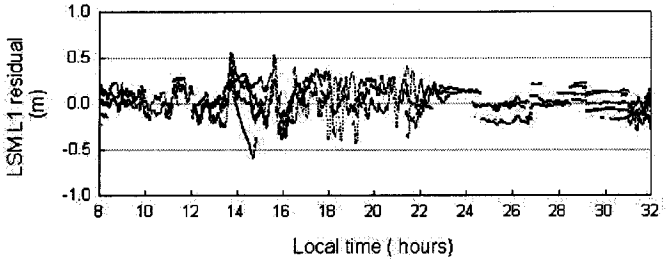

Figure 3-8e. Double-differenced L1 residuals for all the satellites pairs using the Low-order Surface Method (bivariate linear function fitting)

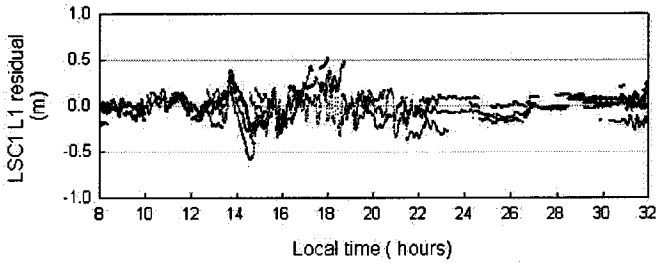

Figure 3-8f. Double-differenced L1 residuals for all the satellites pairs using the Least Squares Collocation Method proposed by Raquet (1998)

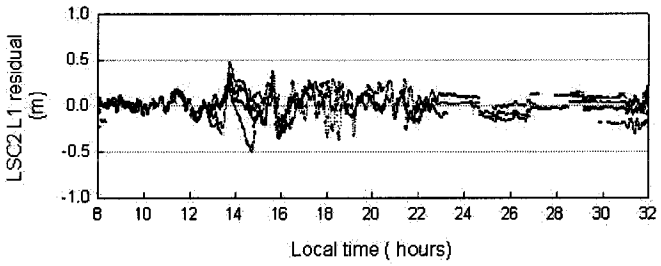

Figure 3-8g. Double-differenced L1 residuals for all the satellites pairs using the Least Squares Collocation Method proposed by Marel (1998)

Figure 3-9 shows the L1, L2, P1 and P2 RMS statistics for the original residuals (ORG) and after the different interpolation methods (LCM, DIM, LIM, LSM, SC1 and LSC2) have been applied. It can be seen for the original residuals (in Figure 3-9) that there are similar RMS values for L1 and P1, and for L2 and P2. This could be due to the dominant ionospheric biases compared to the pseudo-range noise. However, the RMS values for carrier phase are much smaller than for pseudo-ranges after the correction terms are applied. The conclusion can be made again that all the interpolation methods can significantly mitigate the distance-dependent biases in the L1, L2, P1 and P2 double-differenced observables.

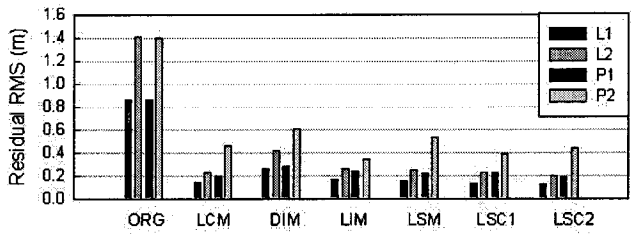

Figure 3-9. L1, L2, P1 and P2 RMS statistics using the different interpolation methods

3.5 Concluding Remarks

In this chapter several interpolation methods suitable for reference station network techniques, including the Linear Combination Model, the Distance-based linear

Interpolation Method, the Linear Interpolation Method, the Low-order Surface Model, and the Least Squares Collocation Method, have been compared in detail. The advantages and disadvantages of each of these techniques has been discussed. For all of the abovementioned methods, the essential common formula has been identified. All use n-1 coefficients and the n-1 independent 'correction terms' generated from a n reference station network to form a linear combination that mitigates spatially correlated biases at user stations.

Test data from several GPS/Glonass reference station networks wer used to evaluate the performance of these methods. The numerical results show that all the proposed methods for multiple-reference receiver implementations can significantly reduce the distance-dependent biases in the carrier phase and pseudo-range measurements at the GPS user station. The performance of all of the methods is similar, although the distance-dependent Linear Interpolation Method does demonstrate slightly worst results in the two experiments studied.

In order to model the distance-dependent errors such as the ionospheric and tropospheric biases, the ambiguities in the GPS/Glonass reference station network should first be resolved to their correct integer values. However, even with precisely known station coordinates, it is still a challenge to fix the ambiguities in the reference station network, especially when a new satellite rises above the tracking horizon. This issue will be investigated in next chapter.

Chapter 4

PREDICTING ATMOSPHERIC BIASES FOR REAL-TIME AMBIGUITY RESOLUTION IN GPS AND GLONASS REFERENCE STATION NETWORKS

4.1 Introduction

Over the past few years the concept of using not just one reference receiver, but a reference station *network* has increasingly been promoted for RTK-GPS positioning. The concept is simple, using pre-determined coordinates of a network of reference receivers and the known (fixed) GPS carrier phase ambiguities, so-called 'correction terms' modelling the atmospheric delays and orbit errors can be generated to support medium-range and long-range carrier phase-based positioning. With modern GPS data processing software packages it is not difficult to precisely determine the coordinates of the reference stations, and to reliably resolve the GPS ambiguities associated with these reference stations, using data sets of several hours or even days in length. However, the challenging issue is to resolve the GPS ambiguities within the reference station network in real-time, to support user-based RTK positioning, particularly in the case of the ambiguities for newly risen satellites.

A four-step algorithm suitable for multiple-reference receiver ambiguity resolution has been suggested by Gao et al. (1997). In their implementation the geometry-free combination is used to determine the initial ambiguities $60N_1 - 77N_2$ and their search ranges. For each ambiguity candidate, the double-differenced ionospheric delay can be derived. Then the computed ionospheric delays are applied to the wide-lane combination, and the wide-lane ambiguities are then resolved. Finally the L1 and L2

ambiguities can be determined. However, one cycle of the $60N_1 - 77N_2$ combination will result in a correction of only 0.01 cycles to the wide-lane combination. Tropospheric delay errors can be up to 10cm (0.12 cycle), or worse, for low elevation satellites.

Rabah & Leinen (1998) have suggested that for real-time crustal deformation monitoring applications over long baselines the wide-lane ambiguity could be rounded-off after five epochs of wide-lane observables have been accumulated. Then the narrow-lane ambiguity using the ionosphere-free combination would be determined, and fixed after the empirical limit is met. Sun et al. (1999) have suggested that ambiguities be fixed in two steps (wide-lane and L1 ambiguity using the ionosphere-free combination) by a search method. However, in the former method, the wrong wide-lane ambiguity may be resolved under conditions of high solar activity or in the case of long baselines. Both methods take quite a long time to fix the narrow-lane ambiguities, especially for a newly risen satellite.

Recently, a regional single-thin layer ionospheric model has been used to increase the success rate of wide-lane ambiguity resolution (see, e.g. Schaer et al., 1999; Vollath et al., 2000). Colombo et al. (1999) and Hernández-Pajares et al. (1999) have proposed a tomographic model, which consists of a two-layer model with boundaries at 60-740-1420 kilometres. It was suggested that this model could provide good accuracy in the double-differenced estimate of the Slant Total Electron Content, and have demonstrated the feasibility of predicting ionospheric delay for real-time wide-lane ambiguity resolution at reference stations. Schaer et al. (1999) have suggested 30-minute linear models for tropospheric refraction as a function of latitude, longitude and height of the user station. Then the corrections can be applied to each user station, each epoch and for each satellite. Zhang (1999) proposed the residual tropospheric zenith delay (RTZD) estimation model (after applying a standard tropospheric delay model), which was derived from the residuals of the ionosphere-free combination generated by a network of reference stations. The predicted RTZD model for a rising satellite at the reference stations can significantly improve the success rate of narrow-lane ambiguity resolution (see, e.g. Chen, 2000; Chen et al., 2000).

In general, with the combination of GPS and Glonass, the volume of observations is increased, which will in turn enhance the reliability of multiple-reference station applications, by providing an improved ability to model residual atmospheric biases, and hence lead to higher success rates for ambiguity resolution. However, due to the different frequencies of the different Glonass satellites, it becomes more difficult to fix the ambiguities in real-time (Wang et al., 2001).

In this chapter, two real-time ambiguity resolution scenarios are described. Both the temporal and spatial correlation characteristics of the atmospheric delays are analysed. A temporal correlation model is used to *recover* ambiguities after initial resolution (or initialisation), whilst the spatial correlation models are used to predict residual ionospheric and tropospheric delays for use in wide-lane and narrow-lane ambiguity resolution for a newly risen satellite (or after a long data gap). The performance of the proposed atmospheric bias prediction models will be demonstrated through case study examples of GPS (and Glonass) reference station data processing.

4.2 Real-Time Ambiguity Resolution: Models and Scenarios

4.2.1 Carrier Phase Equations

The GPS and Glonass double-differenced L1 and L2 carrier phase observables can be expressed in units of metres as (e.g., Leick, 1998):

$$\phi_{kl,n}^{p}\lambda_{n}^{p}-\phi_{kl,n}^{q}\lambda_{n}^{q}=\rho_{kl}^{pq}+N_{kl,n}^{pq}\lambda_{n}^{p}-(\lambda_{n}^{p}-\lambda_{n}^{q})N_{kl,n}^{q}+\frac{I_{kl}^{q}}{(f_{n}^{q})^{2}}-\frac{I_{kl}^{p}}{(f_{n}^{p})^{2}}+T_{kl}^{pq}+O_{kl}^{pq}+\varepsilon_{kl,n}^{pq} \tag{4-1}$$

where the subscripts k and l identify the ground stations, and superscripts p and q denote the satellites. $\phi_{kl,n}^{p}$ and $\phi_{kl,n}^{q}$ are the single-differenced carrier phase observables expressed in units of cycles, and n=1,2 denote the L1 and L2 frequencies (in the following sections, n=3, 4 and 5 denote the ionospheric-free, geometry-free and wide-lane combinations respectively). λ_{n}^{p} and f_{n}^{p} are the wavelength and frequency of the carrier wave for satellite p respectively. Other terms in Equation (4-1) have the

following definitions: ρ_{kl}^{pq} and $N_{kl,n}^{pq}$ are the computed double-differenced geometric range between receivers and satellites, and integer ambiguity respectively; $N_{kl,n}^{q}$ is the single-differenced integer ambiguity related to the reference satellite q; $I_{kl}^{q}/(f_n^q)^2$ and $I_{kl}^{p}/(f_n^p)^2$ are the single-differenced ionospheric delays for satellite q and p respectively (where I is a function of the Total Electron Content); T_{kl}^{pq} and O_{kl}^{pq} are the double-differenced tropospheric delay and orbit error respectively; and $\varepsilon_{kl,n}^{pq}$ is the noise and remaining errors in the carrier phase measurements, such as multipath, antenna phase centre drift (and Glonass inter-channel carrier biases). It should be mentioned that the double-differencing operator is applied to the GPS measurements only or the Glonass measurements only, rather than between the GPS and Glonass measurements. Kozlov et al. (2001) have investigated in detail the effect of the Glonass inter-channel carrier biases, and their results indicate that the magnitude of the biases is usually insignificant and can be neglected.

For simplicity, the frequencies f_n^p and f_n^q in Equation (4-1) related to the ionospheric delay terms for Glonass satellites will be replaced by the mean frequency f_n of the L1 and L2 signals:

$$\begin{aligned}\frac{I_{kl}^{q}}{(f_n^q)^2}-\frac{I_{kl}^{p}}{(f_n^p)^2} &= \frac{I_{kl}^{q}}{(f_n)^2}\cdot(\frac{f_n}{f_n^q})^2-\frac{I_{kl}^{p}}{(f_n)^2}\cdot(\frac{f_n}{f_n^p})^2 \\ &\cong \frac{I_{kl}^{q}}{(f_n)^2}-\frac{I_{kl}^{p}}{(f_n)^2} \\ &= -\frac{I_{kl}^{pq}}{(f_n)^2}\end{aligned} \tag{4-2}$$

where

$$\begin{aligned}-0.0085 < (\frac{f_n}{f_n^q})^2 - 1 < .0085 \\ -0.0085 < (\frac{f_n}{f_n^p})^2 - 1 < .0085\end{aligned} \tag{4-3}$$

The maximum difference in the coefficient $(\frac{f_n^p}{f_n})^2$ or $(\frac{f_n^p}{f_n})^2$ between the correct and approximate values will be less than 0.0085 (Equation (4-3)). The errors caused by approximation (i.e. using the mean frequencies) can be ignored because these single-differenced ionospheric delays $\frac{I_{kl}^q}{f_n^{\,2}}$ and $\frac{I_{kl}^p}{f_n^{\,2}}$ are at the metre level in the worst case. Therefore, for the L1 frequency, Equation (4-1) can be rewritten as:

$$\phi_{kl,1}^p \lambda_1^p - \phi_{kl,1}^q \lambda_1^q = \rho_{kl}^{pq} + N_{kl,1}^{pq} \lambda_1^p - (\lambda_1^p - \lambda_1^q) N_{kl,1}^q - \frac{I_{kl}^{pq}}{f_1^{\,2}} + T_{kl}^{pq} + O_{kl}^{pq} + \varepsilon_{kl,1}^{pq} \qquad (4\text{-}4)$$

It should be noted that the third term – the single-differenced ambiguity bias on the right-hand side of Equation (4-4) – causes another problem in cycle slip detection and ambiguity resolution for Glonass satellites. This problem will be further discussed in Section 4.3.1.

4.2.2 Ambiguity Resolution Scenarios

Although the ambiguities could be initialised at the beginning of network operation, the challenge remains: how to recover an integer ambiguity if a cycle slip or data gap occurs, or if a new satellite rises above the tracking horizon? Based on the temporal and spatial correlation characteristics of the systematic biases, two scenarios are suggested to address this challenge.

From Equation (4-4) it is noted that the factors affecting ambiguity determination are the residual ionospheric delay $I_{kl}^{pq}/f_1^{\,2}$, the tropospheric delay T_{kl}^{pq}, the orbit error O_{kl}^{pq}, the geometric range ρ_{kl}^{pq}, the single-differenced ambiguity related to the reference satellite $N_{kl,1}^q$, the measurement noise and any remaining errors (typically multipath) ε_{kl}^{pq}. In the case of a GPS/Glonass reference station network, station coordinates can be precisely determined using several days of static data before system operation begins. After careful selection of the reference stations, and using state-of-the-art hardware and

software multipath mitigation techniques, the influence of multipath can expect to have been significantly mitigated. The RMS value of 20cm per coordinate component for the CODE (Center for Orbit Determination in Europe) orbits assumes predicted ephemerides from a 2-4 hour extrapolation (Rothacher & Mervart, 1996). Orbital errors can therefore be ignored if predicted ephemerides can be used for real-time reference station data processing. Due to the presence of residual ionospheric delay, tropospheric delay and the single-differenced ambiguity related to the reference satellite, reliable *instantaneous* ambiguity resolution will be a significant problem in medium-to-large scale reference networks (defined here as where the reference stations are typically in the range 50-200km apart), even though the previous epoch's ambiguities have been correctly resolved.

As the systematic biases due to atmospheric delays and orbital errors after double-differencing exhibit a high degree of *temporal* correlation for short time spans, the double-differenced residuals can be represented as a linear function of time for short periods of up to a few minutes. On an epoch-by-epoch and satellite-by-satellite basis, they can be estimated using previous measurements with fixed ambiguities, and precisely predicted for ambiguity resolution for the following measurement epoch. Therefore, this scenario (referred to here as Scenario A) is suitable for ambiguity recovery. However, the assumption is that the ambiguities during the previous epochs have been fixed to their correct values.

On the other hand, atmospheric biases exhibit strong *spatial* correlation between satellite pairs. Therefore, the residual atmospheric delay information derived from other satellites, with fixed ambiguities, can aid in the estimation of the atmospheric delay for a newly risen satellite, and for those satellites that have unknown ambiguities associated with them. Specific residual ionospheric and tropospheric delay models can be developed for this purpose. The predicted ionospheric and tropospheric delay corrections can then be used for wide-lane and narrow-lane ambiguity resolution. As a result, this scenario (referred to here as Scenario B) is suitable for real-time ambiguity resolution for a newly risen satellite, or after a long data gap.

It should be noted that ambiguity resolution within a reference station network is a special case of the general ambiguity resolution procedure, because the ambiguities to be resolved here can be treated individually. For each satellite pair, the double-differenced ambiguity is a scalar. Therefore, the best and second best ambiguity values are the two integers, for example, which are closest to the estimated ambiguity value. According to the ambiguity validation procedure developed in Wang et al. (1998), for this situation, the W-ratio is:

$$W = \frac{d}{\sqrt{Var(d)}} = \frac{1-2r}{2\sigma_N} \tag{4-5}$$

where d is the difference between the quadratic form of residuals for the best and second best ambiguity combinations; r is the round-off value ranging from 0 to 0.5 and σ_N is the standard derivation of the estimated ambiguity parameter. As shown in Sections 4.4.1 and 4.4.2, the prediction of the biases can be very accurate, to one or two centimetres accuracy for Scenario A in single-epoch mode, and for Scenario B in the case of multiple epoch accumulation. Therefore, the standard derivation for the estimated ambiguity values can be set to 0.1 cycles. If the round-off values are less than 0.2 cycles, the W-ratio values are larger than 3, which indicates a confidence level of 99.9% for the statistic test discriminating the best and second best ambiguity combinations. See Ibid (1998) for details.

4.3 Atmospheric Bias Prediction for Use in Real-Time Ambiguity Resolution

4.3.1 Temporally Correlated Biases

Numerous studies have attempted to model the temporal correlation of the residual atmosphere delays and orbit errors in order to improve the performance of GPS positioning (see, e.g., Beutler, et al., 1989; El-Rabbany et al., 1994; Han, 1995; Wang,

1999; Dai et al., 2000a; Fotopoulos & Cannon, 2000). In these investigations it was shown that strong temporal correlation does exist in the measurements between adjacent epochs. Han & Rizos (2000) discuss the strong temporal correlation of the multipath signatures on pseudo-range and carrier-phase observations for static receivers. From Equation (4-4), the biases (including atmospheric delays, orbit errors and the single-differenced ambiguity bias) can be represented as:

$$\begin{aligned} Bias &= -(\lambda_1^p - \lambda_1^q)N_{kl,1}^q - \frac{I_{kl}^{pq}}{f_1^2} + T_{kl}^{pq} + O_{kl}^{pq} \\ &= \phi_{kl,1}^p \lambda_1^p - \phi_{kl,1}^q \lambda_1^q - \rho_{kl}^{pq} - N_{kl,1}^{pq} \lambda_1^p - \varepsilon_{kl,1}^{pq} \end{aligned} \tag{4-6}$$

For a GPS/Glonass reference station network, the biases in Equation (4-6) can be easily computed after the double-differenced ambiguities are fixed. It should be pointed out that the single-differenced ambiguity bias would disappear for the GPS reference satellite, but will be a constant for the Glonass reference satellite if no cycle slips occur.

As mentioned earlier, these biases exhibit a high degree of temporal correlation for short time spans, and hence this can be represented as a function of time for short periods of up to a few minutes. To predict the biases, three methods are proposed. The former two methods are based on a random walk process for the systematic bias called (a) constant bias model, and for the change rate of the systematic bias called (b) linear bias model. The third method will be (c) linear fitting fucntion approach.

Constant Bias Model

$$\begin{aligned} &x_{t+1} = x_t + q_t \\ &\text{with } E(q_t\, q_k) = \delta(t,k) \cdot \delta_{\dot{x}}\, \Delta t^2 \end{aligned} \tag{4-7}$$

where x and $\delta_{\dot{x}}$ are the systematic bias and the variance of velocity noise respectively, t and Δt are the measurement time and interval of sampling rate respectively, $\delta(k,t)$ is

the Dirac function, and a white sequence (q_t) is a sequence of zero-mean random variables that are uncorrelated.

Linear Bias Model:

$$\begin{bmatrix} x \\ \dot{x} \end{bmatrix}_{(t+1)} = \begin{bmatrix} 1 & \Delta t \\ 0 & 1 \end{bmatrix} \begin{bmatrix} x \\ \dot{x} \end{bmatrix}_{(t)} + W_t \tag{4-8a}$$

where $\dot{x}$ is the systematic bias change rate and a white sequence (W_t) is a sequence of zero-mean random variables that are uncorrelated. The covariance matrix associated with W_t is assumed to be known, and denoted as:

$$E\left[W_k W_t^T\right] = \delta(\mathrm{k,t}) \cdot \begin{bmatrix} \frac{\Delta t^2}{2} \\ \Delta t \end{bmatrix} \cdot \delta_{\ddot{x}} \cdot \begin{bmatrix} \frac{\Delta t^2}{2} & \Delta t \end{bmatrix} \tag{4-8b}$$

where $\delta_{\ddot{x}}$ is the variance of acceleration noise.

Linear fitting function approach:

$$x_{t+1} = x_t + \dot{x}\Delta t \tag{4-9}$$

It should be noted that the constant bias model is easy to implement, but gives the lowest accuracy for the predicted biases. The fitting of a linear function needs to keep track of previous residuals, and may bring some inconvenience for real-time coding. The linear bias model approach combines the merits of the two other approaches, and is easy to be implemented by Kalman filtering for real-time applications.

The biases can be estimated using Equations (4-6), (4-7), (4-8a), (4-8b) and (4-9). On an epoch-by-epoch and satellite-by-satellite basis, the bias can be predicted by either Kalman filtering, the linear fitting function approach. The number of epochs used (for

the linear fitting), and the variance of acceleration noise (used for the Kalman filtering), are critical to achieving highly predicted accuracy of the systematic biases. These will be further discussed in Section 4.4.1. The predicted biases can be applied to the next epoch's measurements to assist ambiguity resolution:

$$N_{kl,1}^{pq}\lambda_1^p = \phi_{kl,1}^p\lambda_1^p - \phi_{kl,1}^q\lambda_1^q - \rho_{kl}^{pq} + Bias - \hat{B}ias - (\lambda_1^p - \lambda_1^q)\delta N_{kl,1}^q + \varepsilon_{kl,1}^{pq} \tag{4-10}$$

where $\hat{B}ias$ is the predicted bias and $\delta N_{kl,1}^q$ is the cycle slip related to the reference satellite. It should be emphasised that the cycle slip bias term $\delta N_{kl,1}^q$ depends on the wavelength difference between satellite k and j and the size of the single-differenced cycle slip related to the reference satellite. Normally the $\delta N_{kl,1}^q$ bias term will be zero if no cycle slips are present, or the wavelengths are identical (i.e. for a GPS satellite pair). Otherwise the bias term will destroy the integer nature of the double-differenced ambiguities. In the worst case for the Glonass constellation, one cycle in $\delta N_{kl,1}^q$ will result in a 0.0081 cycle bias in the double-differenced ambiguity $N_{kl,1}^{pq}$ (the 0.0081 cycle is identical for the L2 frequency and other linear combinations). Therefore, 12 cycle errors in the single-differenced ambiguity will only cause less than 0.1 cycle bias in the double-differenced ambiguity. Hence, small cycle slips have no significant influence on Glonass ambiguity resolution. However, larger cycle slips need to be repaired before modelling.

A special two-step procedure is used to deal with cycle slips related to the Glonass reference satellite. The first step is that the Glonass satellite without cycle slips will be selected as the reference satellite. The difference in the single-differenced TEC with ambiguities between two epochs can be used to detect cycle slips. In practice, significant cycle slips are easily detected. The second step, if the Glonass reference satellite has been changed, is that the corresponding double-differenced ambiguities will have to be reconstructed. If all the Glonass satellites are suspected of having a significant number of cycle slips, a new initialisation for all the Glonass satellites is necessary.

The accuracy of the predicated biases depends on the data interval (and the length of data gap), and how smooth the variations in the atmospheric delay (especially due to the ionosphere) and the orbit bias are. Their performances will be demonstrated through case study examples of GPS (and Glonass) reference station data processing. Long data gaps and high ionospheric scintillation may decrease the accuracy of the predicted biases.

The bias modelling based on temporal correlation can be used to *recover* ambiguities for any kind of linear combination, or the L1, L2 frequencies after initialisation (in this study, double–differenced L1 and L2 are used). It should be noted that the proposed method could also be applied to detect and repair cycle slips *before* an ambiguity is fixed. However, the predicted bias is significantly biased by the constant unfixed ambiguity term, and furthermore the 'absolute' double-differenced ambiguity cannot be fixed. In addition, ambiguity validation is a necessary step. If the validation criterion fails, this satellite needs to be considered as a newly risen satellite. In the following sub-section the emphasis will be on modelling spatially correlated biases for real-time ambiguity resolution for newly risen satellites, or after a long data gap.

4.3.2 Spatially Correlated Biases

For a newly risen satellite, the elevation angle is generally very low. Measurements with low satellite elevation angle will be contaminated by significant ionospheric and troposphere delays. Therefore it becomes difficult to fix the corresponding ambiguities.

Modelling Residual Ionospheric Delay

For regional and global station network post-processing, a single-layer ionosphere model which condenses the electron content on a layer of infinitesimal thickness at a height of about 350km above the surface of Earth is typically used to aid wide-lane ambiguity for long baselines (Rothacher & Mervart, 1996). The model consists of a series of harmonic coefficients which are a function of the latitude and hour angle of the sun. The ionospheric delay information derived from other satellites, with fixed

ambiguities, can be used in the estimation of the ionospheric delay for newly risen satellites, and for those satellites that have unknown ambiguities associated with them.

The difference ($L_{kl,4}^{pq}$) (i.e. the geometry-free measurement) between the double-differenced ionospheric delay on the L1 and L2 carrier phase observations of the satellites p and q can be represented as (from Equation (4-4)):

$$L_{kl,4}^{pq} = \frac{f_1^2 - f_2^2}{f_1^2 f_2^2} I_{kl}^{pq}$$
$$= \lambda_1^p \phi_{kl,1}^p - \lambda_2^p \phi_{kl,2}^p - \lambda_1^q \phi_{kl,1}^q + \lambda_2^q \phi_{kl,2}^q + (\lambda_1^p - \lambda_1^q) \cdot N_{kl,1}^q - (\lambda_2^p - \lambda_2^q) \cdot N_{kl,2}^q - \lambda_1^p N_{kl,1}^{pq} + \lambda_2^p N_{kl,2}^{pq} + \varepsilon_{kl,4}^{pq} \quad (4\text{-}11)$$

where $N_{kl,1}^q$ and $N_{kl,2}^q$ are single-differenced ambiguities involving the reference satellite on L1 and L2 respectively. In Equation (4-11) it is obvious that the Glonass $L_{kl,4}^{pq}$ value is biased by the single-differenced ambiguity at the Glonass reference satellite, but this is not the case for the GPS satellites. One cycle bias on $N_{kl,1}^q$ (or $N_{kl,2}^q$) will result in about 1.5mm (or 2.0mm) error in $L_{kl,4}^{pq}$ in the worst case. Therefore small biases related to $N_{kl,1}^q$ and $N_{kl,2}^q$ have no significant influence on the $L_{kl,4}^{pq}$ calculation. Larger cycle-slips associated with the Glonass reference satellite can be treated in the same way as described in Section 4.3.1. In order to obtain the double-differenced ionospheric delay for the Glonass reference satellite it is necessary to use pseudo-range data to estimate the single ambiguity. In general, a satellite with the highest elevation is selected as the reference satellite. Therefore, multipath and atmospheric biases can expect to be reduced. Pseudo-range noise can be significantly mitigated using a multiple epoch data. Therefore, it should not be difficult to obtain the precise value $L_{kl,4}^{pq}$, with sub-centimetres accuracy, after the double-differenced ambiguities are correctly resolved.

Similarly, the double-differenced ionospheric observables based on the pseudo-ranges P1 and P2 can be written as:

$$L_{kl,4}^{pq} = \frac{f_1^2 - f_2^2}{f_1^2 f_2^2} I_{kl}^{pq} = P_{kl,2}^{pq} - P_{kl,1}^{pq} + \varepsilon_{kl,4}^{pq} \quad (4\text{-}12)$$

The question is how to quantify the spatial correlation between the double-differenced ionospheric delays? The assumption can be made that the greater the latitude and longitude differences between the reference satellite and the non-reference satellites, the greater the double-differenced ionospheric delays. Based on this assumption, the following linear model is proposed:

$$L_{kl,4}^{pq} = a_0 + a_1 \cdot \Delta\lambda + a_2 \cdot \Delta\beta \quad (4\text{-}13)$$

where a_0 is the constant coefficient; a_1 and a_2 are the horizontal ionospheric gradient parameters; $\Delta\lambda$ and $\Delta\beta$ are the latitude and longitude differences between the reference satellite and non-reference satellite respectively at the ionospheric pierce point (defined as the point of intersection of the line of sight with the spherical shell at a height of about 350km above the surface of the Earth). The ionospheric gradient parameters a_1 and a_2 are expected to absorb a significant amount of the spatially correlated ionospheric delays.

The measurements in Equations (4-11), (4-12) and (4-13) can be used to estimate the ionospheric spatial correlation model parameters. In order to mitigate measurement noise and increase model accuracy, the previous few epochs of data are used. These parameters can then predict the ionospheric delay for a newly risen satellite, or after a long data gap. It should be emphasised that only measurements with fixed ambiguities in Equation (4-11) have been used. However, all the ionospheric delay biases derived from Equation (4-12) have also be applied, but with lower weight because of the higher pseudo-range noise. In this chapter, the empirical elevation-dependent exponential functions (i.e. $0.02 + 0.05 \cdot exp(-E/20)$ cycles for one-way carrier-phase and $0.2 + 1.0 \cdot exp(-E/20)$ metres for one-way pseudo-range) have been applied for the

stochastic model. After residual ionospheric parameters α_i (i=0, 1 and 2) are estimated, the following significant test should be applied:

$$t_i = \frac{\alpha_i}{\sqrt{\hat{\delta}_0^2 Q_{\alpha_i}}} > t(n-m,\alpha) \quad (\mathrm{i} = 0,1 \text{ and } 2) \tag{4-14}$$

where $\hat{\delta}_0^2$ is the *a posteriori* variance of unit weight and n denotes the number of double-differenced measurements, m is the number of the estimated residual ionosphere parameters, and Q_{α_i} is the co-factor of the parameter α_i. t is the critical value associated with the t-distribution with a given significant level α and n-m degrees of freedom. If Equation (4-14) cannot be satisfied, the associated parameter(s) is (are) not significant and should be removed from the parameter estimation process.

Modelling Residual Tropospheric Delay

After careful selection of the reference stations, and using hardware and software multipath mitigation techniques, the influence of multipath can expect to have been significantly mitigated. If the precise orbits (or real-time predicted orbits) are used, and the reference station coordinates are precisely determined, and provided that the L1 and L2 ambiguities are correctly resolved, the residual double-differenced tropospheric delay can be derived from the ionosphere-free observables $L_{kl,3}^{pq}$:

$$T_{kl}^{pq} = L_{kl,3}^{pq} - \rho_{kl}^{pq} - N_{kl,3}^{pq}\lambda_3^p - (\lambda_3^p - \lambda_3^q)N_{kl,3}^q + \varepsilon_{kl,3}^{pq} \tag{4-15}$$

where

$$N_{kl,3}^{pq} = aN_{kl,1}^{pq} + bN_{kl,2}^{pq} \tag{4-16}$$

$$N_{kl,3}^{q} = aN_{kl,1}^{q} + bN_{kl,2}^{q} \tag{4-17}$$

and the integers a, b are 9, -7 for the Glonass combination and 77, –60 for the GPS combination. λ_3^p and λ_3^q are the wavelengths of the ionosphere-free combination for satellites p and q (6.3mm for a GPS satellite and about 52.3mm for a Glonass satellite) respectively. The wavelength differences $(\lambda_3^p - \lambda_3^q)$ for the Glonass satellites range from 18.5μm to 422μm. However, the differences are zero for GPS satellites. In order to obtain the residual tropospheric delay, the term $(\lambda_3^p - \lambda_3^q)N_{kl,3}^q$ needs to be corrected. The accuracy of this correction will be discussed later.

Tropospheric delays are classically represented using models for the zenith delay and a mapping function to obtain the delay at any other satellite elevation angle. All the deviations of the atmospheric conditions from standard conditions are subsumed within a scaling factor for the zenith delay. This scaling factor for each station is the model parameter for tropospheric delay (Vollath et al., 2000). Zhang (1999) also proposed the estimation of the residual tropospheric delay for the purpose of predicting the residual tropospheric delay for a setting satellite, or newly risen satellite, using a network of reference stations. After neglecting the elevation differences between stations, the relative tropospheric zenith delay (RTZD) can be approximately represented as a function of the residual tropospheric delay after double-differencing and a mapping function with respect to the elevation angles:

$$RTZD = T_{kl}^{pq} / [MF(\varepsilon^p) - MF(\varepsilon^q)] \tag{4-18}$$

where ε^p and ε^q are the average elevation angles of the two receivers for satellites p and q respectively. RTZD is assumed to be a first-order Gauss-Markov process. The variance of RTZD can also be derived:

$$E[(RTZD)^2] = E[(T_{kl}^{pq})^2] / [MF(\varepsilon^p) - MF(\varepsilon^q)]^2 \tag{4-19}$$

where $E[(RTZD)^2]$ and $E[(T_{kl}^{pq})^2]$ are the variance of the residual tropospheric delay bias and the RTZD respectively. It can be seen that the RTZD accuracy estimated by different satellite pairs will be different. The smaller the elevation angle differences for

satellites p and q, the larger the RTZD variances. It should be emphasised that for less than 5° differences of elevation angle, very poor accuracy estimates of RTZD will be obtained. Therefore, the weighted RTZD estimation is very important for estimating precise residual tropospheric zenith delay.

Hence, the relative tropospheric zenith delay can be estimated using Equations (4-15), (4-18) and (4-19). In practice, the tropospheric zenith delay model at the reference stations, using a few epochs of tropospheric delay data (derived from Equation (4-18)), can not only mitigate the observation noise but also increase the predicted tropospheric zenith delay accuracy (5 minutes of data is chosen in the following experiments).

4.3.3 Atmospheric Bias Prediction to Aid Ambiguity Resolution for a Newly Risen Satellite

After the ionospheric and tropospheric delay corrections (derived from Equations (4-13) and (4-18)) have been computed, the corrected double-differenced wide-lane linear combination for a newly risen satellite can be written as:

$$L_{kl,5}^{pq} = \rho_{kl}^{pq} + N_{kl,5}^{pq}\lambda_5^p + (\lambda_5^p - \lambda_5^q)N_{kl,5}^q - \frac{I_{kl}^{pq} - \hat{I}_{kl}^{pq}}{f_1 f_2} + T_{kl}^{pq} - \hat{T}_{kl}^{pq} + \varepsilon_{kl,5}^{pq} \tag{4-20}$$

where $\hat{I}_{kl}^{pq}/f_1 f_2$ and $\hat{T}_{kl}^{pq}$ are the predicted ionospheric and tropospheric corrections respectively. λ_5^p and λ_5^q are the wavelengths of the wide-lane combination for satellites p and q respectively. The wide-lane wavelength differences $(\lambda_5^p - \lambda_5^q)$ for Glonass satellites range from 0.3mm to 6.75mm. In the worst case, one cycle in $N_{kl,5}^q$ will result in 0.0081 cycles bias in the wide-lane double-differenced ambiguity $N_{kl,5}^{pq}$. In order to fix the double-differenced wide-lane ambiguity, the term $N_{kl,5}^q$ needs to be corrected as precisely as possible. The single-differenced wide-lane ambiguity related to the Glonass reference satellite can be determined using a combination of single-differenced wide-lane phase and narrow-lane pseudo-range measurements:

$$N_{kl,5}^{q} = \phi_{kl,1}^{q} - \phi_{kl,2}^{q} - \frac{1}{(f_1^q + f_2^q)\lambda_5^q}(f_1^q P_{kl,1}^{q} + f_2^q P_{kl,2}^{q}) + \varepsilon_{kl,5}^{q} \tag{4-21}$$

The accuracy of the term $N_{kl,5}^{q}$ depends very much on the noise of the pseudo-range measurements. If the one-way pseudo-range accuracy is 3m, the $N_{kl,5}^{q}$ accuracy, derived from Equation (4-21), will be of the order of 3.6 cycles. Therefore this will cause less than 0.03 cycles bias in the wide-lane ambiguity determination, in the worst case. In practice, the multiple-epoch average can significantly improve the accuracy of $N_{kl,5}^{q}$. As a result, the $N_{kl,5}^{q}$ error can be ignored in wide-lane ambiguity determination.

After the wide-lane ambiguity has been correctly resolved, and the tropospheric delay has been predicted, the corrected ionosphere-free combination can be rewritten as:

$$\begin{aligned} L_{kl,3}^{pq} &= \rho_{kl}^{pq} + N_{kl,3}^{pq}\lambda_3^p + (\lambda_3^p - \lambda_3^q)N_{kl,3}^{q} + T_{kl}^{pq} - \hat{T}_{kl}^{pq} + \varepsilon T_{kl,3}^{pq} \\ &= \rho_{kl}^{pq} + N_{kl,1}^{pq}(a+b)\lambda_3^p - bN_{kl,5}^{pq}\lambda_3^p + (\lambda_3^p - \lambda_3^q)N_{kl,3}^{q} + T_{kl}^{pq} - \hat{T}_{kl}^{pq} + \varepsilon_{kl,3}^{pq} \end{aligned} \tag{4-22}$$

$$\begin{aligned} N_{kl,3}^{q} &= aN_{kl,1}^{q} + bN_{kl,2}^{q} \\ &= (a+b)N_{kl,1}^{q} - bN_{kl,5}^{q} \end{aligned} \tag{4-23}$$

In Equation (4-22), the integer ambiguity $N_{kl,1}^{pq}$, with associated wavelength $(a+b)\lambda_3^p$ (about 10.7cm), should be resolved. The term $N_{kl,3}^{q}$ also should be corrected. It should be pointed out that one cycle error in $N_{kl,3}^{q}$ will result in only 0.004 cycles bias in the L1 double-differenced ambiguity $N_{kl,1}^{pq}$ using the ionosphere-free combination (it is referred to as the narrow-lane ambiguity because of the 10.7cm wavelength), in the worst case. The accuracy of the corrected $N_{kl,3}^{q}$ term depends on the accuracy of the two parts ($N_{kl,1}^{q}$ and $N_{kl,5}^{q}$). If the $N_{kl,1}^{q}$ and $N_{kl,5}^{q}$ can be corrected to within 10 and 3.6 cycles respectively, the computation effect on the narrow-lane ambiguity and on the tropospheric delay would be less than 0.13 cycle and 1.36cm respectively.

If the ambiguity validation criterion can not be satisfied, more epochs of data need to be accumulated. In most circumstances, only a few ambiguities (for a newly risen satellite or a re-gained satellite after a long data gap) will need to be resolved.

4.4 Experimental Results and Analysis

In order to test the performances of the two proposed scenarios for real-time ambiguity resolution for GPS/Glonass reference station networks, two experiments have been carried out.

4.4.1 Sydney: Temporary GPS/Glonass Reference Stations

This experiment was carried out on 15 May 2000, using three dual-frequency integrated GPS/Glonass JPS receivers to simulate a reference station network (Figure 4-1). One of the reference stations was located on the roof of the Geography and Surveying building, at The University of New South Wales. The other reference stations were located at Camden and Richmond. The distances between the reference stations were 55.9km, 48.2km and 49.5km. The experiment commenced at 8:30AM and concluded at 12:30PM. A total of four hours of GPS and Glonass measurements, with one-second sampling rate and 15° cut-off angle, were collected. During the period between 5 and 9 GPS, and between 3 and 5 Glonass satellites were tracked.

The reference station positions were precisely determined in the post-processing mode using the recorded GPS and Glonass measurements. The precise orbits from the CODE were used in the data processing. The ambiguities that were correctly resolved using the whole data set were used as the true values to test the proposed algorithms.

Figure 4-2 shows the L1 residuals for the GPS satellite pairs 11-15 and the Glonass satellite pair 39-41 for the baseline UNSW-RICHMOND. It can be seen that the residuals without the predicted models can reach up to 20cm. Therefore the ambiguities are difficult to resolve instantaneously (with one epoch of data). Figure 4-3 shows the

corresponding residuals after the temporally correlated bias model using the linear bias model approach was applied. It can be seen that the residuals can be reduced significantly (to less than 1cm), and hence the ambiguities can be correctly resolved by simply rounding-off to the nearest integer value.

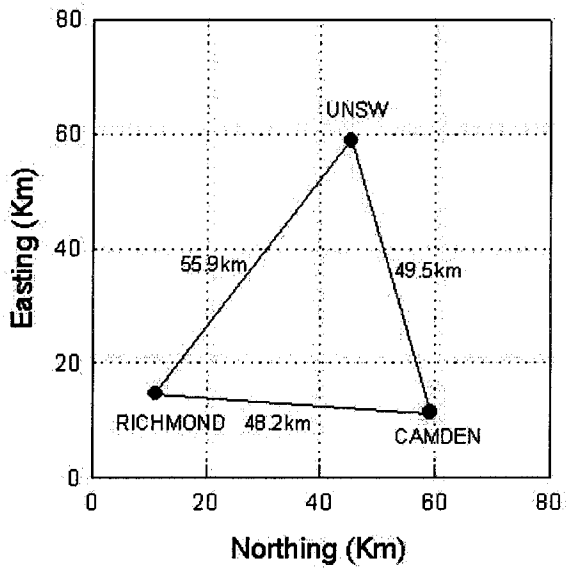

Figure 4-1. Configuration of the Sydney GPS/Glonass reference station experiment

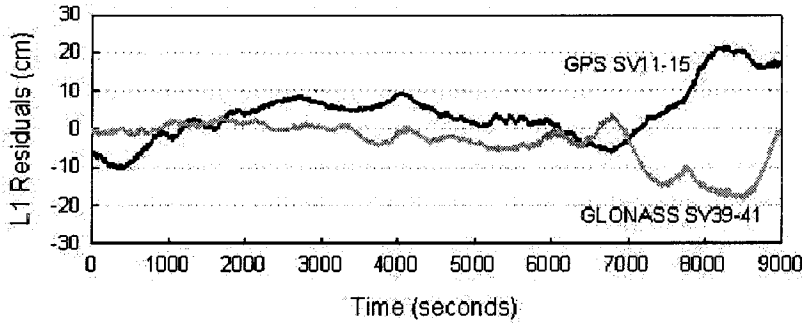

Figure 4-2. L1 residuals without model for GPS SV11-15, and Glonass SV39-41

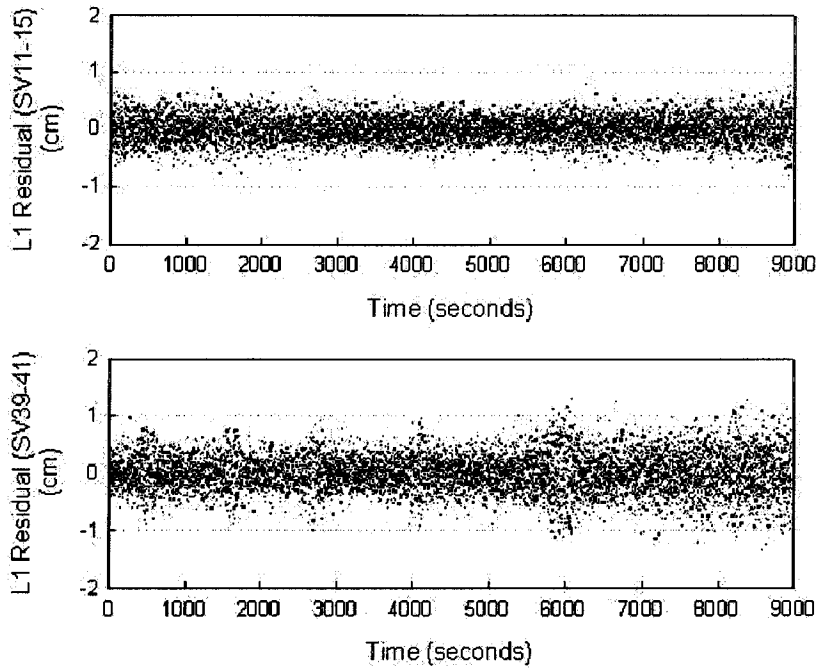

Figure 4-3. L1 residuals after application of the temporal correlation model, linear bias model approach

Figure 4-4 shows the optimised variance of acceleration noise in the Kalman filtering, for the satellite pairs 11-15 and 39-41 for the baseline UNSW-RICHMOND, in the case of L1 residual prediction. 0.05-0.1mm/sec^2 variance of acceleration noise is the best accuracy of the predicted bias in this experiment. The level of variance of acceleration noise depends on how smooth the variations in the systematic biases are. In the linear fitting approach, different numbers of fitting epochs were tested, yielding different levels of performance. The optimal fitting number for L1 residual prediction of the satellite pairs 11-15 and 39-41 is shown in Figure 4-5. Further testing indicates that the optimal number is between 10 – 30 epochs (for a 1 second sampling rate).

Table 4-1 shows the performance of the three different temporal correlation approachs: constant bias model, linear fitting and linear bias model. It can be seen that all three methods can significantly reduce the residual RMS, but the linear bias model approach yields the minimum RMS values. The constant bias model approach has the lowest predicted accuracy. The results show that the double-differenced residuals do exhibit a high degree of temporal correlation, and they can be estimated using previous residuals

(derived with fixed ambiguities), and can support ambiguity resolution at subsequent measurement epochs.

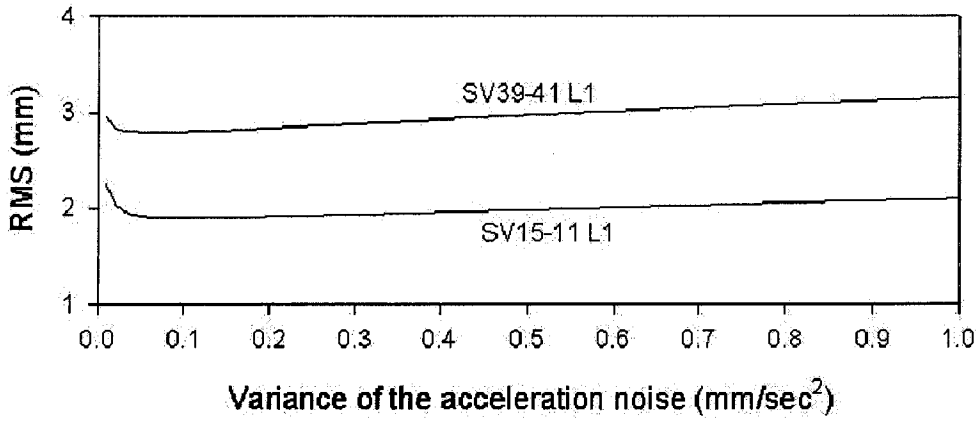

Figure 4-4. Optimal variance of acceleration noise for temporally correlated bias model

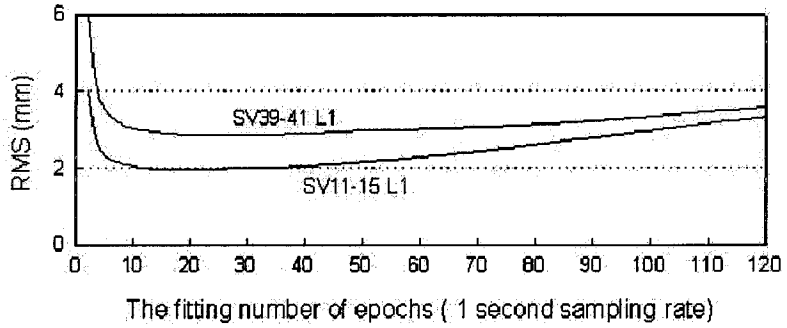

Figure 4-5. Optimal number of epochs for linear fitting for temporally correlated bias model

Table 4-1. Performance of the different temporal correlation modelling options, for different satellite pairs

SV / Type	**Sat11-15 RMS L1 (mm)**	**Sat39-41 RMS L1 (mm)**	**Sat25-15 RMS L1 (mm)**	**Sat11-15 RMS L2 (mm)**	**Sat39-41 RMS L2 (mm)**	**Sat25-15 RMS L2 (mm)**
Original	81.22	57.38	67.59	133.81	94.71	110.23
Constant bias model	2.21	2.21	3.36	2.29	2.29	3.53
Linear fitting	2.02	1.99	3.03	2.19	2.09	3.37
Linear bias model	1.89	1.86	2.79	2.03	1.98	3.27

In order to test the prediction accuracy for the bias temporally correlated model, 30 second, 2 minute and 5 minutes data gaps after every epoch were simulated. The results for the satellite pair 25-15 (L1 residuals) and baseline UNSW-CAMDEN are shown in Figure 4-6. It can be seen that after the correction for the predicted bias was applied the remained residuals for the 30 second and 2 minute data gap does not change much (it is still less than 2cm and 5cm respectively). The round-off method therefore still is appropriate. For the 5 minute data gap the rounding-off approach to ambiguity resolution becomes unreliable because the remaining errors are sometimes quite large (of the order of 10cm). The main reason for this is that the temporal correlation becomes weaker as the size of the data gap increases. The accuracy of the predicted biases depends on the sampling rate between epochs (and the length of the data gap), and how smooth the atmospheric biases (especially due to the ionosphere) and orbit error are. A long data gap and/or high ionospheric scintillation may decrease the accuracy of the predicted biases.

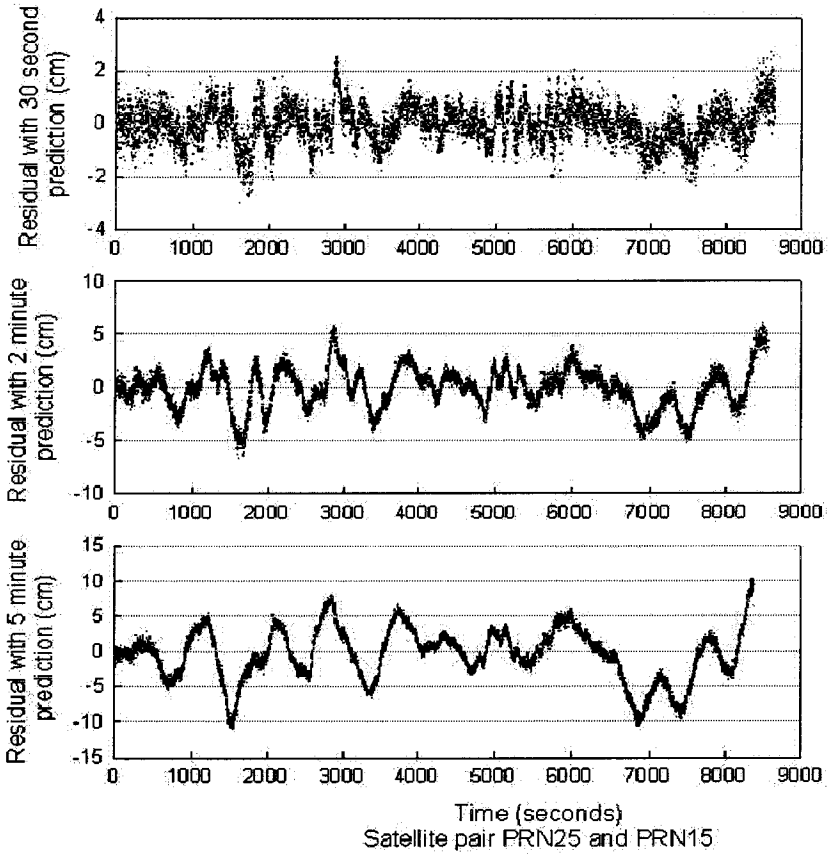

Figure 4-6: Residuals for bias prediction with simulated 30 second, 2 and 5 minute data gaps

Figure 4-7 shows the computed (true), predicted wide-lane residuals, and the difference between the two, for the newly risen satellite 19 and baseline UNSW-RICHMOND. It can be seen that the wide-lane ambiguity without the application of the residual ionospheric delay modelling cannot be fixed correctly for the first 15 minutes. However, the wide-lane residual can be significantly reduced after the residual ionospheric model is applied. The estimated constant a_0, and horizontal ionospheric gradient parameters a_1 and a_2, are shown in Figure 4-8. Though this model cannot precisely predict the ionospheric delay for the newly risen satellite, it does reduce the required time for wide-lane ambiguity resolution. Figure 4-9 shows the values of the significance test for the estimated residual ionospheric model parameters. For a given significant level α = %95 and 30 to 100 epochs data, the critical values of the test is approximately equal to 2. It can be seen that, for most of the time, the estimated parameters are statistically significant. Figure 4-10 shows the optimal number of epochs in the residual ionospheric model. Results from Figure 4-10 indicate that 30 – 100 epochs (of 1 second sampling rate) yield the best predicted accuracy for the residual ionospheric delays in this experiment.

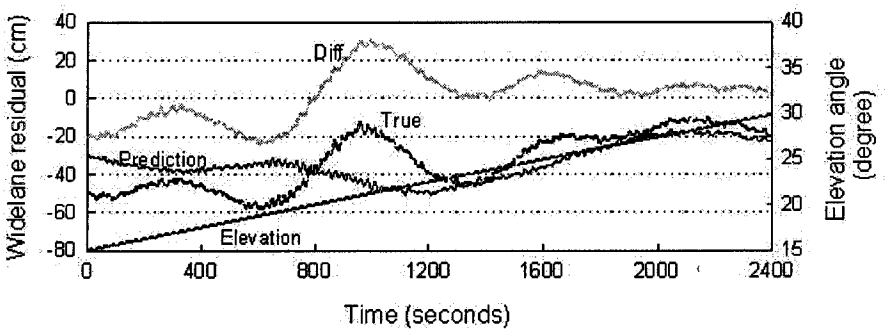

Figure 4-7. Residual ionospheric delay modelling for satellite pair 19-25

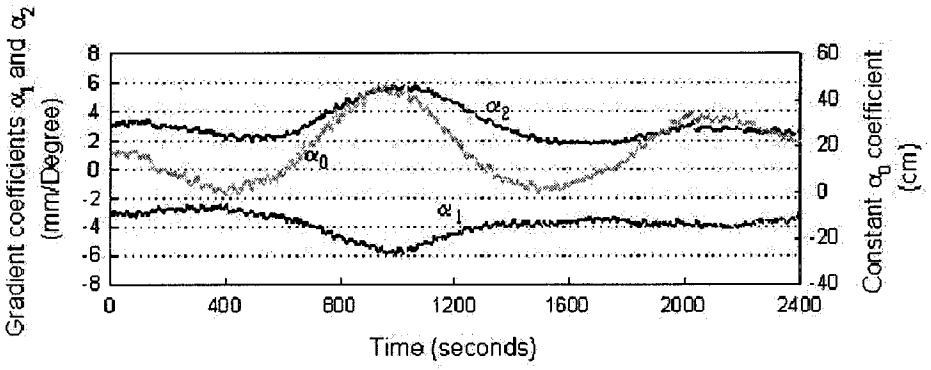

Figure 4-8. Constant and horizontal gradient coefficients for residual ionospheric modelling

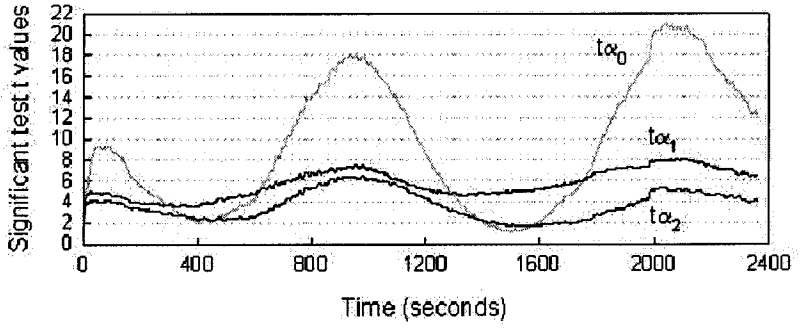

Figure 4-9. Significance test for residual ionospheric modelling parameters

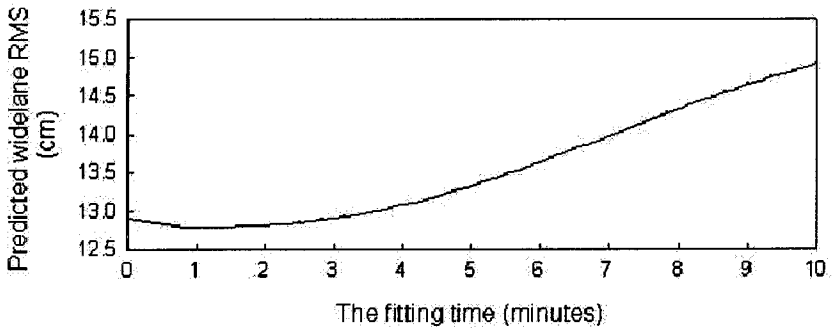

Figure 4-10. Optimal number of epochs for the residual ionospheric model (1 second sampling)

Figure 4-11 shows the narrow-lane residuals with and without the spatially correlated tropospheric delay model for the newly risen satellite 16 and the baseline UNSW-CAMDEN. It can be seen that the narrow-lane ambiguity without the application of the relative tropospheric zenith delay model cannot be fixed correctly at the beginning of

the session. The estimated RZRD values are shown in Figure 4-12. The results indicate that this model can predict the residual tropospheric delay for a newly risen satellite, significantly improve the success rate of ambiguity resolution, and decrease the time required to resolve ambiguities.

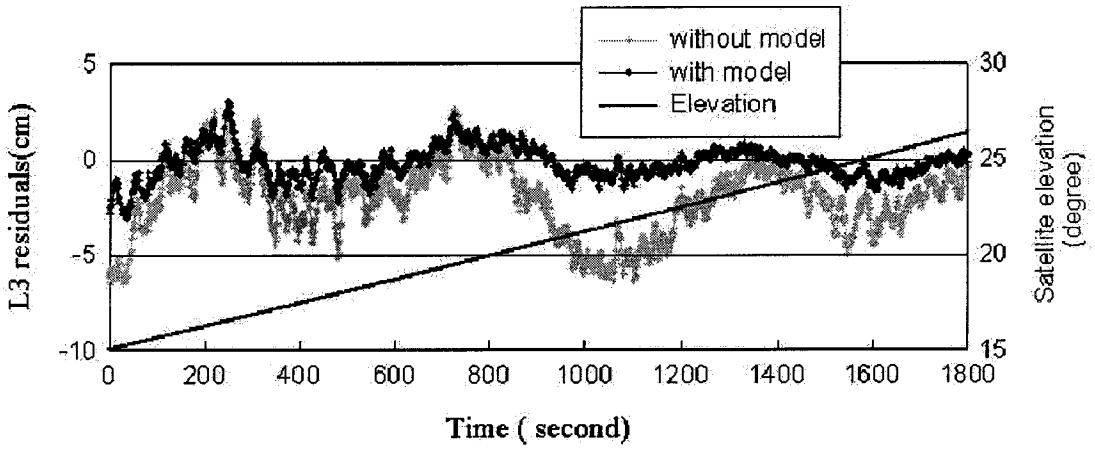

Figure 4-11. Residual tropospheric delay modelling for satellite pair 16-25

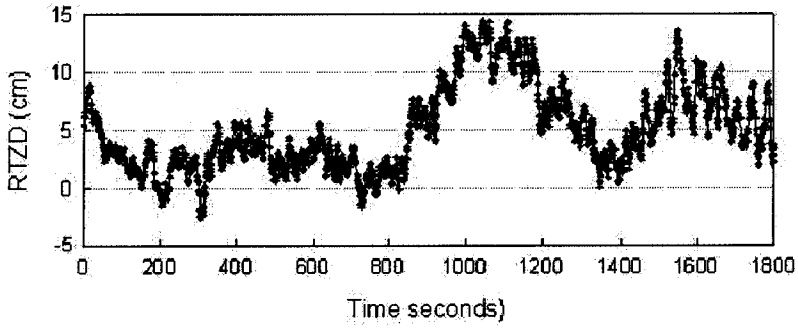

Figure 4-12. Estimated residual tropospheric zenith delay values

The results from the Sydney experiment show that ambiguities can be recovered correctly, after initialisation, using the proposed temporal correlation bias modelling. Because the baseline lengths are not too long, all wide-lane ambiguities except one can be fixed correctly through direct rounding-off of values. But they can be fixed correctly after the residual ionospheric delay model was applied.

4.4.2 Japan: GPS Reference Station Network

To further test the performance of the two proposed senarios, data from one part of the Geographical Survey Institute's (GSI) permanent GPS network in Kyushu, Japan (Figure 4-13) has been analysed. The experimental period was six days from 29 September to 4 October (DoY 272-277) in 1997, logged at a 30 second sampling rate and a cut-off angle of 15°. The approximate distances between the reference stations are 154.4km, 103.5km and 140.2km for #7-#122, #122-#138 and #138-#7 respectively.

Figure 4-14 shows the L1 and L2 residuals for all the satellite pairs, for baseline #7-#122, during the six days from DoY 272 to DoY 277, after the temporal correlation bias model was used. It can be seen that residual errors in L1 and L2 are less than 5cm. Therefore all the cycle slips are easily detected and repaired (in this experiment there were a total of 393 cycle slips that were successfully repaired). It should be emphasised that some L1 and L2 residuals (larger than 5cm) are due to the existence of a long data gap or due to measurement outliers.

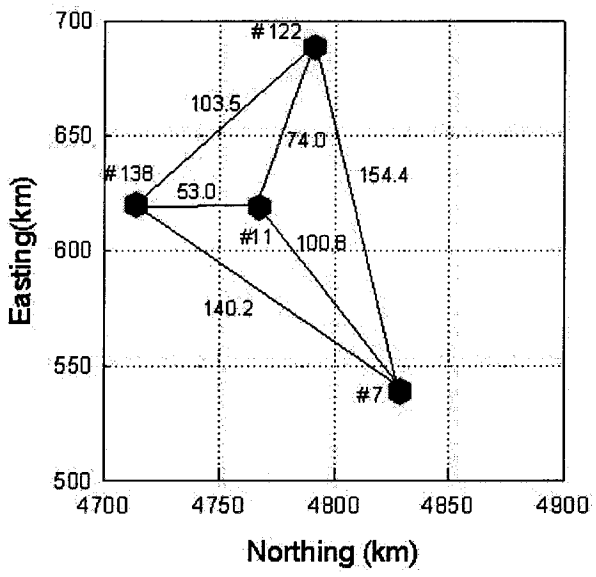

Figure 4-13. Configuration of the GSI reference stations in Kyushu, Japan

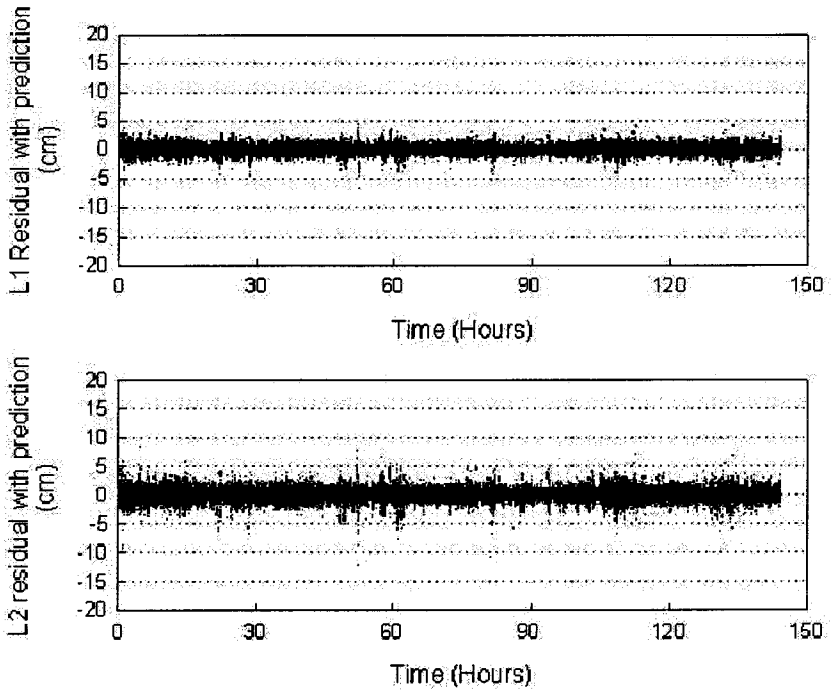

Figure 4-14. L1 and L2 residuals using the proposed temporally correlated bias model

In order to further test the prediction performance of the proposed residual atmospheric modelling procedure for a newly risen satellite, the data from *every* newly risen satellite at the beginning 60 epochs (satellite elevation range from 15°–30°) was analysed. There were 33 satellites rising (out of a total of 25 satellites) on each of the days tested, for the period DoY 272-277, and 8 satellites with two rising times each day.

Figure 4-15 shows the wide-lane residuals, with and without the application of the proposed residual ionospheric models, for every newly risen satellite, for baseline #7-#138 and DoY 272. It can also be seen that all the RMSs larger than 15cm for the wide-lane residuals can be decreased significantly after applying the proposed bias model. However, for some satellites (s4, s5, s7, s16, s18, s31) with smaller RMS values of the wide-lane residuals, the wide-lane residual RMS did increase slightly after the proposed model was applied. It should be emphasised that a slight increase in the RMS of the wide-lane residuals does not have a signifcant effect on wide-lane ambiguity resolution. The average RMS for the wide-lane residuals decreased from about 14.3cm to 9.2cm, an improvement of about 35.5%. In the computation of the wide-lane residual, only residual ionospheric delay modelling was applied.

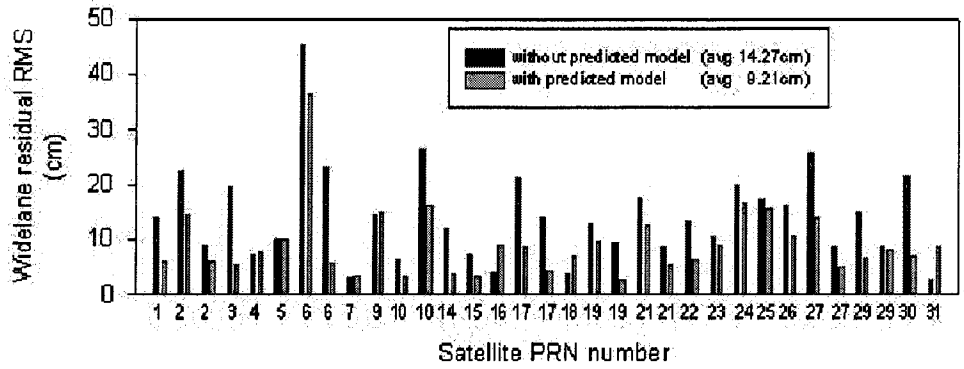

Figure 4-15. Improvement of wide-lane residual RMS, with and without bias modelling

Figure 4-16 shows the RMS of the narrow-lane residuals, with and without the application of the proposed residual tropospheric models, for every newly risen satellite, for baseline #7-#138 and DoY 272. For the residual tropospheric delay modelling, RTZD models without and with weighting using Equation (4-19) have been tested. From Figure 4-16 it can be seen that for most newly risen satellites, after applying the spatial correlation tropospheric delay model with the same weight, the RMS values in the L3 residuals are decreased. However, for some satellites the L3 residual RMS values did increase slightly after the tropospheric model was applied. The average RMS has decreased (for the same weight model) from 6.4cm to 4.9cm, an improvement of about 24%. However, for *every* newly risen satellite the RMS value of the L3 residuals has decreased significantly after the weighted RTZD model was applied. The average RMS value has decreased significantly from 6.4cm to 2.9cm, an improvement of about 54%. Figure 4-16 clearly shows that the weighted TTZD model can give good prediction performance.

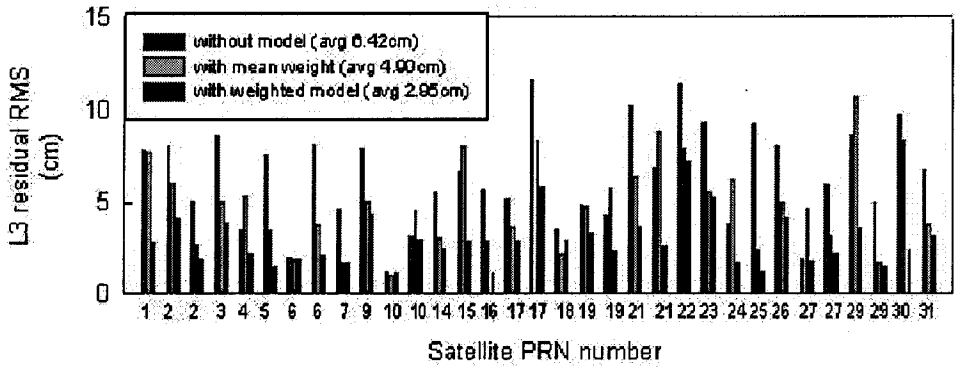

Figure 4-16. Improvement of L3 residual RMS, with and without bias modelling

In this experiment the wide-lane ambiguities were successfully determined using a few epochs of data after applying the linear ionospheric model for newly risen satellites. Figure 4-16 shows the required time-to-fix for the narrow-lane ambiguity for newly risen satellites. It can be seen that when the predicted relative tropospheric zenith delay was applied the required time-to-fix for the ambiguities becomes less. The average time taken without a model is 18.1 minutes. However, this was significantly shortened to 5.5 minutes after the predicted tropospheric delay model was applied. It should be pointed out that for satellite 19 it took almost one hour to fix the ambiguities because the satellite elevation always was quite low (from 15° - 20° - 15°)!

4.5 Concluding Remarks

In this chapter two scenarios for real-time ambiguity resolution appropriate for GPS/Glonass reference station networks have been proposed. The temporal correlation bias model is used to recover ambiguities after initialisation, and spatially correlated residual ionospheric and tropospheric models can aid the resolution of the wide-lane and narrow-lane ambiguities for a newly risen satellite, or after a long data gap. Other associated issues, such as the criterion to fix ambiguities and the different signal frequencies for the Glonass satellites, have also been addressed.

The experimental results show that the temporal correlation bias model can predict the bias for the next measurement epoch and aid instantaneous ambiguity resolution. In the experiment reported here, the average RMS for the wide-lane residuals decreased from 14.3cm to 9.2cm, an improvement of about 35.5%. The average RMS for the tropospheric delay can be significantly reduced, from 6.4cm to 2.9cm, an improvement of 54.%. The average time-to-fix required for the narrow-lane ambiguities can be significantly shortened, in this experiment from 18.1 minutes to 5.5 minutes, after the predicted relative tropospheric zenith delay model was applied.

The conclusion that can be drawn is that the atmospheric delay information derived from other satellites, with fixed ambiguities, can be used to predict the atmospheric

delay for a newly risen satellite, or after a long data gap, and hence aid ambiguity resolution.

Chapter 5

MODELLING ISSUES FOR GPS AND PSEUDOLITE INTEGRATION

5.1 Introduction

In satellite-based positioning, some of the most important factors influencing accuracy and reliability are the number and geometric distribution of the satellites tracked by the receivers. With global navigation satellite systems such as GPS, Glonass and Galileo, four visible satellites are the minimum requirement for three-dimensional positioning. In general, the more satellites that are tracked, the more accurate and reliable the positioning solution. However, in some situations, such as in urban canyons and in deep open-cut mines, the number of visible satellites may not be sufficient to reliably carry out positioning operations.

The geometric distribution of the satellites being tracked will have a significant impact on the accuracy of the estimated position components. It is well known that the horizontal components of the position or baseline component solutions are much better determined than the height component. It is due to systematic errors in height not being compemsated as much as they are in the horizontal components (satellites can be well spread horizontally – but there are never any signal to be received below horizontal).

These two abovementioned problems with space-borne satellite positioning systems can be addressed by the inclusion of additional ranging signals transmitted from ground-based "pseudo-satellites" – also referred to as pseudolites (PLs). Actually, in 1970's, even before the launch of the GPS satellites, pseudolites had been used to test the initial GPS user equipment (Harrington & Dolloff, 1976). In the mid 1980s, the RTCM committee SC-104 ('Recommended Standards for Differential Navstar GPS Service')

designated the Type 8 Message for the pseudolite almanac, containing the location, code and health information of pseudolites (Kalafus et al., 1986). With the development of pseudolite technology and GPS user equipment during the last decade, the pseudolites can now be used to enhance the availability, reliability, integrity and accuracy in a range of applications, such as aircraft landing (Holden & Morley, 1997; Hein et al., 1997), deformation monitoring (Dai et al., 2000b, 2001a), Mars exploration (Lemaster & Rock, 1999), precision approach applications, and others (Barltrop et al., 1996; Dai et al., 2001f; Weiser, 1998; Choi et al., 2000; Wang et al., 2000; Stone & Powell, 1999; O'Keefe et al., 1999).

Compared with satellites in space, pseudolites usually have a great flexibility to be located, which can significantly improve the geometric strength of positioning solutions, particularly for the height component. However, due to the comparatively small separation between pseudolites and receivers (users), there are some challenging issues in modelling that need to be addressed, such as non-linearity, pseudolite location errors, tropospheric delays, multipath and noise. In this chapter, some of these issues will be investigated.

5.2 Modelling Pseudolite Measurements

5.2.1 Pseudolite Measurement Models

The one-way pseudolite observables can be expressed in a similar form to GPS satellite observations.

Pseudo-range:

$$R_k^p = \rho_k^p + c \cdot (t^p - t_k) + T_k^p + O_k^p + mR_k^p + \varepsilon_k^p \tag{5-1}$$

Carrier phase:

$$\phi_k^p = \frac{1}{\lambda_p}\rho_k^p + \frac{c}{\lambda_p} \cdot (t^p - t_k) + N_k^p + \frac{1}{\lambda_p}T_k^p + \frac{1}{\lambda_p}O_k^p + m\Phi_k^p + e_k^p \tag{5-2}$$

where R_k^p and ϕ_k^p are pseudo-range and carrier phase measurements from receiver k to pseudolite p respectively; λ_p is the wavelength of the carrier frequency for pseudolite p; ρ_k^p is the topocentric distance between receiver k and pseudolite p; c is the speed of light; t^p is the pseudolite clock error; t_k is the receiver clock error; N_k^p is the integer carrier phase ambiguity; T_k^p is the tropospheric delay; O_k^p is the pseudolite location error (analogous to 'orbit error'); mR_k^p and $m\Phi_k^p$ are multipath errors, ε_k^p and e_k^p are noise (and unmodelled) errors for the pseudo-range and carrier phase measurements respectively.

It should be emphasised that no terms need to be introduced to account for ionospheric delay for the ground-based pseudolites. This is because pseudolite signal transmitters and the user receiver antennas are both ground-based. Hence the pseudolite signals will not propagate through the ionosphere, which lies approximately between 50km and 1000km above the surface of the Earth. Though the pseudolite equations for carrier phase and pseudo-range are similar to the GPS observation equations, some factors such as the effects of non-linearity ρ_k^p, the pseudolite-location bias O_k^p, tropospheric delay T_k^p and multipath have to be considered carefully in a different way to the GPS observations. These modelling issues are further discussed in the following Sections (5.3 to 5.6).

Because there is the opportunity to optimise the selection of pseudolite signal frequency, a promising approach is to expand on the principles employed by dual-frequency GPS receivers and to develop a multi-frequency system that can instantaneously resolve the ambiguities. A four-frequency pseudolite system which uses two frequencies in the 900MHz ISM band and two in the 2.4GHz ISM band (S-band) has been suggested by Zimmerman et al. (2000). Undoubtedly, multi-frequency pseudolite development will make it more feasible to implement a pseudolite-based positioning and navigation system. On the other hand, the pseudolite power could be very strong relative to the nominal GPS signal power. However, this will cause a signal jamming problem. This issue called Near-Far problem will be discussed in the next section.

5.2.2 Near-Far Problem

GPS receivers are designed to track the GPS satellite signals transmitted at an altitude of about 20200km, and at a large and relatively constant distance from all the user receivers. The power level of these signals received by GPS antennas on the surface of the Earth is very weak (around –130dBm), but relatively constant. This is the 'far-field' situation. The situation with pseudolites is, of course, quite different. Normally, the distance between pseudolites and receivers may be highly variable, of the order of tens, hundreds or thousands of metres. The strong pseudolite signals can cause interference with the GPS satellite signals, and can jam the receivers if they are situated inside the 'near-field' region. Beyond the far-field boundary, the pseudolite signals will be too weak to be tracked by the GPS receivers. Between these near-field and far-field regions is the 'dynamic range' (Cobb & O'Connor, 1998) within which the pseudolite and GPS satellite signals are balanced, and they can both be tracked by a GPS receiver. It is this so-called 'near-far problem' which must be resolved before many pseudolite applications can be satisfied.

The Near-Far Problem limits the coverage area. To overcome this problem, a couple of methods have been developed. The first method is signal 'pulsing'. The RTCM SC-104 has a recommendation on tackling this 'near-far' problem involving the use of the Time Division Multiple Access (TDMA) approach (Stansell, 1986). It recommended that pseudolites transmit pulsed signals at the 10% duty cycle with selected Gold Codes (i.e. 93 code chips), and varying every signal pulse position from millisecond to millisecond such that each of the 11 portions of the Gold Code will be transmitted within a 10-millisecond interval. The second method would be to use a best-fit antenna diagram (Martin, 1999). The type of antenna used would depend on the application and environment. Ibid (1999) suggests that microstrip patch antennas, which provide a uniform spherical pattern, are optimal for small areas, e.g. indoor usage, and high-gain parabolic or helix antennas are suitable for longer-range coverage. Possible reflectors could be excluded by notches in the antenna pattern, or by beam sharpening using different kinds of ground planes.

5.3 Effects of Non-linearity

The use of ground-based pseudolites will have different implications for some aspects of positioning operations. For example, for short baselines, the effects of non-linearity on the measurement equations are negligible for the space-borne satellites, but could be significant in the case of pseudolites on the ground. The reason for this is that pseudolites are much closer to the user receivers than the satellites are.

In positioning applications the key geometric information from the measurements is 'distance' or 'range' between two points, which are generally represented through 'coordinates' or the 'baseline vector' defined in some reference frame. The relationship between the measurements (distances) and the unknown parameters (coordinates or baseline vector) is of course non-linear. Because the estimation techniques for the linear models have attractive statistical properties, the non-linear measurement equations, such as Equations (5-1) and (5-2), are usually linearised using a Taylor series expansion. In GPS data processing, different selection of parameterisation schemes may have different effects on non-linerarity. The non-linerarity effects for two parameterisation schemes (i.e. *rover station coordinates* and *baseline components*) are discussed below.

Consider a function $F(x)$ is expanded into a Taylor series up to the first order:

$$F(x) = F(x_0) + A\delta x + R \tag{5-3}$$

where x_0 is the approximate values for the parameters x; $A = \partial_x F(x_0)$ is the vector of first order partial derivatives evaluated at x_0, which is also called the line-of-sight (LOS) vector; $\delta x = x - x_0$; and R is the second order remainder term expressed as:

$$R = \frac{1}{2}\delta x^T \partial_{xx}^2 F(x_0 + t \cdot \delta x)\delta x,\ 0 < t < 1 \tag{5-4}$$

where $\partial^2_{xx}F(x)$ is the Hessian matrix constructed using the second order partial derivatives. In standard data processing, the remainder term R is ignored, resulting in a non-linearity error in the measurement model. The bounds of this error term are given by (Teunissen, 1987):

$$\frac{1}{2}\lambda_{\min}\cdot\|\delta x\|^2 \le R \le \frac{1}{2}\lambda_{\max}\cdot\|\delta x\|^2 \tag{5-5}$$

where $\lambda_{\min}$ and $\lambda_{\max}$ are the minimum and maximum eigenvalues of the Hessian matrix $\partial^2_{xx}F(x)$. For the distance model:

$$d_{ij} = \sqrt{x_{ij}^2 + y_{ij}^2 + z_{ij}^2}\,, \tag{5-6}$$

where x_{ij}, y_{ij}, z_{ij} are the differences between the coordinates for the two points (i, j) associated with the measurement. The Hessian matrix is:

$$\partial^2_{xx}d_{ij} = \frac{1}{\sqrt{d_{ij}^3}}\begin{bmatrix} y_{ij}^2+z_{ij}^2 & -x_{ij}y_{ij} & -x_{ij}z_{ij} \\ -x_{ij}y_{ij} & x_{ij}^2+z_{ij}^2 & -y_{ij}z_{ij} \\ -x_{ij}z_{ij} & -y_{ij}z_{ij} & x_{ij}^2+y_{ij}^2 \end{bmatrix} \tag{5-7}$$

with the extreme eigenvalues being $\lambda_{\min} = 0$ and $\lambda_{\max} = 1/d_{ij}$. From Equation (5-5), the bounds for the non-linearity error caused by ignoring the remainder term R are:

$$0 \le R \le \frac{\|\delta x\|^2}{2d_{ij}} = \frac{\left(\delta_{x_{ij}}^2 + \delta_{y_{ij}}^2 + \delta_{z_{ij}}^2\right)}{2d_{ij}} \tag{5-8}$$

In integrated GPS-pseudolite positioning, the length of the distances for linearisation may vary from 20000km between GPS satellites and user, and 200m (even as short as a few metres) between pseudolites and user. Figures 5-1 and 5-2 show the linearisation error bounds for these two different lengths.

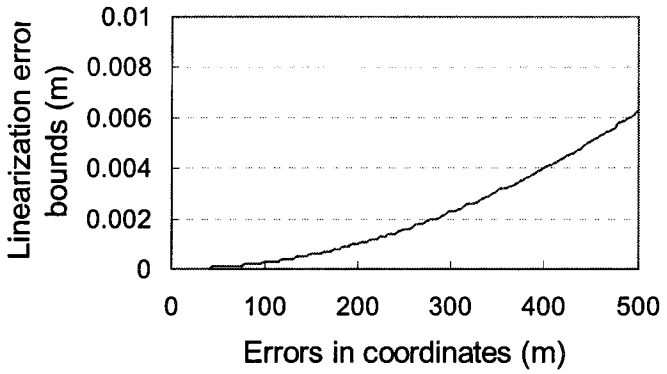

Figure 5-1. Linearisation error for the distance between satellites and user (about 20000km)

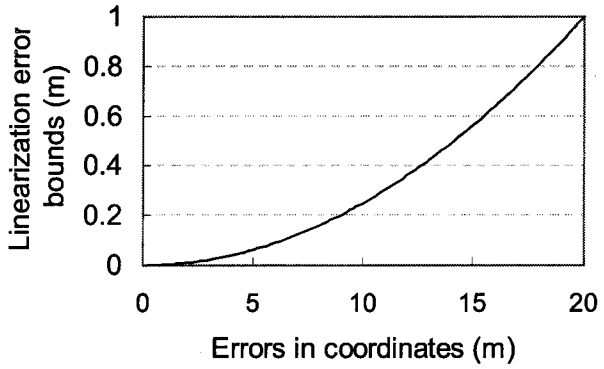

Figure 5-2. Linearisation error for the distance between pseudolites and user (200m)

For distances such as between GPS satellites and users on the ground, the linearisation error for a 200m error in the coordinates is just 1mm, which is clearly negligible. However, when the separation between pseudolites and users is 200m, an error of 15m in coordinates may result in a linearisation error of as much as 0.6m, which is much larger than the phase measurement errors and may lead to divergence of the computation process.

The effects on non-linerarity have been discussed if the coordinates for rover station are processed as the unknown parameters. However, if the baseline vector is chosen as the parameters being estimated (as shown in Equation (5-9)) in data processing, there is a different effect on non-linerarity (Stone & Powell, 1998; Lawrence, 1996):

$$-\overline{e}\Delta\overline{X} = (\Delta\phi + N\lambda) + |\overline{P}|(1-\cos(\theta)) \tag{5-9}$$

where $\overline{e}$ is line-of-sight vector from user to transmitter; $\Delta\overline{X}$ is the baseline vector from user to reference station; $\Delta\phi$ is single-differenced carrier phase measurements; N is the ambiguity; $\overline{P}$ is the distance between pseudolite transmitter and reference station; and θ is intersectional angle between pseudolite and two receivers. Because the wavefronts are planar, a non-linear correction term $|\overline{P}|(1-\cos(\theta))$ needs to be accounted for as shown in Figure 5-3. The approximate error for GPS satellites due to linearisation is:

$$|\overline{P}|(1-\cos(\theta)) = 2\sin^2(\theta/2)|\overline{P}| \cong \frac{|\Delta\overline{X}|^2}{2|\overline{P}|} \text{ where} \left(\sin(\theta/2) \cong \frac{|\Delta\overline{X}|}{2|\overline{P}|}\right) \tag{5-10}$$

For a five kilometre long GPS baseline, this error is approxomately half a metre (Lawrence, 1996). Due to uncertainty in the exact position of the user, the corrected phase will also be in error. It should be noted that Equation (5-10) is not suitable for pseudolite measurments because θ could be very large. It is obvious that for pseudolite measurement processing, the non-linearised errors may become very serious.

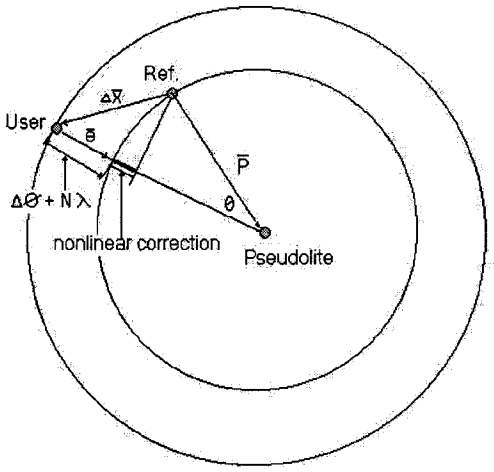

Figure 5-3 Example of pseudolite non-linear correction

The effects of non-linearity have been analysed from a theoretical point of view. The formulas derived in this section show that special attention has to be given to the effects

of non-linearity in pseudolite positioning applications. To prevent this from happening in reality, at the beginning of the Least Squares computation, a large variance for the pseudolite measurements is introduced (Elrod & Van Dierendonck, 1996). In most cases, if multipath effects are not significant, differential pseudo-range solutions will provide the initial coordinates of sufficient accuracy for iterative processing using the non-linear measurements

5.4 Effects of Orbital Errors

The orbit errors, or errors in the coordinates of the phase centres of the transmitter antennas, are one of the major biases in satellite/pseudolite-based positioning. In GPS relative positioning applications, the impact of the orbital errors on baseline length is approximated by the following 'rule-of-thumb' (Bauersima, 1983):

$$\frac{db}{b} = \frac{dr}{r} \tag{5-11}$$

where db is the baseline error; dr is the orbital error; b is the baseline length and r is the distance between satellite and user(s).

Equation (5-11) indicates that, in the case of short-range GPS relative positioning, satellite orbit errors have little impact on the solutions. However, as pseudolites are close to users, the impact of the orbital errors needs more detailed analysis (see, e.g., Hein et al., 1997; Morley, 1997; Wang et al., 2000; Dai et al., 2000b).

Without loss of generality, the relationship between a baseline (AB) and a transmiter antenna (T) can be represented schematically as in Figure 5-4. The distances between T, A and B, are then expressed as:

$$S_A = \sqrt{x^2 + y^2 + z^2} \tag{5-12}$$

$$S_B = \sqrt{x^2 + (y-b)^2 + (z-h)^2} \tag{5-13}$$

If dx, dy and dz are the errors in the coordinates x, y and z respectively, the impact of these errors on the single-differenced (SD) measurement between A and B is:

$$dS_{AB} = dS_{AB}(x) + dS_{AB}(y) + dS_{AB}(z) \tag{5-14}$$

where

$$dS_{AB}(x) = x \cdot (\frac{1}{S_A} - \frac{1}{S_B}) \cdot dx \ , \tag{5-15}$$

$$dS_{AB}(y) = (\frac{y}{S_A} - \frac{y-b}{S_B}) \cdot dy , \tag{5-16}$$

$$dS_{AB}(z) = (\frac{z}{S_A} - \frac{z-h}{S_B}) \cdot dz \tag{5-17}$$

are the model errors caused by the orbital errors dx, dy and dz respecitvely. It is noted from Equations (5-15), (5-16) and (5-17) that these model errors are geometry-dependent. For instance, if $S_A = S_B = S$:

$$dS_{AB}(x) = 0 ; \tag{5-18}$$

$$dS_{AB}(y) = \frac{b}{S} \cdot dy ; \tag{5-19}$$

$$dS_{AB}(z) = \frac{h}{S} \cdot dz . \tag{5-20}$$

In this situation, whilst the term dx causes no model errors, the impact of terms dy and dz on the measurement model are inversely propotional to S (the separation between the transmiter and the user), and are proportional to b (horizontal baseline distance) and

h (the baseline height difference). If the height difference is equal to zero ($h = 0$), then $dS_{AB}(z) = 0$. In such an event the 'rule-of-thumb' at Equation (5-11) is identical to Equation (5-19). Therefore Equation (5-11) is a special case of Equation (5-14), which provides a general tool for analysing the impact of orbital errors on the (SD) measurement models.

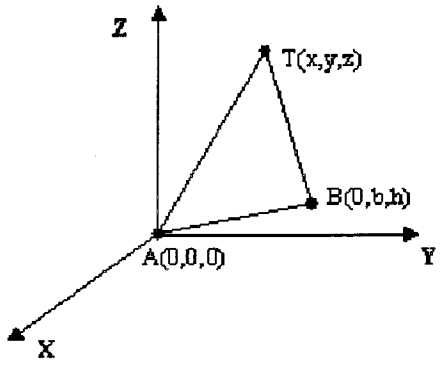

Figure 5-4. Set-up of the baseline (AB) and the transmitter (T)

In some situations, the geometric relationship between pseudolite transmitter and users is quite different from that for the satellite transmitters and users. Hein et al. (1997) and Morely (1997) discuss two special set-ups for the pseudolite and users, as illustrated in Figure 5-5. These set-ups can be analysed using Equation (5-14).

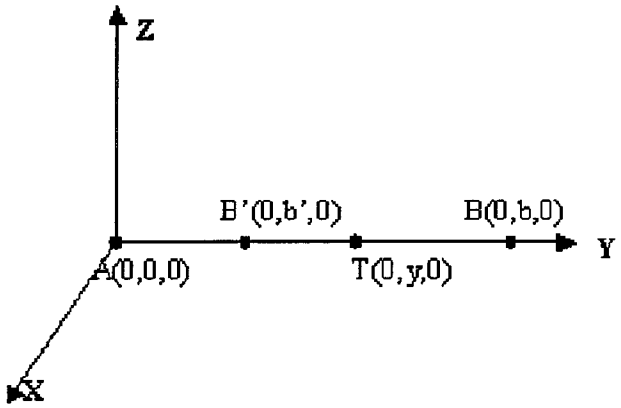

Figure 5-5. Special set-ups for the pseudolite and baselines

In the case of the baseline AB, $y = S_A$ and $S_A + S_B = b$. Then, from Equation (5-16) $dS_{AB}(y) = 2 \cdot dy$, which means that the single-differencing procedure doubles the size

of the orbital error in the Y axis direction in the measurements. However, for the baseline AB', since $S_A - S_B' = b'$, $dS_{AB'}(y) = 0 \cdot dy$, indicating that orbital error in the Y axis direction is cancelled out in differencing. However, the impact of the orbit errors in the X and Z axis directions is different from the Y axis direction. Figures 5-6 and 5-7 show an example of the influence of a 5cm pseudolite location error on single-differenced observables in the two special user locations (B and B'), as shown in Figure 5-5. It can be seen from Figure 5-6 that the effects of the 'orbit errors' are different for different elevation and azimuth related to the mobile pseudolite location T. In the worse case, for the user location B, the influence of the pseudolite 'orbit error' on the differenced range becomes doubled. However, in the best case, the pseudolite 'orbit error' can be reduced significantly and ignored after single-differencing. It can also be seen from Figure 5-7 that for the user location B' the influence of pseudolite 'orbit error' is so small (less than 2μm) after single-differencing that they can be ignored. Therefore, the conclusion can be made that the pseudolite location errors can significantly bias the precise carrier phase observations in some cases, even though they are only of the order of a few centimetres in magnitude.

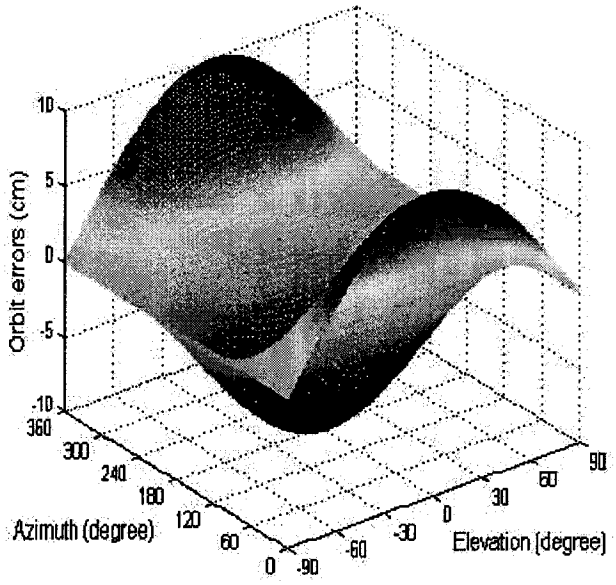

Figure 5-6 Influence of 5cm pseudolite location bias on the user location B

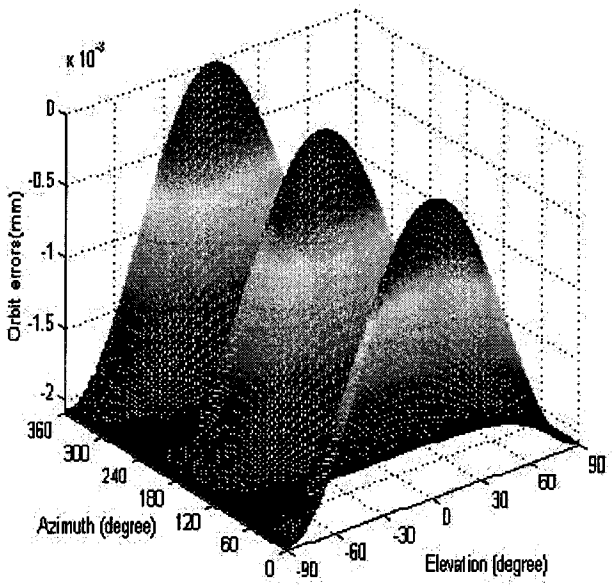

Figure 5-7. Influence of 5cm pseudolite location bias on the user location B'

In the worst case, the influence of the pseudolite-location bias on the differenced range becomes doubled. Good selection of pseudolite location can mitigate the effect of the bias. Due to the pseudolite being stationary (unlike the moving GPS satellites) the pseudolite-location bias will be a constant. If the reference and mobile receiver are both stationary, orbit error will contribute an invarant bias to the differenced observables. The constant (or very near invariant) bias can be predicted and removed for some applications, such as deformation monitoring. It should be emphasised that for kinematic applications, the pseudolite location should be precisely determined beforehand, using GPS surveying, 'total station' or other traditional surveying techniques.

5.5 Pseudolite Tropospheric Delay

For GPS signals, a simple way to compensate for the tropospheric delay is to apply a model to derive the delay, such as the Saastamoinen, Hopfield, or Black models. The delay derived from all of these models is very dependent on the satellite elevation angle, and only suitable for satellites in space. The standard tropospheric models can not be

used to compensate for pseudolite tropospheric delay. This is because the model parameters are designed for signals from GPS satellites, more than 20000km away.

Hein et al. (1997) has proposed a simple troposphere model that can be used to compensate for pseudolite tropospheric delay, where the refractivity n at the base of the atmosphere is described as a function of the meteorological parameters:

$$N = (n-1)\cdot 10^6 = 77.6\frac{P-e}{T} + 71.98\frac{e}{T} + 3.75\cdot 10^5 \frac{e}{T^2} \tag{5-21}$$

where P is the air pressure in hectopascals, e is partial pressure of the water vapour in hectopascals, and T is the absolute temperature in degrees Kelvin. The partial pressure of the water vapour can be calculated via the relative humidity (RH):

$$\mathrm{e} = \mathrm{R}H\cdot\exp(-37.2465 + 0.2133\mathrm{T} - 2.569*10^{-4}\mathrm{T}^2) \tag{5-22}$$

If the meteorological parameters can be assumed the same, the tropospheric delay after between-receiver single-differencing can be represented by (Dai et al., 2000c):

$$\Delta\delta_{trop} = (77.6\frac{P}{T} + 5.62\frac{e}{T} + 375000\frac{e}{T^2})10^{-6}\Delta\rho \tag{5-23}$$

where $\Delta\rho$ is the difference in geometric ranges between the pseudolite transmitter and the two receivers. For the standard meteorological parameters (P=1013mPa, T=20°, RH=50%), from Equation (5-23), the tropospheric delay correction can reach 320.5ppm (32.05cm per km). The influence of the tropospheric delay is shown in Figure 5-8. It can be seen that the pseudolite tropospheric delay can reach up to 600ppm under some weather conditions. Similar conclusions have been drawn by Hein et al. (1997). It is obvious that local weather conditions have a significant effect on the magnitude of the correction. Barltrop et al. (1996) suggests that the local refractivity should be estimated as a slowly varying parameter using the pseudolite measurements. Equation (5-23) indicates that if the pseudolite site can be located with the differences $\Delta\rho$ as small as possible, the tropospheric error can be significantly reduced.

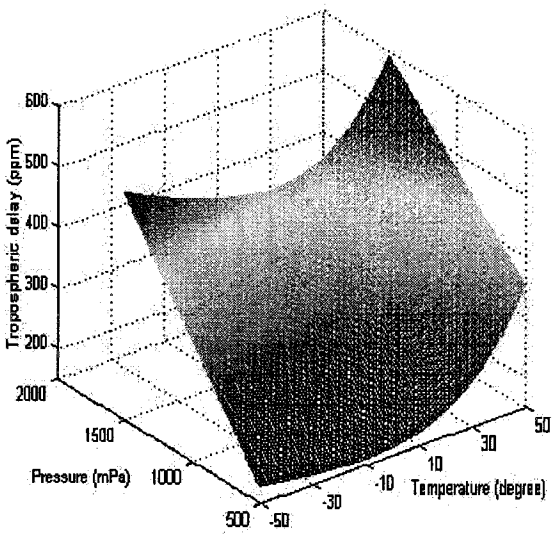

Figure 5-8. Pseudolite tropospheric delay with 50% RH

5.6 Pseudolite Multipath and Noise Level

5.6.1 Pseudolite Multipath

If one or more reflected signals arrive at the receiver antenna in addition to the direct signal, multipath will be present in both the code and carrier measurements. The effect of multipath on code observations is two orders of magnitude larger than on the carrier phase observations. The theoretical maximum multipath bias that can occur in pseudo-range data is approximately half a chip length of the code, that is, 150m for C/A code ranges and 15m for the P(Y) code ranges (Rizos, 1996). Typical errors are much lower (generally <10m). The carrier phase multipath for one-way measurements does not exceed about one-quarter of the wavelength (5-6cm for L1 or L2) (Rizos, 1996)

Compared with multipath from GPS signals, the pseudolite multipath has some peculiar characteristics. The multipath from pseudolites is not only due to reflected signals from surfaces, but also from the pseudolite transmitter itself (Ford et al., 1996). Bartone (1999) has shown that the standing-wave multipath in an airport pseudolite ground-to-ground link can essentially be eliminated by the use of a Multipath-Limiting-Antenna for both the pseudolite transmission and reception antennas. If the pseudolite and

receiver are both stationary, the multipath bias will be a constant. Hence, the influence of multipath from pseudolites cannot be mitigated and reduced to the same extent over time as in the case of GPS. Therefore the multipath will significantly increase the noise level of the measurement in a dynamic environment. An example of pseudolite multipath in a static environment is shown in Figures 5-9 and 5-10. The mean value and standard deviation for the pseudo-range data are -1.25m and 0.21m respectively, and for the carrier phase are -0.105 cycles and 0.008 cycles respectively. It can be clearly seen that the influence of multipath remains at significant levels. Furthermore, it is very hard to avoid, even though precautions may have been taken. However, because of the constant characteristics of the multipath from a pseudolite transmitter in a static environment, it is relatively easy to calibrate in advance. The constant (or very near invariant) bias can be predicted and removed during data processing, or can be estimated together with other unknown parameters. Therefore, pseudolite signals can, in principle, make a contribution to improving the performance for some static applications such as deformation monitoring.

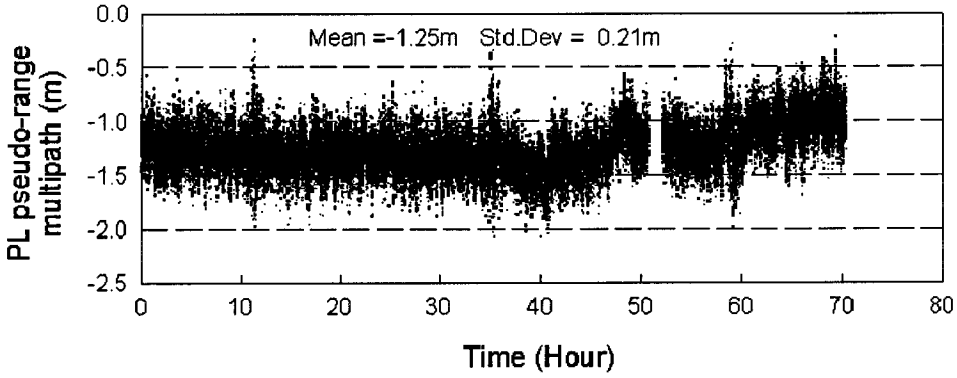

Figure 5-9. Multipath influence on the double-differenced pseudo-range

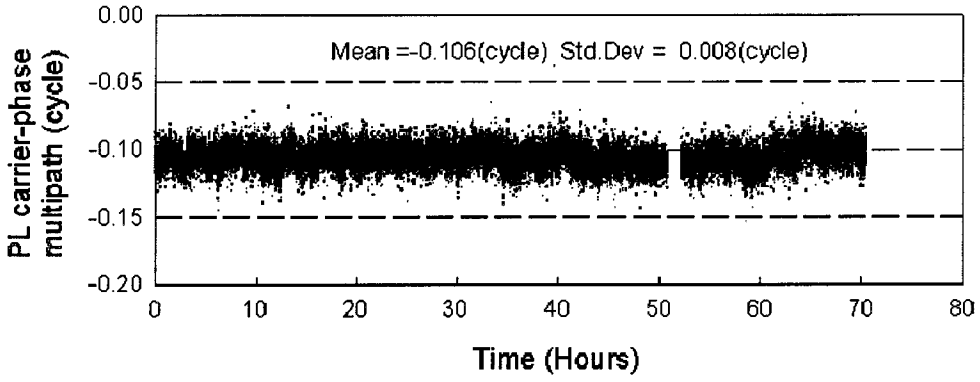

Figure 5-10. Multipath influence on the double-differenced carrier phase

Pseudolite multipath is a challenging issue that needs to be addressed for kinematic applications. Good hardware design, including receivers, receiver antennas and pseudolite transmitter antennas, as well as software-based multipath mitigation techniques will be needed.

5.6.2 Pseudolite Noise Level

A zero-baseline test was carried out on 14 March 2000 to evaluate the quality of the pseudolite carrier phase and pseudo-range measurements under ideal conditions. The influence of multipath, pseudolite-location bias and atmospheric errors on the differenced observable is cancelled completely.

A total of 30 minutes of data were collected using two NovAtel GPS receivers and one IN200CXL pseudolite, with a 1Hz-sampling rate. GPS satellite PRN29, with the highest elevation angle, was selected as the reference satellite. The double-differenced carrier phase and pseudo-range residuals for pseudolite PL32 and GPS satellite PRN31 have been plotted in Figures 5-11 and 5-12. From Figure 5-11 the standard deviations of the pseudo-range residuals for the transmitter pairs PL32-PRN29 and PRN31-PRN29 are 0.11m and 0.08m respectively. It can be seen that only small biases (0.02m and 0.01m) exist in the residual errors. Figure 5-11 also shows that the quality of the pseudolite pseudo-range data is almost the same as for GPS pseudo-range measurements. From Figure 5-12 the standard deviations of the carrier phase residuals for the transmitter pairs PL32-PRN29 and PRN31-PRN29 are 1.3mm and 0.8mm respectively. It can be

seen that only small biases (-0.03mm and -0.01mm) exist in the residual errors. Figure 5-12 also shows that the quality of the pseudolite carrier phase data is as almost the same as for GPS measurements.

The zero-baseline experiment shows that the pseudolite, as a 'satellite-on-the-ground', can provide similarly high quality observations as a GPS satellite. Hence it is, in principle, possible to improve the performance of a GPS-based positioning system using pseudolite data. It should be noted that in the case of pseudolite measurements, it would not be appropriate to weight the pseudolite measurements by their elevation angles because they may not be less reliable in quality than the GPS measurements taken at higher elevation angles.

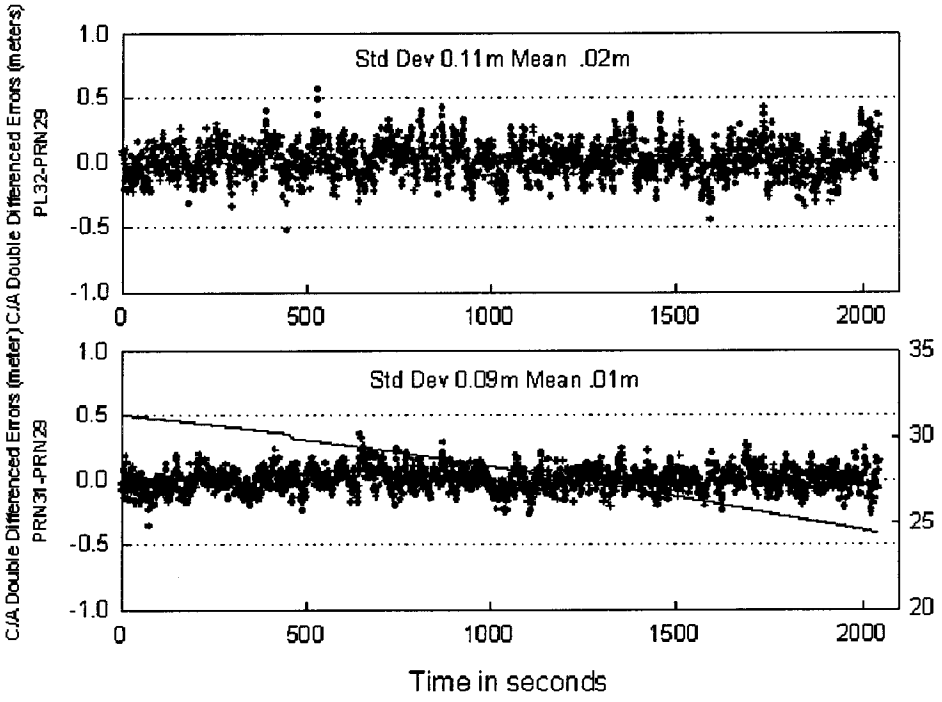

Figure 5-11 Noise level of the double-differenced pseudo-range

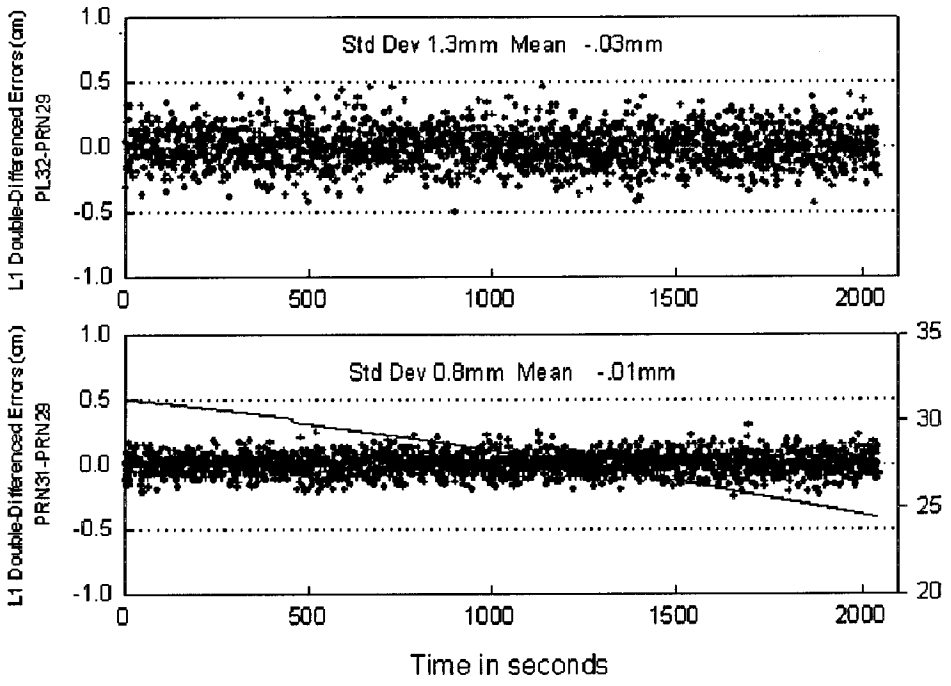

Figure 5-12 Noise level of the double-differenced carrier phase

Another issue that needs to be addressed is the effect of additional pseudolite signal(s) on ambiguity resolution. Pseudolite signals can aid the algorithm to resolve the carrier phase ambiguity quickly and reliably in the moving receiver case. This is because the line-of-sight vector between epochs changes by a large angle, which results in a well-conditioned matrix of ambiguity parameters. If the observation takes place in a static environment, pseudolite ambiguities maybe need to be resolved with the help of GPS observations, or other external sensor observations.

5.7 Concluding Remarks

The reliability and accuracy of satellite-based positioning are very dependent on both the number of visible satellites and their geometric distribution. The integration of pseudolite and GPS signals is one of the options for improving system performance, particularly in poor operational environments.

In this chapter, modelling issues for GPS and pseudolite integration such as non-linearity, pseudolite location errors, tropospheric delays, multipath and noise, have been

discussed. The effects of non-linearity, orbit errors and tropospheric delay on pseudolite use have been analysed from a theoretical point of view. The formulas derived in this chapter show that special attention has to be given to these error sources within pseudolite positioning applications. The experimental results have shown that the noise level of the PL carrier phase measurements is comparable with, or even lower than, that of GPS measurements. However, the mitigation of the (unmodelled) systematic errors identified in the PL measurements, such as multipath, is a challenging issue for kinematic applications.

Chapter 6

PSEUDOLITE APPLICATIONS FOR PRECISE POSITIONING AND NAVIGATION

6.1 Introduction

Due to the high precision of the carrier phase measurements, the GPS technology has been widely used for geodetic applications such as measuring crustal motion, for geodetic engineering applications such as monitoring ground subsidence and the deformation of man-made structures such as bridges, dams and buildings, and a wide range of other engineering survey applications (e.g. Dai & Liu, 1998; Ashkenazi et al, 1998; Behr et al, 1998; Moore et al, 2000). As is well known, the accuracy, availability, reliability and integrity of the GPS positioning solutions is heavily dependent on the number, and geometric distribution, of the satellites being tracked. However, in some situations, such as in urban canyons, in deep valleys and in open-cut mines, the number of visible satellites may not be sufficient to reliably determine precise coordinates. Furthermore, it is impossible to use GPS for indoor positioning applications. On the other hand, due to limitations of the GPS satellite geometry, the accuracy of the height component is generally 2 or 3 times worse than the horizontal components. These factors make it difficult to address GPS positioning applications in areas where the number of visible satellites is limited or satellite geometry is poor, especially where high accuracy height component determination is required. Therefore, in order to improve the performance of GPS-only positioning systems, the integration of GPS with other technologies has been extensively investigated. Some well known examples include the integration of GPS with Glonass, and the integration of GPS and inertial navigation systems.

Pseudolites, which are ground-based transmitters of GPS-like signals, can significantly enhance the satellite geometry, and even replace the GPS satellite constellation in some circumstances. In this chapter, three configurations of pseudolites for precise positioning and navigation are discussed. They include *GPS and pseudolite integration*, *indoor pseudolite-only system*, and *pseudolite 'inverted' positioning*. Several potential applications of pseudolite positioning systems have been identified, including deformation monitoring and navigation services based on pseudolite installed on stratospheric airships. Some experiments have been carried out using NovAtel GPS receivers and IntegriNautics IN200CXL pseudolite instruments.

6.2 Three Configurations for Pseudolite Positioning Systems

There are three general pseudolite configurations for precise positioning.

6.2.1 Integrated GPS and Pseudolite System

An integrated GPS and pseudolite positioning system would be suitable for such environments as urban canyons, deep valleys and open-cut mines, where the number of visible satellites is limited, the geometry is poor, and/or high precision height monitoring is needed. Applications with implementation constraints such as solution reliability and availability can be addressed by the pseudolite augmentation of GPS. The additional pseudolite signal(s) can significantly enhance the performance of the GPS system in a number ways, including reducing the dilution-of-precision (DOP) and improving the accuracy, integrity, availability and reliability of the solution results. The general configuration of such a system is indicated in Figure 6-1.

The geometry of the 'satellite constellation' can be improved by the careful selection of the pseudolite location(s). In the case of GPS, the measurements with low elevation angles are usually rejected in order to avoid serious multipath, tropospheric delay and ionospheric bias. However, this is not necessary in the case of pseudolites. For example, in one experiment (described later in this chapter), the quality of the measurements with less than half-degree elevation angle (from the pseudolite transmitter to the GPS

receivers) is still very high. Therefore, high quality pseudolite measurements with low elevation angles, when included in data processing, can be expected to significantly improve the ambiguity resolution performance and solution accuracy, especially for the height component. The availability is also increased because a pseudolite provides an additional ranging signal to augment the GPS constellation. More measurements make it easier to isolate outliers in the carrier phase measurements, and hence this enhances the system reliability. Furthermore, the number of pseudolites can be configured according such criteria as the accuracy requirement, system cost considerations and environmental conditions.

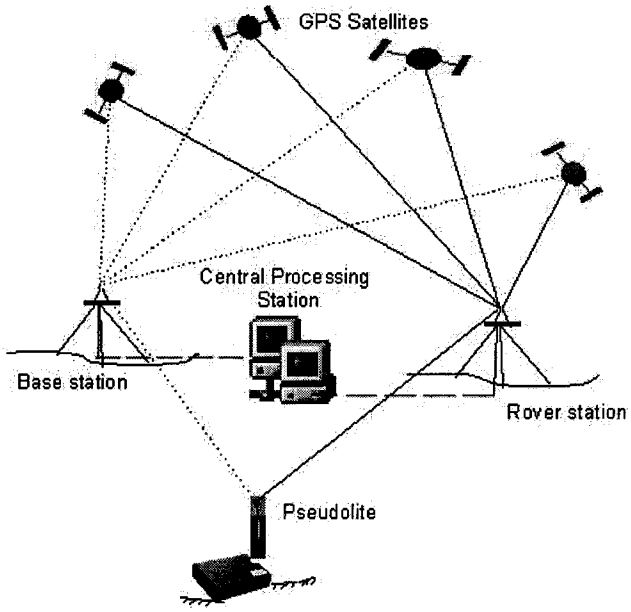

Figure 6-1. Configuration of an integrated GPS and pseudolite system

6.2.2 Pseudolite-Based Positioning Systems

As is well known, GPS techniques cannot be used when the signals are completely blocked by obstacles, natural and man-made. However, monitoring of man-made structures may be needed in areas such as canyons, underground or in tunnels. In these situations, GPS-only positioning becomes difficult, even impossible. However, pseudolite arrays, in principle, can completely replace the GPS satellite constellation, as shown in Figure 6-2. This can extend the concept of 'satellite-based' positioning

indoors, for applications in tunnels or underground, where GPS satellite signals cannot be tracked.

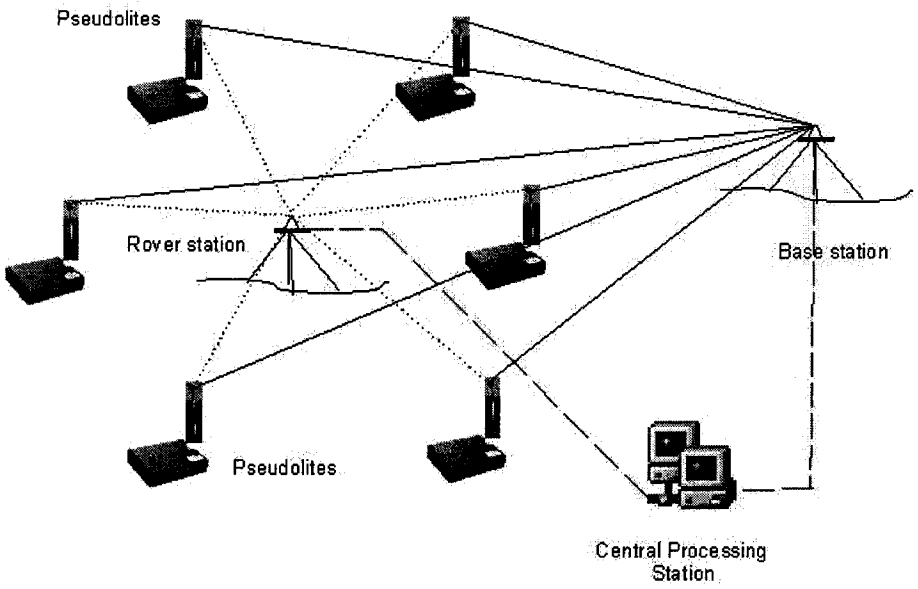

Figure 6-2. Configuration of a pseudolite-based positioning system

In the case of an indoor pseudolite-based positioning system, the pseudolite transmitters can be placed at arbitrary locations. Therefore, the pseudolite geometry can be optimally designed in advance so that the best results can be obtained (this is discussed in Section 6-4). According to the different requirements of the applications, different design scenarios can be considered. For example, in order to monitor ground subsidence, the monitoring system scenario may consist of only two receivers and two pseudolites. In this system, one double-differenced carrier phase observable can be used to derive the height deformation if the constraint of no horizontal deformation is applied. Furthermore, due to the potentially low cost of pseudolite instruments (expected to be of the order of a few thousand dollars when produced in commercial quantities), many more pseudolites can be used in the system design. The transmitted frequency can also be selected so that it is optimal for the particular situation. In a pseudolite-based positioning system, all the instruments, including receivers and pseudolites, are under user control, unlike the case with GPS. Hence, users have more options.

In a pseudolite-based positioning system, if receivers and pseudolites are both stationary, the geometry doesn't change with time. Therefore ambiguity resolution becomes a big issue. The simple way to overcome this problem in the case of deformation monitoring applications is to use the precise initial coordinate of the pseudolite to 'round off' the ambiguity. However, for some deformation monitoring applications with large displacements, such as following an earthquake or landslide as well as kinematic applications, this will significantly degrade the system performance. Because there is the opportunity to optimise the selection of pseudolite signals, a promising approach is to expand on the principles employed by dual-frequency GPS receivers and to develop a multi-frequency system that can instantaneously resolve the ambiguities. A four-frequency pseudolite system which uses two frequencies in the 900MHz ISM band and two in the 2.4GHz ISM band (S-band) has been suggested by Zimmerman et al. (2000). Undoubtedly, multi-frequency pseudolite development will make pseudolite-based positioning much more feasible.

6.2.3 Pseudolite 'Inverted' Positioning Systems

The last scenario involves a pseudolite-based *inverted* positioning system, where a fixed 'constellation' of GPS receivers with precisely known coordinates tracks a mobile pseudolite. The concept of inverted pseudolite positioning was first suggested by Raquet et al. (1995). In their study, a ground-based test was conducted to investigate the feasibility of using mobile pseudolites for the precise positioning of military aircraft. O'Keefe et al. (1999) and Dai et al. (2001d, 2002b) presented experimental results and discussed the pseudolite-based inverted GPS concept for local-area positioning.

The system consists of an array of GPS receivers, the reference pseudolite (or GPS reference satellite) and the mobile pseudolite. There are two configurations for an inverted positioning system (Figure 6-3), where the only difference is whether a pseudolite is selected as the 'reference' (referred to here as type I configuration), or a GPS satellite is selected as the 'reference' (referred to here as the type II configuration). The reference satellite, or pseudolite, is needed in order to form double-differenced observables, and to eliminate the GPS receivers' clock biases, as well as mitigate other code and phase biases. It should be emphasised that both the type I&II configurations

have the same dilution-of-precision (DOP) factor because the DOP value is only a function of the relative locations of the mobile pseudolite and GPS receiver array. In this system, the central computer can download the pseudolite and/or the GPS measurements, and generate the mobile pseudolite positioning information in real-time.

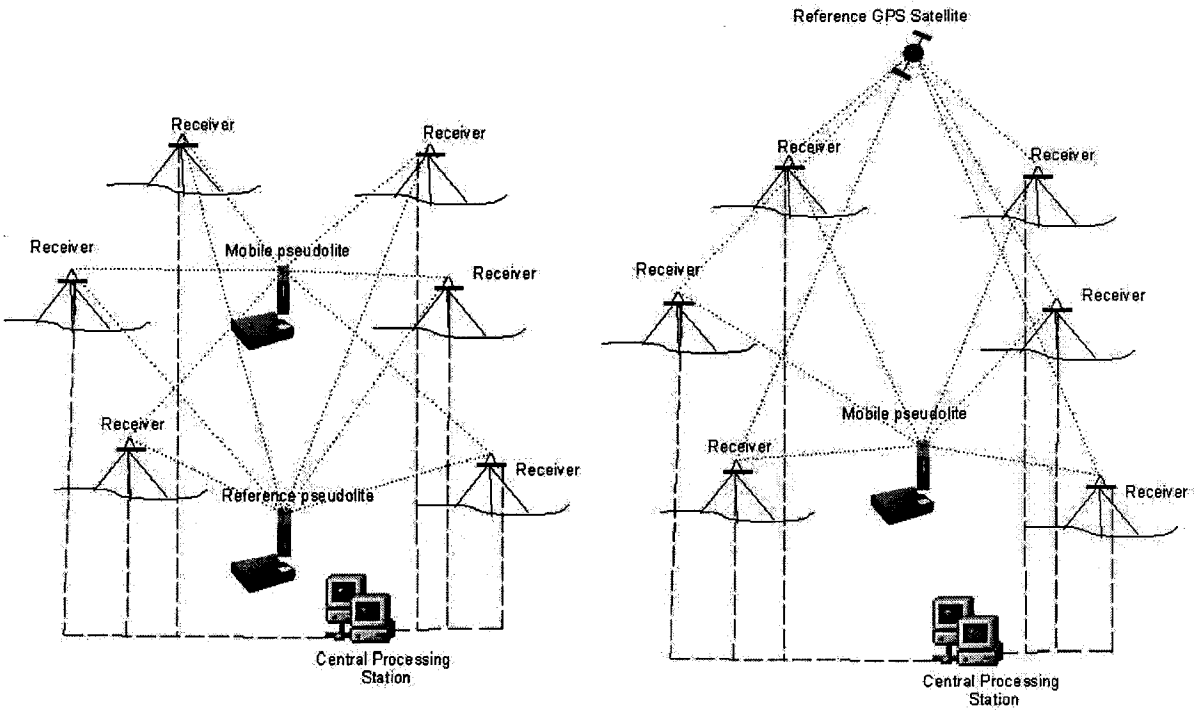

Figure 6-3. Inverted pseudolite positioning configurations
(Left: two pseudolites, and Right: a pseudolite and a GPS satellite)

There are different advantages and disadvantages for the two configurations. In the type I configuration, orbit error and atmospheric delay bias related to the GPS reference satellite are insignificant and can be ignored, particularly in the case of short distances between the GPS receivers. However, in the type II configuration these errors, related to the reference pseudolite, may be significant because of the short distances between reference pseudolite and GPS receivers. Their influence will be discussed in the next section. The type I configuration can overcome the limitations of 'satellite-based' positioning indoors, for applications in tunnels or underground, where GPS satellite signals can not be tracked. Furthermore, all the hardware equipment and software are configured on the ground, where the power, size and computational load constraints can be easily resolved. However, in the type II configuration, one GPS satellite in view is

selected as the reference, and hence reduces the overall system cost. It is suitable for some applications in urban canyons, dam monitoring in valleys and in deep open-cut mines, where the number of visible satellites may not be sufficient to reliably determine coordinates. Furthermore, in the type II configuration, GPS satellite time can be used to synchronise the GPS receivers to within one millisecond. System time synchronisation needs to be addressed in the type I configuration.

Applications with implementation constraints such as solution reliability and availability, and severe design constraints such as space and weight could be addressed by a pseudolite-based inverted positioning system. In such a system, flexibility is increased and cost is reduced because all the hardware equipment and software are configured on the ground, where the power, size and computational load constraints can be easily resolved. Furthermore, the whole system may be able to operate in the presence of jamming at GPS frequencies.

6.3 Potential Applications of Pseudolite-Related Positioning Systems

Based on the aforementioned pseudolite positioning configurations, some applications – deformation monitoring and navigation services based on pseudolite installed on stratospheric airships – have been investigated.

6.3.1 Deformation Monitoring

As is well known, GPS techniques can not be used when the signals are completely blocked. Therefore, the monitoring of structures by GPS-only techniques becomes difficult in such cases. The potential deformation monitoring applications using the pseudolite positioning configurations have been investigated by Dai et al. (2001a, 2002a). This can extend the concept of 'satellite-based' deformation monitoring indoors, where GPS satellite signals cannot be tracked. In practice, constant systematic biases from multipath and the 'orbit' errors can be calibrated beforehand.

6.3.2 Navigation Services Based on Pseudolites Installed on Stratospheric Airships

Feasibility studies and R&D projects concerning high altitude platform systems are being conducted in a number of countries. Japan has been investigating the use of an airship system that will function as a stratospheric platform (altitude of about 20km) for applications such as environmental monitoring, communications and broadcasting. Remote sensing from such an airship would be very effective because it floats above the same ground area, permitting continuous monitoring of the surface. However, the precise positioning of the airship is one of the most important technical challenges for such a project. If the pseudolite transmitter is installed on the underside of the airship, its position can be precisely determined by the receiver array on the ground using the inverted positioning method (Tsujii et al., 2001). In addition, the pseudolites could be considered as additional GPS satellites, which would improve the accuracy, availability, and integrity of GPS-based positioning systems.

6.4 Geometric Analysis

In the case of pseudolite-only or hybrid pseudolite-GPS positioning systems, there are different issues that need to be addressed vis-a-vis GPS-only systems. Systematic biases such as multipath, atmospheric delay effects and pseudolite/receiver location-dependent biases need to be considered in a different way (see Chapter 5 for more details). Another important issue that needs to be addressed is the optimisation of the locations of the pseudolites (and receiver array).

It is well known that pseudolites can be used to improve the geometric strength of positioning solutions, particularly for the height component. Pseudolite location with respect to the mobile receiver will be critical. In practice, constraints that GPS satellite signals may be blocked need to be considered. Optimisation of the pseudolite location is therefore necessary. 'Geometric optimisation' refers to the need to find locations for the pseudolite transmitters that will minimise the Position DOP (PDOP), Relative Position DOP (RDOP) or other similar factors (in this chapter, RDOP is used).

Two cases of geometric optimisation are investigated below, which include pseudolite location optimisation for GPS augmentation by pseudolite, and pseudolite (receiver) array optimisation for a pseudolite-based (inverted) positioning system.

6.4.1 Augmentation of GPS with Pseudolites

To optimise pseudolite location, a simulation has been carried out with the following characteristics. Cut-off angle 15°, 10° pseudolite elevation angle with respect to mobile receiver and the constraint has been assumed that all the satellites lie in the azimuth range from 100° to 150°, and elevation angles less 25° will be rejected.

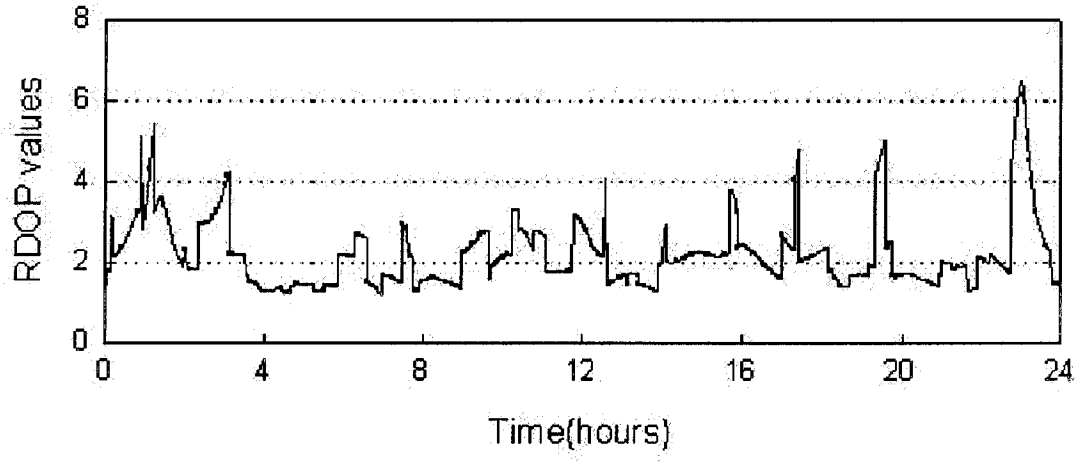

Figure 6-4. 24-hour RDOP values at UNSW, 24 April 2000, without pseudolite

Figure 6-4 shows the 24-hour the RDOP values at UNSW, on 24 April 2000, without a pseudolite. It can be seen that RDOP values are larger than 2 most of the time, and sometime up to 6. Figure 6-5 is a plot of the 24-hour RDOP values when one pseudolite is assumed deployed, but with varying azimuth from 0° to 360°. It can be seen from Figure 6-5 that RDOP values are still very large if the pseudolite were located in the azimuth band 240° to 360°, or from 0° to 60°. However, very good RDOP (less than 2) values can be achieved if the pseudolite were located in the azimuth band 60° to 240°. It is obvious that different pseudolite locations can change the geometry significantly. It should be emphasised that the constraints rejecting all the satellites with azimuth

between 100° and 150°, and elevation angle less 25° has been assumed. Intuitively, pseudolites should be located in azimuth sectors where GPS satellite signals are blocked.

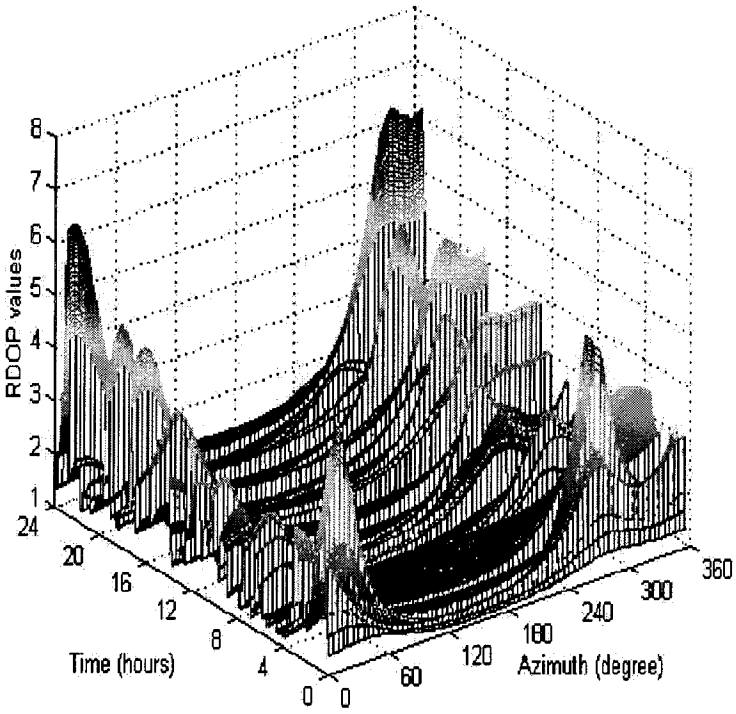

Figure 6-5. 24-hour RDOP values at UNSW, 24 April 2000, with one pseudolite

6.4.2 Pseudolite-based (Inverted) Positioning

In terms of geometric optimisation, there is no significant difference between pseudolite-based positioning and inverted positioning. Hence, the following discussion is focused on inverted pseudolite positioning only. 'Geometric optimisation' refers to the process of finding locations for the receiver array and the pseudolite transmitter that will minimise the RDOP. Poor geometry of GPS receiver arrays was investigated by Pachter & Mckay (1998). If the receiver array and pseudolite transmitter all lie approximately in the one plane, or the LOS vectors drawn from the pseudolite transmitter to the receivers have similar angular orientations (i.e. the pseudolite transmitter is very far away from the receiver array, in the same direction), poor geometry will result. Therefore the measurement errors as mapped into the estimated coordinates will be greatly amplified.

The results of a computer simulation showing the minimum RDOP values as a function of the number of receivers are plotted in Figure 6-6 (after the constraint that the receiver elevation angle related to the mobile pseudolite cannot be less than 0° is applied). It can be seen that the RDOP values will reduce as the number of receivers increases. For a four-receiver array, the minimum RDOP values can still reach 1.63. The simulation also shows that if the receivers are equally spaced in the horizontal plane, and at a zero elevation angle relative to the mobile receivers, and one receiver is at the zenith, the minimum RDOP value is obtained. Figure 6-7 shows the optimal configuration in the case of a four-receiver array. R1-R4 indicates the location of the four receivers, and the mobile pseudolite is indicated as PL. Figure 6-8 shows the minimum RDOP values as a function of the elevation cut-off angle for a four-receiver array configuration. It should be emphasised that very good geometry can still be obtained (RDOP value less than 3) even though the cut-off angle is up to 30°. This means that there is considerable flexibility when considering receiver array optimisation.

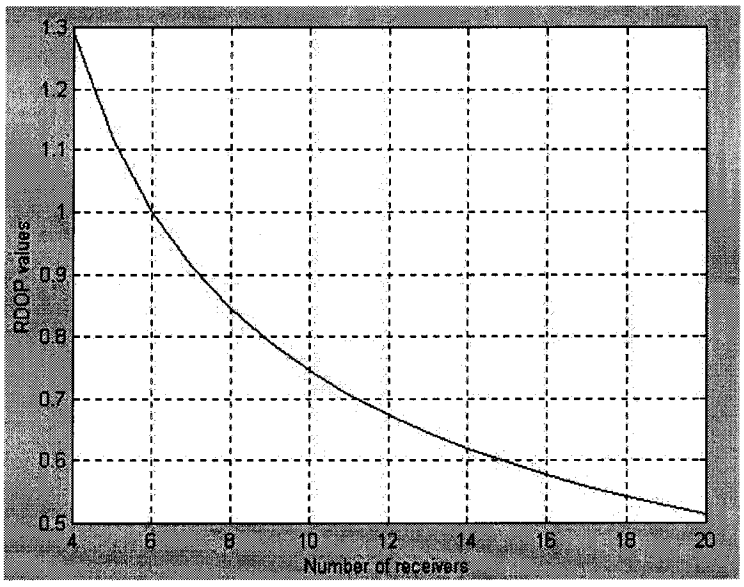

Figure 6-6. Minimum RDOP values

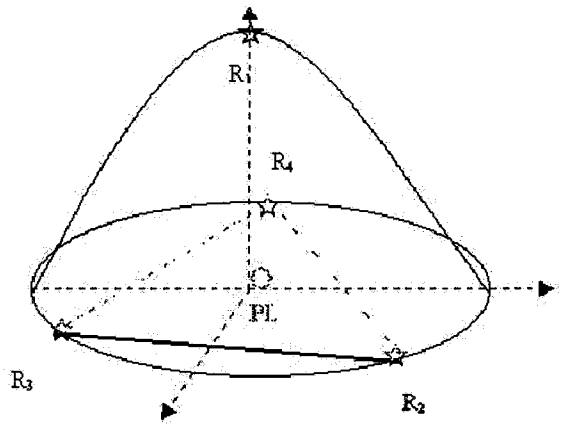

Figure 6-7. Optimum four-receiver array to minimise RDOP value

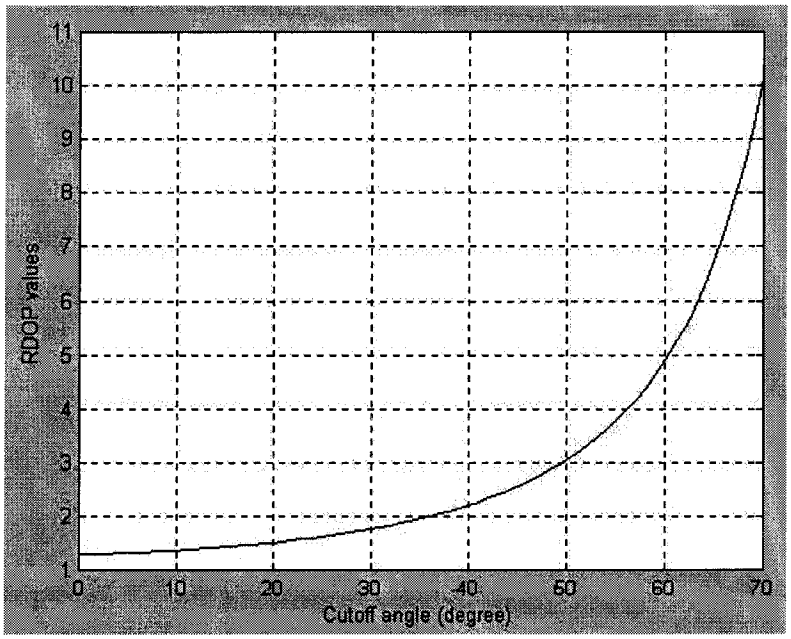

Figure 6-8. Minimum RDOP as a function of cut-off angle for four receivers

6.5 Experimental Results and Analysis

Static and kinematic experiments were carried out to investigate the potential applications of pseudolites for precise positioning. The NovAtel Millennium™ GPS receivers and the IntegriNautics IN200CXL pseudolite instruments were used in these experiments. The pseudolites transmitted only GPS L1 signals. In order to avoid signal

interference, the RTCM recommended pulsing signals at 1/11 cycle was used, and 32dB attenuation was applied to the signal power. In the case of the NovAtel GPS receivers, channels can be easily assigned to the specific PRN codes used by the pseudolites. Each pseudolite can be programmed to transmit a PRN code (either one of the 36 assigned to GPS satellites, or several others that can still be recognised by the NovAtel receiver). The remaining channels were used to track GPS satellite signals.

6.5.1 GPS and Pseudolite Integration Experiment

The experiment was conducted using two NovAtel receivers and three IntegriNautics IN200CXL pseudolite instruments at a factory site on 3 January 2001. Heavy industry, such as steelworks, are very challenging environments for precise positioning due to heat, dust, cramped and dangerous conditions, vibration, moving machinery, elevated sites, line-of-sight obstructions, gas fumes and steam. These constraints make conventional and GPS surveying sub-optimal. The three pseudolites were set up on tripods, on the ground, where some GPS satellites were blocked by the buildings. Therefore very good geometry could be assured. The pseudolites were programmed to transmit PRN codes 12, 16 and 18. Two NovAtel Millennium GPS receivers, spaced approximately 7 m apart, were used to collect the GPS and pseudolite data (see Figure 6-9 – PL indicates the location of the pseudolites and the two GPS receivers are indicated as BASE and ROVE).

The distances from the reference GPS receiver to pseudolites PL12, PL16 and PL18 were 54m, 55m and 109m respectively, and the corresponding elevation angles were 0.02°, 0.39° and 0.26°. During this experiment five GPS satellites were tracked and an hour of GPS and pseudolite measurements were collected at a 1-second sampling rate. The pseudolite and GPS data were processed together in post-processing mode using the BASELINE^{TM} software developed at The University of New South Wales (UNSW).

Figure 6-10 shows the DD carrier phase residuals from the ambiguity-fixed baseline solutions (the highest satellite SV17/PRN17 was used as the reference satellite). The mean value and RMS of the residuals were 0.0363 and 0.0167 cycles respectively. These residuals indicate that the pseudolite measurements were contaminated by

systematic errors, which are most likely due to multipath. The biases from multipath, tropospheric delay and pseudolite-location-dependent errors can be calibrated beforehand in the case of static environments. Therefore the pseudolite measurements can make a significant contribution to high accuracy deformation monitoring applications. (However, such biases may seriously degrade positioning accuracy for kinematic positioning applications.)

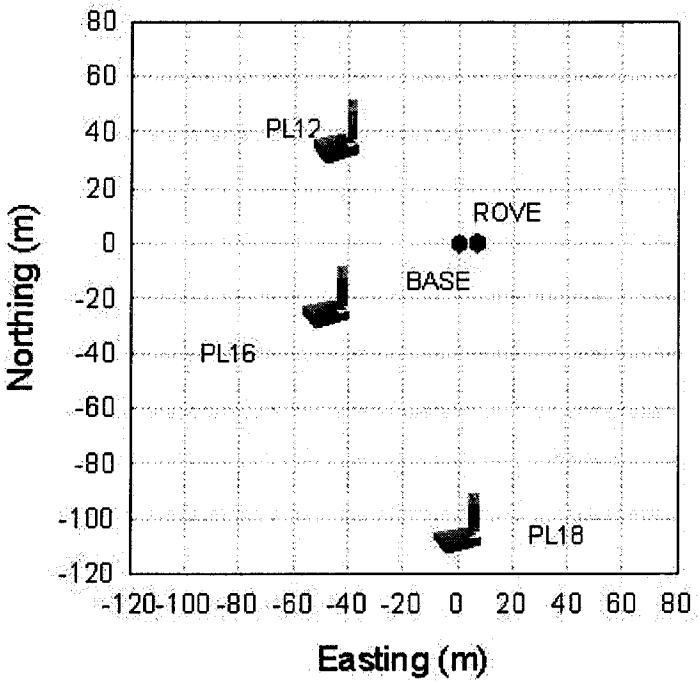

Figure 6-9. Location of instruments for the multiple pseudolite experiment

It can be seen from Figure 6-10 that the quality of the measurements is very good, even though the elevation angles from the pseudolites to the receivers are quite low (less than half degree). The Horizontal Dilution-of-Precision (HDOP) and Vertical Dilution-of-Precision (VDOP), with and without pseudolites, are plotted in Figures 6-11 and 6-12 respectively. It can be seen that the VDOP and HDOP values without pseudolites can reach values of 15 and 6 respectively. It is obvious that the DOP values (especially the VDOP values) with pseudolites have been reduced significantly – to less than 2. The differences between the E, N, U components of the static GPS-only fixed solution, and the static integrated GPS-pseudolite solution are 0mm, 3mm, 5mm respectively. Figures

6-13, 6-14 and 6-15 show the differences between the single-epoch GPS-only solutions, and the single-epoch solutions with pseudolite augmentation. The standard deviations of the single-epoch solutions for the E, N and U components are 3.4mm, 2.5mm and 4.4mm for the integrated GPS-pseudolite solutions, and 3.6mm, 4.2mm and 16.2mm for the GPS-only solutions respectively. The incorporation of pseudolite data into the GPS solution results in reduced solution RMS. In particular, the RMS of the vertical component is reduced by a factor 4. Clearly, pseudolites can be used to improve the positioning accuracy of a GPS-based positioning system, especially where high accuracy height component monitoring is needed, as in such applications as ground subsidence measurement or for monitoring the deformation of man-made structures.

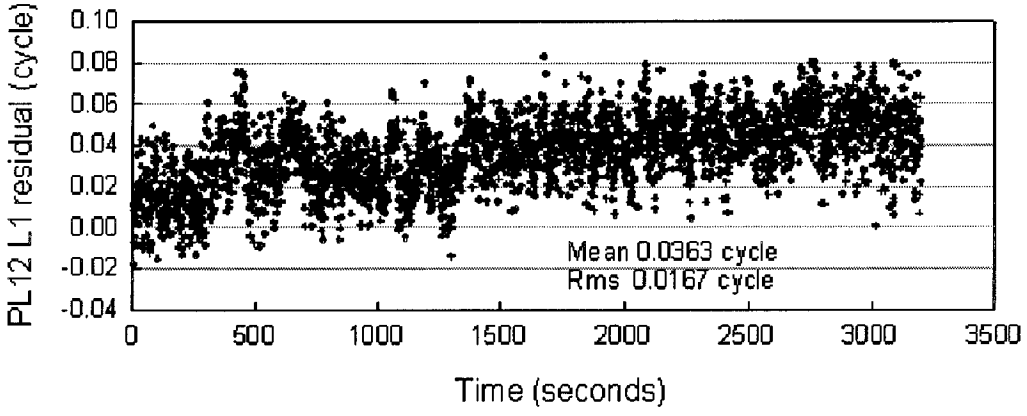

Figure 6-10. DD carrier phase residuals for PL12 – SV17

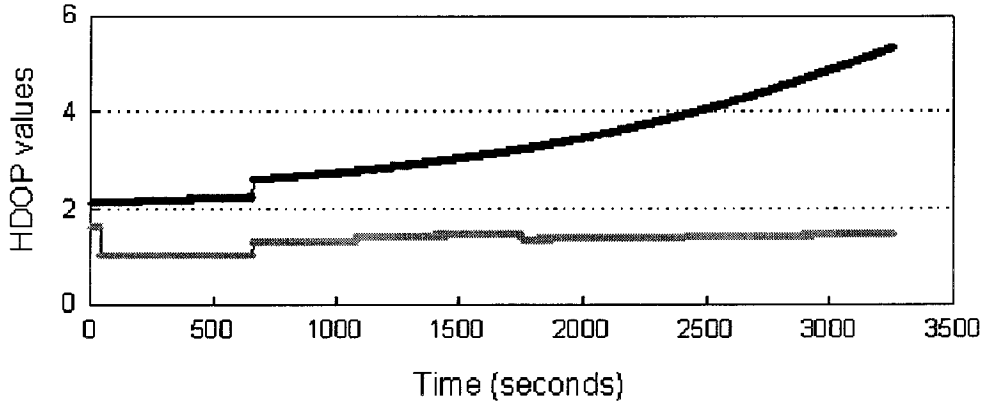

Figure 6-11. HDOP with (grey plot)and without pseudolites (black plot)

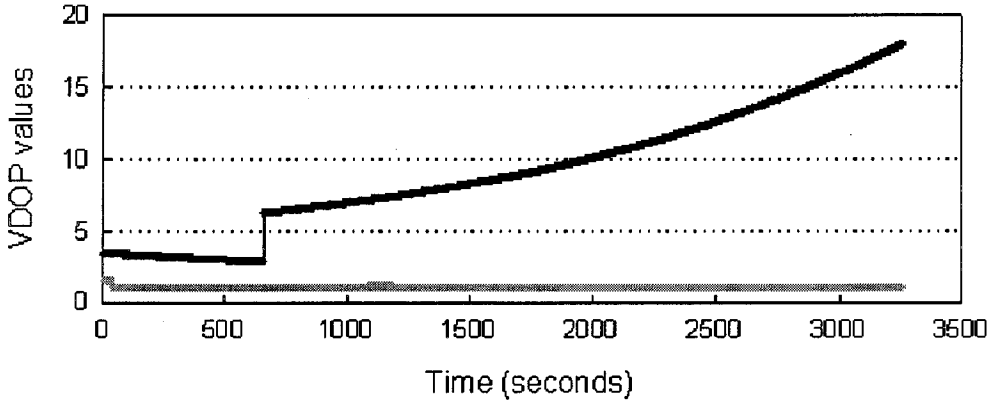

Figure 6-12. VDOP with (grey plot)and without pseudolites (black plot)

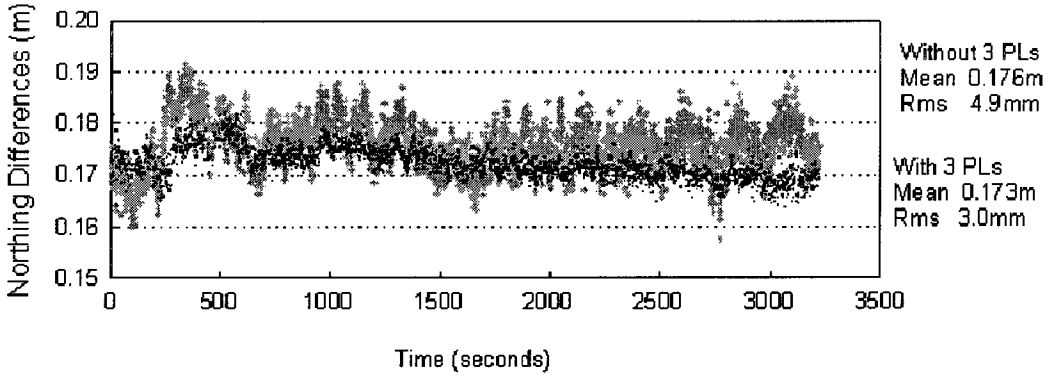

Figure 6-13. North component of the carrier phase solutions with GPS-pseudolite integration (black plot) and GPS-only (grey plot)

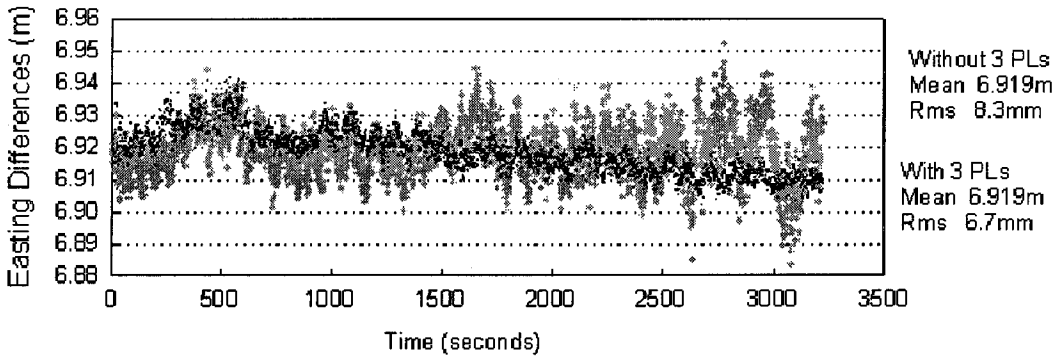

Figure 6-14. East component of the carrier phase solutions with GPS-pseudolite integration (black plot) and GPS-only (grey plot)

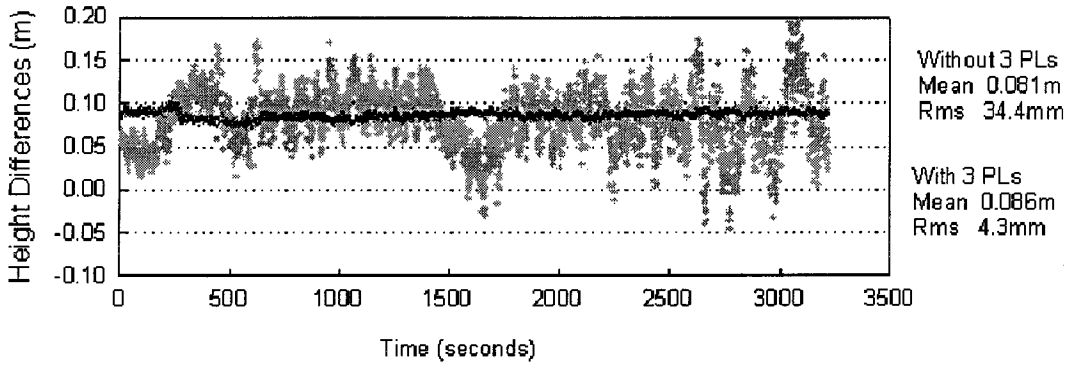

Figure 6-15. Height component of the carrier phase solutions with GPS-pseudolite integration (black plot) and GPS-only (grey plot)

6.5.2 Inverted Pseudolite Positioning Experiments

Static and kinematic experiments for pseudolite inverted positioning system were conducted using six NovAtel receivers (four Millennium™ and two Beeline™) and two IntegriNautics IN200CXL pseudolite instruments on the UNSW campus, on the 4th and 20th April 2001 respectively. The six NovAtel receivers were placed on the roof of the Electrical Engineering building of The University of New South Wales, and a pseudolite (PL) antenna was set on the wooden rail fixed on the two pillars (Figure 6-16). The pseudolite could be slid along on the wooden rail for the kinematic test. Also, an antenna for an Ashtech GG24 receiver was mounted on the PL antenna in order to determine the correct position of the PL antenna, and can be slid along the rail together with the PL antenna. As discussed in the previous Section, it is easy to establish a good geometry for the inverted pseudolite positioning system because a receiver can be placed directly underneath the PL.

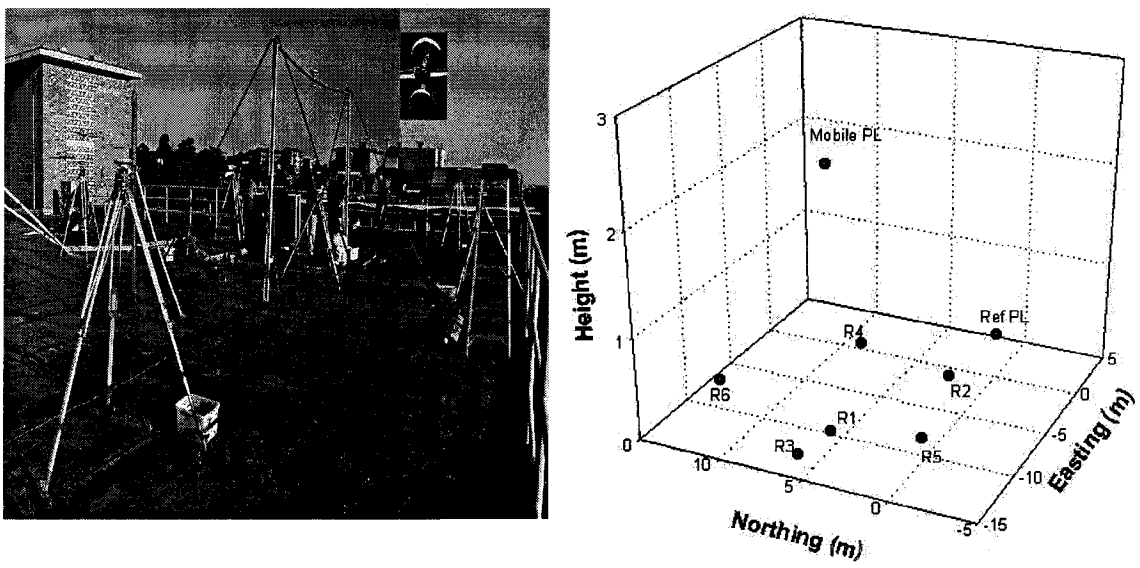

Figure 6-16. Location of instruments for inverted pseudolite positioning experiment

Static Experiment

About 40 minutes of static GPS and pseudolite measurements were collected with a one-second sampling rate. The coordinates of the six GPS receivers and the two pseudolite sites were precisely determined beforehand using the data collected by the GPS receivers. Figure 6-17 shows the HDOP and VDOP values for the mobile pseudolite PL16 during the experiment. 5-6 receivers tracked both pseudolite signals, therefore different combinations of receivers result in different HDOP and VDOP values. It can be seen from Figure 6-17 that very good geometry (HDOP and VDOP both less than 2) was obtained because of the optimised receiver locations (through careful selection of antenna locations).

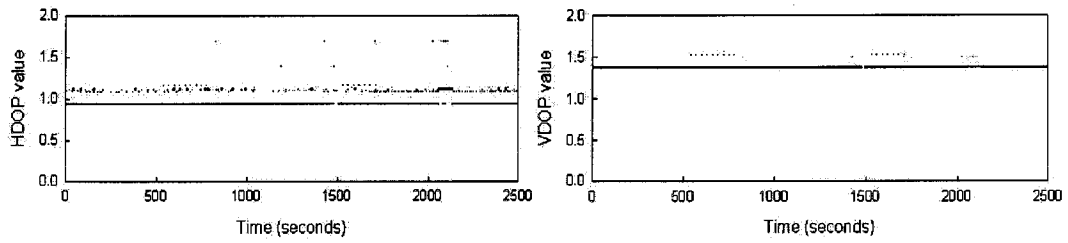

Figure 6-17. HDOP (Left) and VDOP (Right) values

Carrier phase ambiguity resolution could not be attempted in the normal manner because the receivers and pseudolites were stationary. The carrier phase processing was conducted by rounding-off the double-differenced ambiguity to the nearest integer using the known initial position of the mobile pseudolite. During data processing it was found that significant constant biases existed in the pseudolite carrier phase measurements. The constant biases may come from the invariant multipath, attributable to the high multipath environment on the roof. The carrier phase multipath for the one-way signal does not exceed about one-quarter of the wavelength (*5-6*cm for L1 or L2). However, the double-differenced measurements, involving four one-way signals, could be seriously contaminated by multipath. It is therefore necessary to calibrate the constant biases, for static environments, before data processing. In this experiment, each receiver not only tracks the two pseudolite signals but also the GPS signals. Therefore GPS measurements can be used to calibrate the residual biases in the pseudolite measurements. Figure 6-18 shows the values of the double-differenced L1 residual biases between receivers and the two pseudolites, or one pseudolite and one GPS satellite. The constant biases for receivers 1, 2, 3, 4, 5 are -0.0742, 0.0918, 0.2048, 0.0446 and 0.1663 cycles in the type II configuration, and 0.3374, -0.3477, 0.0747, -0.0688, -0.1288 cycles in the type I configuration (receiver 6 was selected as the reference 'satellite' in this configuration). It should be pointed out that the RMS of these bias values are less than 1cm (0.05 cycle).

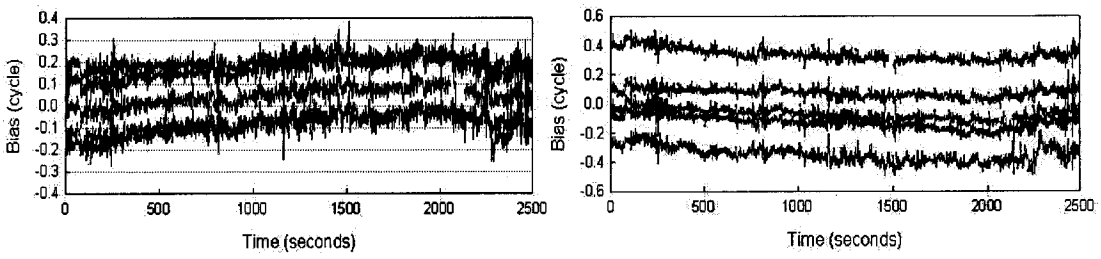

Figure 6-18. Double-differenced L1 residuals (Left: type II, and Right: type I)

The data was processed in single-epoch mode using both configurations (type II&I). The highest satellite (PRN7) was chosen as the reference 'receiver'. The positioning results are plotted in Figure 6-19. The RMS of the North, East and Height components are 2.6mm 5.0mm and 4.9mm for the type II configuration, and 2.9mm, 4.7cm and

4.8mm for the type I configuration respectively. Because the constant biases in the pseudolite carrier phase measurements are calibrated beforehand, the positioning solutions are not biased. The conclusion can be drawn that high accuracy positioning results can indeed be achieved using both the type I and II configurations.

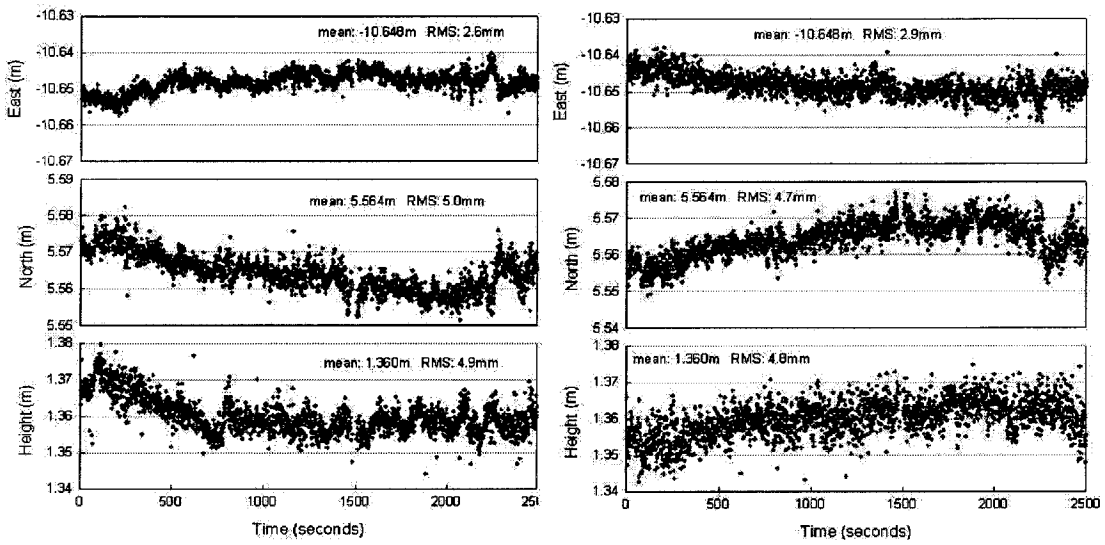

Figure 6-19. The East (upper plot), North (middle plot) and Height (lower plot) results for inverted carrier phase positioning (Left: type II, and Right: type I)

Kinematic Experiment

In the kinematic mode, the PL antenna was slid on the wooden rail, together with the GG24 antenna, by pulling a rope attached to the antenna mount. The trajectory of the GG24 antenna derived by the standard kinematic GPS positioning is shown in Figure 6-20. The antennas were moved very slowly so as not to lose signal tracking. However, some receivers did lose signal lock, as shown in Figure 6-21.

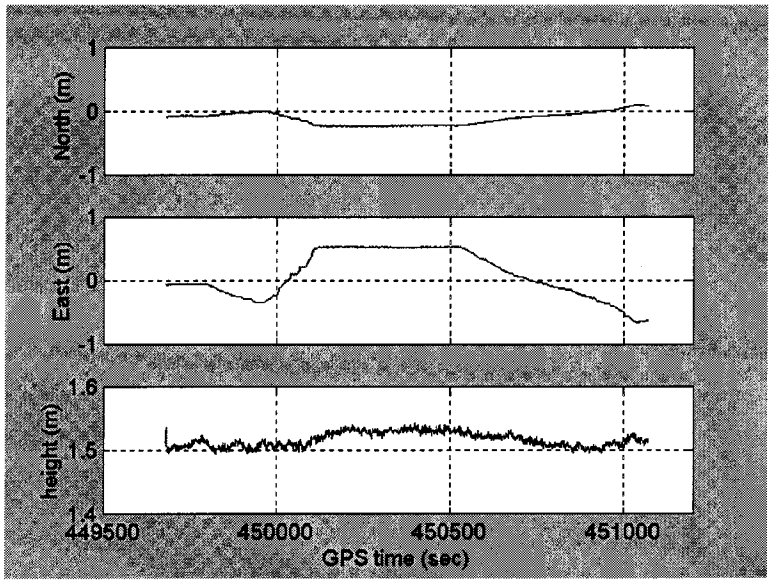

Figure 6-20. Trajectory of GG24 antenna in the kinematic test

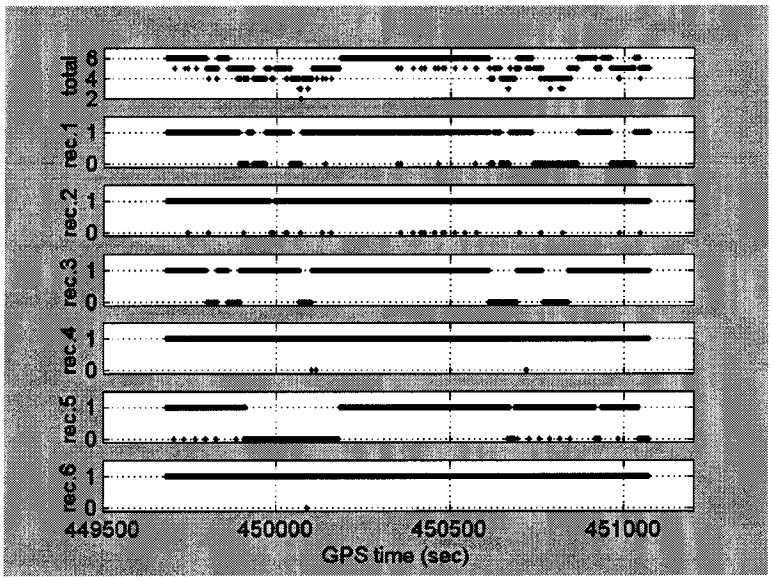

Figure 6-21. Number of receivers tracking PL signal (top), and the tracking status (1:tracked, 0:not tracked)

Because there is only a 12cm constant difference in the height component, the trajectory of the GG24 antenna shown in Figure 6-20 was used to define the true position of the PL antenna. The true position of the PL antenna could be used to resolve the carrier

phase ambiguities in this kinematic pseudolite-inverted system. The residuals of the double-differenced carrier phase were computed (an example shown in Figure 6-22). The residuals change very quickly due to the motion of PL antenna compared to the static period (time 449679-449803, 450123-450530). This is a reasonable result considering the characteristics of the multipath, because the angle between the PL antenna and the ground antenna changes dramatically in such a micro-configuration, even if the motion of the PL is slight. With such large residuals, ambiguity resolution would be very difficult. Even if the ambiguities were resolved by some method, the positioning solution would be degraded, as indicated in Figure 6-23. Error sources could be mainly from multipath, possibly from the phase polarisation and the phase centre variation. The pseudolite multipath is therefore a challenging issue that needs to be addressed if pseudolites are to find wide acceptance for kinematic applications.

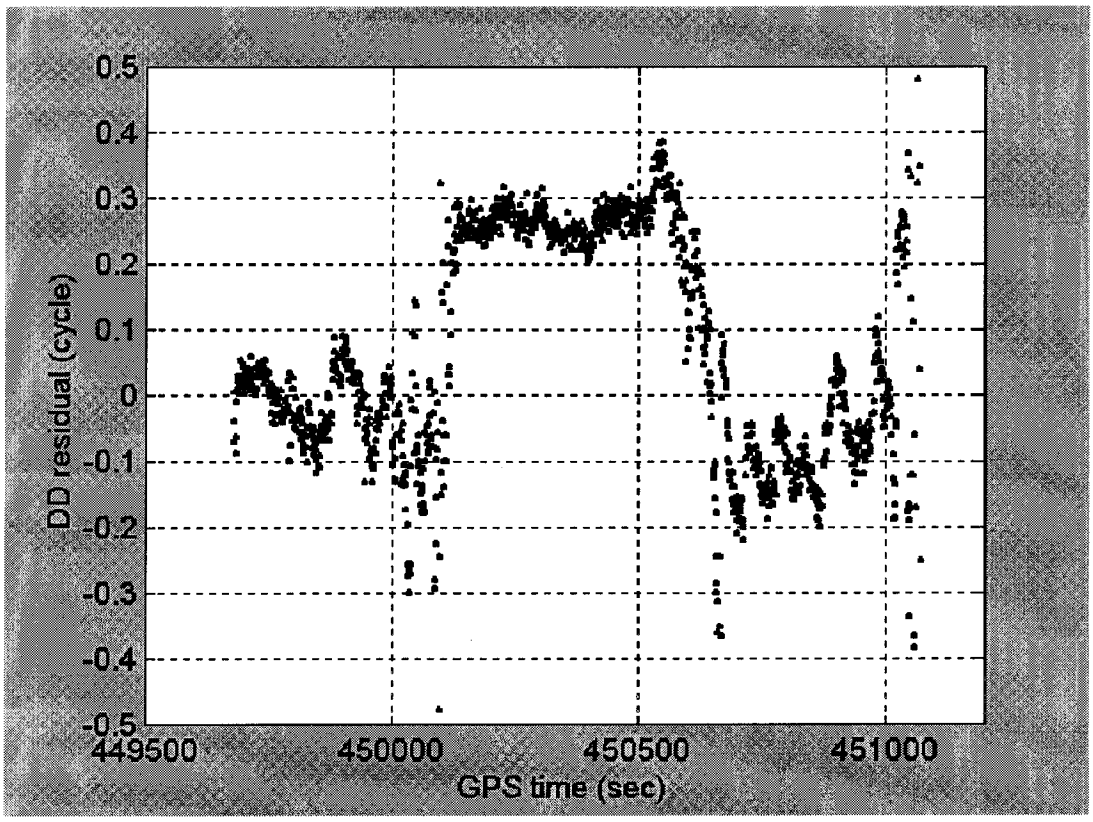

Figure 6-22. DD residuals of L1 carrier phase between receiver pairs R4 and R6

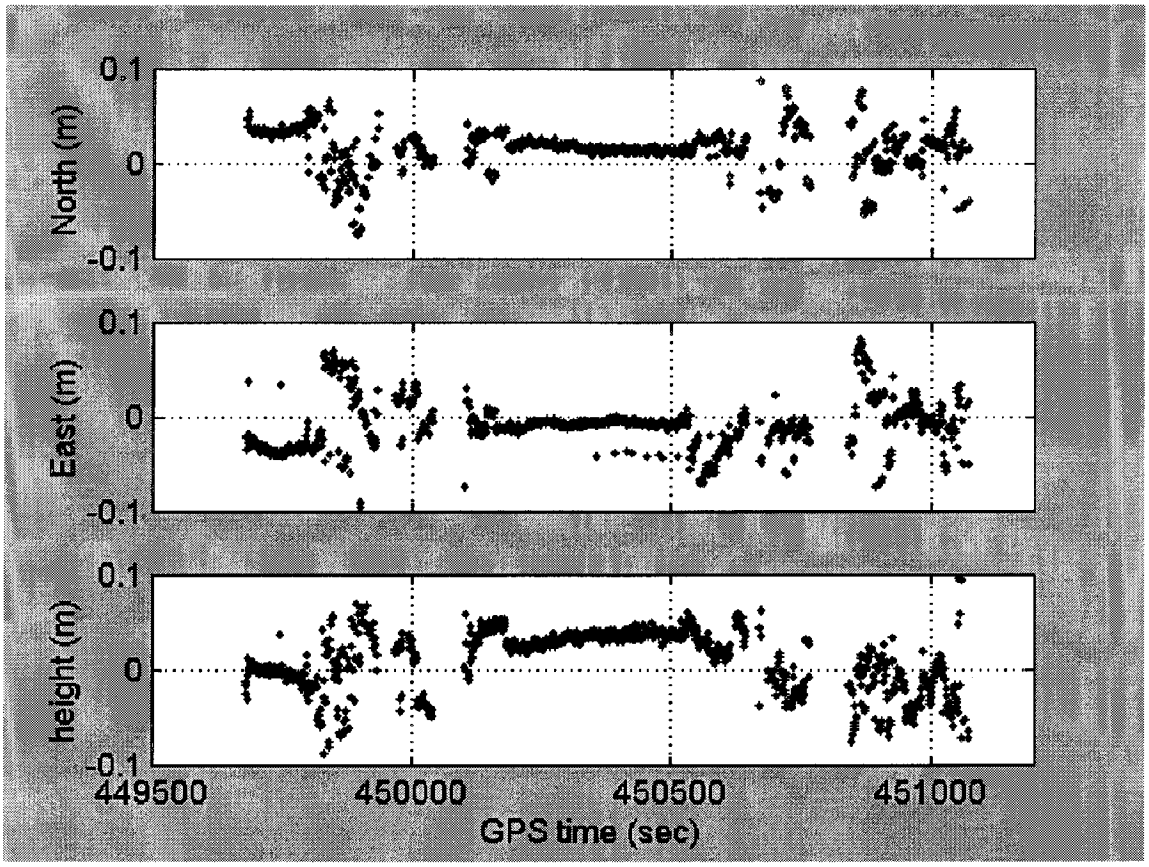

Figure 6-23. Kinematic positioning results in the inverted pseudolite test

6.6 Concluding Remarks

In this chapter, the three different pseudolite configurations (integrated GPS and pseudolite, pseudolite-only, and pseudolite-based 'inverted' positioning) have been investigated. The advantages and disadvantages of each configuration were discussed. The feasibility of using pseudolites for deformation monitoring and stratospheric navigation applications have been investigated in a series of tests. Practical considerations concerning geometric optimisation have been addressed.

Several experiments have been carried out using NovAtel GPS receivers and up to three IntegriNautics IN200CXL pseudolites. The first experimental results indicate that the accuracy of the height component can indeed be significantly improved (the RMS of the vertical is reduced by a factor 4), to the same level as the horizontal components. The

accuracy, reliability, availability and integrity of the solutions from an integrated GPS and pseudolite system can also be improved. The static test results for the pseudolite 'inverted' positioning show excellent positioning stability (Std. deviation less than 5mm), and indicate again that the accuracy of the height component can be significantly improved. The kinematic test shows that pseudolite multipath is a challenging issue that needs to be addressed. Good hardware design, including receivers, receiver antennas and pseudolite transmitter antennas, as well as software-based multipath mitigation techniques will be needed.

Chapter 7

SUMMARY AND RECOMMENDATIONS

7.1 Summary and Concluding Remarks

Real-time kinematic GPS carrier phase-based positioning is playing an increasing role in surveying and navigation, and has become an essential tool for precise relative positioning. However, there are two main problems that must be addressed for carrier phase-based GPS positioning to be accurate and reliable. As is well known, reliable and correct ambiguity resolution depends on observations to a large number of GPS satellites which constrains its applications, making it difficult to address positioning applications in areas where the number of visible satellites is limited. On the other hand, carrier phase-based positioning applications have been constrained to 'short range' due to the presence of distance-dependent biases such as orbital errors, tropospheric and ionospheric delays.

To address these problems, GPS augmentation for carrier phase-based positioning by the existing Glonass satellite system, the use of GPS and Glonass multiple reference station networks, and the incorporation of additional ground-based pseudo-satellite signals has been the focus of this study.

7.1.1 Integrated Procedure for GPS and Glonass Precise Positioning

Due to the different signal frequencies for the different Glonass satellites, the commonly used double-differencing procedure for carrier phase data processing cannot be

implemented in its straightforward form, as in the case of GPS. In Chapter 2, an integrated procedure for GPS and Glonass data processing has been proposed, consisting of a three-step procedure to improve the functional model, an associated real-time stochastic model estimated using residuals from the previous epochs, and a fault detection and adaptive procedure. The proposed functional model improves the performance because the ambiguity resolution process is insensitive to the residual clock biases and the inter-channel biases, and hence reliable and precise positioning results are obtained. The real-time stochastic model estimated from the residuals can significantly improve the ambiguity resolution success rates, as well as the accuracy of the final solutions. The fault detection and adaptive procedure includes an outlier detection algorithm based on correlation analysis, which can locate rapidly and reliably the outliers or biases even in the case of highly correlated observations. It is especially powerful for only one outlier with small degrees of freedom. This procedure can significantly improve the ambiguity resolution success rate and the number of valid kinematic positioning solution epochs.

The experimental results in Chapter 2 indicate that using the integrated procedure results in a 99.3% success rate for single-epoch solutions, based on the analysis of four static GPS/Glonass experiments. This is a significant improvement on the success rate of 81.4%, obtained using the standard procedure. The success rate of single-epoch solution for kinematic positioning using dual-frequency GPS-only receivers and single-frequency GPS/Glonass receivers increased to 98.2%, compared with 62.4% when the proposed procedures and modelling was not applied.

7.1.2 Comparison on GPS and Glonass Multiple-Reference Station Techniques

High precision GPS (and Glonass) surveying and navigation applications have been constrained to a comparatively 'short range' (<10km) due to the presence of distance-dependent biases in the between-receiver single-differenced observables. Over the past few years, the use of a GPS reference station network, to extend the inter-receiver distances (user-to-reference station), has been proposed by several investigators. One core challenge for multi-reference station techniques is how to interpolate the distance-

dependent biases generated from the reference receiver network for the user's location? In order to account for the distance-dependent residual biases, such as the atmospheric biases and orbit errors, several techniques have been developed. They include the Linear Combination Model, the Distance-based Linear Interpolation Method, the Linear Interpolation Method, the Low-order Surface Model, and the Least Squares Collocation Method.

In Chapter 3, the abovementioned interpolation methods for GPS multiple-reference receiver techniques have been compared in detail. The advantages and disadvantages of each of these interpolation methods have been discussed. For all of the interpolation methods, the essential common formula has been identified, which uses the n-1 coefficients and the n-1 independent 'correction terms' generated from a n reference station network, to form a linear combination that mitigates spatially correlated errors at user stations. The formulas of the coefficient determination for each method have been derived. In fact, the coefficients can be considered as weighting for the 'correct terms'. Therefore, the major differences between all the methods are essentially the coefficients. Based on a simulated reference station network, the coefficients for each method have been compared.

Test data from GPS and Glonass reference stations were used to evaluate the performance of these interpolation methods. The numerical results show that all the methods for multiple-reference receiver implementation can significantly reduce the distance-dependent biases in the carrier phase and pseudo-range measurements at the GPS user station. The performance of all of the methods is similar, though the Distance-Dependent Linear Interpolation method does demonstrate slightly worst results in the two experiments reported in Chapter 3.

7.1.3 Real-Time Carrier Phase Ambiguity Resolution for GPS and Glonass Reference Station Networks

When using reference station networks to support real-time kinematic positioning, the ambiguities in the GPS and/or Glonass reference station network should first be resolved to their correct integer values. Although precise coordinates can be pre-

determined for the GPS (and Glonass) reference stations, it is still a big challenge to resolve the integer ambiguities correctly between the reference stations, in real-time, when a cycle-slip, or when a new satellite rises, or after a long data gap occurs.

In Chapter 4, two scenarios for real-time ambiguity resolution appropriate for GPS/Glonass reference station networks were investigated. The first scenario involved temporally correlated bias modelling, which is used to *recover* ambiguities correctly after initialisation. As the distance-dependent errors (atmosphere biases and orbit errors) exhibit a high degree of temporal correlation for short time spans, the double-differenced residuals can be represented as a linear function of time for short periods of up to a few minutes. Three methods, including the random-constant stochastic process, linear function fitting and Kalman filtering, have been proposed. On an epoch-by-epoch and satellite-by-satellite basis, these systematic errors (biases) can be estimated using previous measurements with fixed ambiguities, and precisely predicted for use in ambiguity resolution during the following measurement epochs.

The second scenario involved spatially correlated residual ionospheric and tropospheric modelling, which can aid the resolution of the wide-lane and narrow-lane ambiguities for a newly risen satellite or after a long data gap. Atmospheric biases exhibit strong spatial correlations between satellite pairs. The linearly residual ionospheric model and RTZD model are tested. The atmospheric delay information derived from other satellites, with fixed ambiguities, can be used to predict the atmospheric bias for a newly risen satellite, and for those satellites that have unknown ambiguities associated with them. Other associated issues, such as the criterion to fix ambiguities and the different signal frequencies for the Glonass satellites, have also been addressed.

The experimental results from a GPS and Glonass reference station network show that the temporally correlated bias model can predict the bias for the next measurement epoch and aid ambiguity recovery, and all the cycle slips are easily detected and repaired. In the experiment reported in Chapter 4, the test results show that after the spatially correlated bias models are applied, the average RMS for the wide-lane residuals decreased from 14.3cm to 9.2cm, an improvement of about 35.5%. The average RMS for the tropospheric delay can be significantly reduced, from 6.4cm to

2.9cm, an improvement of 54.%. The average required time-to-fix for the narrow-lane ambiguities can be significantly shortened, in this experiment from 18.1 minutes to 5.5 minutes, after the predicted relative tropospheric zenith delay model was applied.

7.1.4 Pseudolite Modelling Issues and Applications

The Global Navigation Satellite Systems, comprising of the GPS and Glonass systems (supplemented later in the decade with the proposed Galileo system), have been revolutionised positioning and navigation techniques. However, the performance of such space-borne systems may suffer from poor satellite visibility under hash operational environments, such as in urban canyons, deep open-cut mines, etc. In the worst situations, such as underground and inside buildings, the GPS signals may be completely lost. These problems can be adequately addressed by the inclusion of additional ranging signals transmitted from ground-based "pseudo-satellites" (or pseudolites). Pseudolites are an exciting technology that can be explored for a wide range of positioning and navigation applications, either as a substantial augmentation tool of the space-borne systems or as an independent system for indoor positioning applications.

However, due to the comparatively small separation between pseudolites and receivers/users, there are some challenging issues in modelling and geometric design that need to be addressed. In Chapter 5, modelling issues for GPS and pseudolite integration such as non-linearity, pseudolite location errors, tropospheric delays, multipath and noise, have been investigated. The effects of non-linearity, and orbital errors and tropospheric delay, have been analysed from a theoretical point of view. The formulas derived in Chapter 5 show that special attention has to be given to these error sources in pseudolite positioning applications. Based on use of the appropriate quality indicators, the impact of the pseudolite-user geometry in final positioning solutions was analysed. Optimal geometric designs for various positioning scenarios have been proposed.

In Chapter 6, the three different pseudolite configurations (integrated GPS and pseudolite, pseudolite-only, and pseudolite-based 'inverted' positioning) have been

investigated. The advantage and disadvantage of each configuration were discussed. The feasibility of pseudolites for applications in deformation monitoring and to support navigation services based on stratospheric airships has been investigated.

From experimental results obtained using NovAtel GPS receivers and up to three IntegriNautics IN200CXL pseudolites, the following conclusions can be drawn:

1. The noise level of the PL carrier phase measurements is comparable with, or even lower than, that of GPS measurements. Systematic errors identified in the PL measurements such as orbit bias and multipath are constant for many cases.

2. For GPS and pseudolite, after carefully optimising pseudolite location, the accuracy of the height component can be significantly improved (the RMS of vertical reduced by a factor 4), to the same level of accuracy as the horizontal components. The accuracy, reliability, availability and integrity of the solutions from an integrated GPS and pseudolite system can also be significantly improved.

3. For the pseudolite 'inverted' positioning, the static test results show excellent positioning stability (std. dev. less than 5mm), and indicate again that the accuracy of the height component can indeed be significantly improved, to approximately the same level as the horizontal components.

4. The kinematic test shows that pseudolite signal multipath is a challenging issue that needs to be addressed if pseudolites are to be used in future for kinematic applications.

7.2 Recommendations for Future Research

Based on both the theoretical and experimental results obtained in this study, the following recommendations are made for further research:

1. When the Galileo satellites become operational (around the end of the decade), and then combined with GPS and Glonass, the volume of observations will be

increased. This will significantly enhance the reliability, availability, integrity and accuracy of an integrated GNSS carrier phase-based positioning system. The modelling issues for such an integrated system should be investigated.

2. The impact of the third GPS frequency carrier phase-based kinematic positioning systems should be analysed and appropriate data processing algorithms developed. In particular, triple-frequency techniques will be able to extend GPS precise positioning to medium-range and long-range.

3. For multiple-reference station techniques, better spatially correlated bias modelling for the ionospheric and tropospheric delays is required. In the case of real-time operation the problem of data latency needs to be considered, which includes the receiver data download and transfer delay, data link delay, and baseline or network computation delay.

4. Pseudolite multipath is a challenging issue that needs to be addressed for kinematic applications. Improvements to the hardware, including receivers, receiver antennas and pseudolite transmitter antennas, as well as the development of software-based multipath mitigation techniques will be needed.

5. Pseudolite kinematic positioning techniques needs to be further investigated. Techniques for mitigating the (unmodelled) systematic errors identified in the Chapter 5 for kinematic applications should be investigated.

REFERENCES

Abidin, H.Z. (1993), Computational and geometrical aspects of on-the-fly ambiguity resolution, Dept. of Geodesy & Geomatic Eng., University of New Brunswick, Canada, Tech. report. no.164, 290pp.

Ashkenazi, V., R. Bingley, A. Dodson, N. Pena & T. Baker (1998), GPS monitoring of vertical land movements in the UK, 11th Int. Tech. Meeting of the Satellite Division of the U.S. Inst. of Navigation GPS ION-98, Nashville, Tennessee, 15-18 Sept., 99-107.

Baarda W. (1968), A testing procedure for use in geodetic networks, Netherlands Geodetic Commission, Publications on Geodesy, New Series, Vol.2, No.5.

Barltrop, K.J., J.F. Stafford & B.D. Elrod (1996), Local DGPS with pseudolite augmentation and implementation considerations for LAAS, 9th Int. Tech. Meeting of the Satellite Division of the U.S. Inst. of Navigation GPS ION-96, Kansas City, Missouri, 17-20 Sept., 449-459.

Bartone, C.G. (1999), Multipath considerations for ground based ranging sources, 12th Int. Tech. Meeting of the Satellite Division of the U.S. Inst. of Navigation GPS ION-99, Nashville, Tennessee, 14-17 Sept., 1491-1498.

Bauersima, I. (1983), NAVSTAR/Global Positioning Sytems (GPS), II, Mitteilungen der Satellitenbeobatungsstation Zimmerwald, Nr.10, Astronomical Institute, University of Berne, Switzerland.

Behr, J.A., K.W. Hudnut & N.E. King (1998), Monitoring structural deformation at Pacoima Dam, California, using continuous GPS, 11th Int. Tech. Meeting of the Satellite Division of the U.S. Inst. of Navigation GPS ION-98, Nashville, Tennessee, 15-18 Sept., 59-68.

Beutler, G., Bauersima I., Gurtner, W., Rothacher, M., Schildknecht, T. & Geiger, A., (1989), Atmospheric refraction and other important biases in GPS carrier phase observations, In monograph 12, "Atmospheric Effects on Geodetic Space Measurements", F.K.Brunner (Ed.), School of Geomatic Engineering (formerly Surveying), The University of New South Wales, 15-44.

Chen, D. (1993), Fast Ambiguity Search Filter (FASF): a novel concept for GPS ambiguity resolution, Proc. 6th Int. Tech. Meeting of the Satellite Division of the U.S. Inst. of Navigation, 22-24 September, 1993, 781-787.

Chen H.Y. (2000), An instantaneous ambiguity resolution procedure suitable for medium-scale GPS reference station networks, 13th Int. Tech. Meeting of the Satellite Division of the U.S. Inst. of Navigation, Salt Lake City, Utah, 19-22 September, 1061-1070.

Chen, H.Y., Dai, L., Rizos, C., & Han, S. (2002). Ambiguity recovery using the triple-differenced carrier phase type approach for long-range GPS kinematic positioning. Submitted to Marine Geodesy.

Chen X., S. Han, C. Rizos & P.C. Goh (2000), Improving real-time positioning efficiency using the Singapore Integrated Multiple Reference Station Network (SIMRSN), 13th Int. Tech. Meeting of the Satellite Division of the U.S. Inst. of Navigation, Salt Lake City, Utah, 19-22 September, 9-18.

Choi I.K., Wang J., Han S. and Rizos C. (2000), Pseudolites: A new tool for surveyors? 2nd Trans Tasman Survey Congress, Queenstown, New Zealand, 20-26 August, 141-149.

Cobb H.S. (1997), GPS pseudolites: Theory, design, and applications, PhD Dissertation, Stanford University, 152pp.

Cobb, S. & M. O'Connor (1998), Pseudolites: enhancing GPS with ground-based transmitters, GPS World, 9(3), 55-60.

Colombo O.L., M. Hernández-Pajares, J.M. Juan, J. Sanz & J. Talaya (1999), Resolving carrier phase ambiguities on the fly, at more than 100km from nearest reference site, with the help of ionospheric tomography, 12th Int. Tech. Meeting of the Satellite Division of the U.S. Inst. of Navigation, Nashville, Tennessee, 14-17 September, 1635-1642.

Dai L. & J. Liu (1998), GPS data automatic transfer and realization in the Geheyan Dam deformation monitoring system, Journal of Wuhan Technical University of Surveying & Mapping, 23, Suppl. 28-31.

Dai L. (1998), Point and Differential Positioning Using Combined GPS and GLONASS Code, Special report on GPS and Glonass, School of Geomatic Engineering, The University of New South Wales, Sydney, Australia, 53pp.

Dai L., S. Han & C. Rizos (1999), A multiple outlier detection algorithm for instantaneous ambiguity resolution for carrier phase-based GNSS positioning, Int. Symp. on Digital Earth (ISDE), Beijing, P.R. China, 29 November - 2 December, 321-332.

Dai L., H.Y. Chen, S. Han, C. Rizos & A.H.W. Kearsley (2000a), Ambiguity recovery for long-range kinematic GPS positioning using a triple-difference-type approach, Pres. at Western Pacific Geophysics Meeting, Tokyo, Japan, 26-30 June.

Dai, L., J. Zhang, C. Rizos, S. Han & J. Wang (2000b), GPS and pseudolite integration for deformation monitoring applications, 13th Int. Tech. Meeting of the Satellite

Division of the U.S. Inst. of Navigation GPS ION-2000, Salt Lake City, Utah, 19-22 Sept., 1-8.

Dai, L. (2000), Dual-frequency GPS/GLONASS real-time ambiguity resolution for medium-range kinematic positioning. 13th Int. Tech. Meeting of the Satellite Division of the U.S. Inst. of Navigation GPS ION-2000, Salt Lake City, Utah, 19-22 Sept, 1071-1080.

Dai, L., Wang, J., Rizos, C., & Han, S. (2001a), Applications of pseudolites for deformation monitoring systems, Pres. 10th FIG Int. Symp. on Deformation Measurements, Orange, California, 19-22 March, 11-22.

Dai L., Wang J., Rizos C. & Han S. (2001b), Real-time carrier phase ambiguity resolution for GPS/Glonass reference station networks, Int. Symp. on Kinematic Systems in Geodesy, Geomatics & Navigation (KIS2001), Banff, Canada, 5-8 June, 475-481.

Dai L., J. Wang, T., Tsujii & C. Rizos (2001c), Pseudolite applications in positioning and navigation: Modelling and geometric analysis, Int. Symp. on Kinematic Systems in Geodesy, Geomatics & Navigation (KIS2001), Banff, Canada, 5-8 June, 482-489.

Dai, L., Wang J., Tsujii, T., and Rizos, C (2001d), Pseudolite-Based Inverted Positioning and its Applications, The 5th International Symposium on Satellite Navigation Technology & Applications, Canberra, Australia, July 24-27, paper 9, CD-ROM proceedings.

Dai, L., Han, S., Wang, J., & Rizos, C. (2001e) A study of GPS/Glonass multiple reference station techniques for precise real-time carrier phase-based positioning, 14th Int. Tech. Meeting of the Satellite Division of the U.S. Inst. of Navigation. Salt Lake City, Utah, 11-14 September, 392-403.

Dai L., C. Rizos & J. Wang (2001f), The role of pseudo-satellite signals in precise GPS-based positioning, Journal of Geospatial Eng., HK Inst. of Engineering Surveyors, 3(1), 33-44.

Dai L., S. Han & C. Rizos (2001g), Performance analysis of integrated GPS/Glonass carrier phase-based positioning, Journal of Geospatial Information Science, 4(4), 9-18.

Dai L., J. Wang, C. Rizos & S. Han (2002a), Pseudo-satellite applications in deformation monitoring, GPS solutions 5(3), 80-87.

Dai L., J. Wang, T. Tsujii & C. Rizos (2002b), Inverted pseudolite positioning and some applications, Accepted by Survey Review.

Dai L., Wang J., Rizos C. & Han S. (2002c), Predicting atmospheric biases for real-time ambiguity resolution in GPS/Glonass reference station networks, Accepted by Journal of Geodesy.

Dai, L., Han S., Rizos, C. & Wang J. (2002d), An adaptive procedure to improve GPS/Glonass ambiguity resolution success rate, submitted to Geomatics Research Australasia.

Dai, L., Han, S., Wang, J., & Rizos, C., (2002e). Comparison of interpolation methods in network-based GPS techniques. Submitted to Navigation.

Derambure X., J. M. Pieplu, D. Flament, J. C. Levy, E. Sales, J. Ventura-Traveset (1999), Assessment of EGNOS continuity from position to range domain, ION GPS-99, Nashville, TN, Sept. 14-17, 1999.

El-Rabbany A.E.S. (1994), The effect of physical correlations on the ambiguity resolution and accuracy estimation in GPS differential positioning, PhD

Dissertation, Dept. of Geodesy & Geomatics Engineering, Tech. Rept. No. 170, University of New Brunswick, Fredericton, New Brunswick, Canada, pp161.

Elrod B.D. & Van Dierendonck A.J. (1996), Pseudolites, in: B.W. Parkinson & J.J. Spilker (eds.), Global Positioning System: Theory and Applications (Vol. II), American Institute of Astronautics, Washington D.C., 51-79.

Enge, P. K. and A. J. Van Dierendonck (1996), Wide Area Augmentation System, In: Parkinson B. et al (ed), Global Positioning System: Theory and Applications, Vol II, American Institute of Aeronautics and Astronautics, Inc., Washington DC, 117-142.

Ford, T., J. Neumann, W. Petersen, C. Anderson, P. Fenton, T. Holden & K.J. Barltrop (1996), HAPPI - a High Accuracy Pseudolite/GPS Positioning Integration, 9th Int. Tech. Meeting of the Satellite Division of the U.S. Inst. of Navigation GPS ION-96, Kansas City, Missouri, 17-20 Sept., 1719-1728.

Fotopoulos G. & M.E. Cannon (2000), Spatial and temporal characteristics of DGPS carrier phase errors over a regional network, U.S. Institute of Navigation Annual Meeting, San Diego,California, 26-28 June, 54-64.

Fotopoulos G. (2000), Parameterization of carrier phase corrections based on a regional network of reference stations, 13th International Technical Meeting of the Satellite Div. of the U.S. Institute of Navigation, Salt Lake City, Utah, 19-22 September, 1093-1102

Fotopoulos G. & M.E. Cannon (2001), An overview of multi-reference station methods for cm-level positioning, GPS Solutions, 4(3), 1-10.

Frei, E. & Beutler, G. (1990), Rapid static positioning based on the Fast Ambiguity Resolution Approach "FARA": theory and first results, Manuscripta Geodaetica, 15, 325-356.

Gao Y., Z. Li & J.F. McLellan (1997), Carrier phase based regional area differential GPS for decimeter-level positioning and navigation, 10th Int. Tech. Meeting of the Satellite Division of the U.S. Inst. of Navigation, Kansas City, Missouri, 16-19 September, 1305-1313.

Gao Y. & Li. Z. (1998), Ionosphere effect and modelling for regional area differential GPS network, 11th Int. Tech. Meeting of the Satellite Div. of the U.S. Institute of Navigation, Nashville, Tennessee, 15-18 September, 91-97.

Gianniou, M. & E. Groten (1996), An advanced real-time algorithm for code and phase DGPS, Proc. 5th Int. Conf. on Differential Satellite Navigation Systems, St. Petersburg, Russia, 20-24 May, 1-7.

Global Satellite Navigation System GLONASS Interface Control Document (19997), Navtech Seminars & GPS Supply, Inc. Feb 1997, 45pp.

Habrich, H., G. Beutler, W. Gurtner & M. Rothacher (1999), Double difference ambiguity resolution for Glonass/GPS carrier phase, 12th Int. Tech. Meeting of the Satellite Division of the U.S. Inst. of Navigation, Nashville, Tennessee, 14-17 September, 1609-1618.

Han, S. (1995), Ambiguity recovery for GPS long range kinematic positioning, Proc. 8th Int. Tech. Meeting of the Sat. Div. of the U.S. Inst. of Navigation, Palm Springs, California, 12-15 Sept., 349-360.

Han S. & C. Rizos (1995), A new method for constructing multi-satellite ambiguity combinations for improved ambiguity resolution, 8th Int. Tech. Meeting of the Satellite Division of the U.S. Inst. of Navigation GPS ION'95, Palm Springs, California, 12-15 September, 1145-1153.

Han S. & C. Rizos (1996), GPS network design and error mitigation for real-time continuous array monitoring system, 9th Int. Tech. Meeting of the Satellite

Division of the U.S. Inst. of Navigation, Kansas City, Missouri, 17-20 September, 1827-1836.

Han S. & Rizos C. (1997), Instantaneous ambiguity resolution for medium-range GPS kinematic positioning using multiple reference stations, International Association of Geodesy Symposia, vol. 118, Advances in Positioning and Reference Frames, Rio de Janeiro, Brazil, 283-288.

Han S. (1997), Quality control issues relating to ambiguity resolution for real-time GPS kinematic positioning, Journal of Geodesy, 71(6), 351-361.

Han S. & C. Rizos (1998), Instantaneous ambiguity resolution for medium-range GPS kinematic positioning using multiple reference stations, in "Advances in Positioning and Reference Frames", Springer-Verlag, ISBN 3-540-64604-3, 283-288.

Han S., L. Dai & C. Rizos (1999), A new data processing strategy for combined GPS/Glonass carrier phase-based positioning, 12th Int. Tech. Meeting of the Satellite Division of the U.S. Inst. of Navigation GPS ION'99, Nashville, Tennessee, 14-17 September, 1619-1627.

Han S. & C. Rizos (2000), GPS multipath mitigation using FIR filters, Survey Review, 35(277), 487-498.

Harrington, R.L. & J.T. Dolloff (1976), The inverted range: GPS user test facility, IEEE PLANS'76, San Diego, California, 1-3 Nov., 204-211.

Hatch, R.R. (1990), Instantanous Ambiguity Resolution, Kinematic Systems in Geodesy, Surveying and Remote Sensing, IAG Symposia 107, Spring Verlag, New York, pp299-308.

Hein, G.W., B. Eissfeller, W. Werner, B. Ott, B.D. Elrod, K.J. Barltrop & J.F. Stafford (1997), Practical investigations on DGPS for aircraft precision approaches augmented by pseudolite carrier phase tracking, 10th Int. Tech. Meeting of the Satellite Division of the U.S. Inst. of Navigation GPS ION-97, Kansas City, Missouri, 16-19 Sept., 1851-1960.

Hernández-Pajares M., J.M. Juan, J. Sanz & O.L. Colombo (1999), Precise ionospheric determination and its application to real-time GPS ambiguity resolution, 12th Int. Tech. Meeting of the Satellite Division of the U.S. Inst. of Navigation, Nashville, Tennessee, 14-17 September, 1409-1417.

Hofmann-Wellenhof, B., H. Lichtenegger and J. Collins (1994), GPS Theory and Practice, Third Revised Edition, Springer-Verlag, Wien New York, 355pp.

Holden, T. & T. Morley (1997), Pseudolite augmented DGPS for land applications, 10th Int. Tech. Meeting of the Satellite Division of the U.S. Inst. of Navigation GPS ION-97, Kansas City, Missouri, 16-19 Sept., 1397-1403.

Jin, X.X. (1995), The change of GPS code accuracy with satellite elevation, Proc. 4th Int. Conf. on Differential Satellite Navigation Systems, Bergen, Norway, 24-28 April, poster No. 6, pp8.

Kalafus, R.M., A.J. Van Dierendonck & N. Pealer (1986), Special Committee 104 Recommendations for Differential GPS Service, Global Positioning System (red book), The Institute of Navigation, Vol. III, 101-126.

Kee C., H. Jun, D. Yun, B. Kim, Y. Kim, B.W. Parkinson, T. Langestein, S. Pullen & J. Lee (2000), Development of indoor navigation system using asynchronous pseudolites, 13th Int. Tech. Meeting of the Satellite Division of the U.S. Inst. of Navigation, Salt Lake City, Utah, 19-22 Sept, 1038-1045.

Kozlov, D. (1997), Instant RTK cm with low cost GPS+GlonassTM C/A receivers, 10th Int. Tech. Meeting of the Satellite Division of the U.S. Inst. of Navigation, Kansas City, Missouri, 16-19 September, 1559-1569.

Kozlov D., Tkachenko M. and Tochilin A. (2000), Statistical characterization of hardware biases in GPS+GLONASS receivers, 13th Int. Tech. Meeting of the Satellite Division of the U.S. Inst. of Navigation, Salt Lake City, Utah, 19-22 September, 817-826.

Landau, H. and H. J. Euler (1992), On-The-Fly Ambiguity Resolution for Precise Differential Positioning, Proceedings of ION GPS-92, Albuquerque, New Mexico, 16-18 September, 607-613.

Lawrence, D.G. (1996), Development and evaluation of a real time system for kinematic positioning using the Global Positioning System, PhD thesis, Stanford University, pp166.

Leick, A. (1998), GLONASS satellite surveying, Journal of Surv. Eng., 121, 91-99.

Lemaster, E. and S. Rock (1999), Mars exploration using self-calibrating pseudolite arrays, 12th Int. Tech. Meeting of the Satellite Division of the U.S. Inst. of Navigation GPS ION-99, Nashville, Tennessee, 14-17 Sept., 1549-1558.

Liu J., and L. Dai (1999), A method to fix ambiguity for GPS long baseline precisely rapid static positioning, Journal of Wuhan Technical University of Surveying and Mapping, 24, Suppl. 5-8.

Lucas R., J. H. Hahn, S. Dinwiddy, M. Lugert, G. Gatti, J. Benedicto (2000), Galileo Space and Ground Segment Definition:System and Performance, 13th Int. Tech. Meeting of the Satellite Division of the U.S. Inst. of Navigation, Salt Lake City, Utah, 19-22 September, 1755-1760.

Marel H. van der (1998), Virtual GPS reference stations in the Netherlands, 11th Int. Tech. Meeting of the Satellite Div. of the U.S. Institute of Navigation, Nashville, Tennessee, 15-18 September, 49-58.

Martin, S. (1999), Antenna diagram shaping for pseudolite transmitter antennas – a solution to the near-far problem, 12th Int. Tech. Meeting of the Satellite Division of the U.S. Inst. of Navigation GPS ION-99, Nashville, Tennessee, 14-17 Sept., 1473-1482.

Moore, T., G. Close & R. Moore (2000), RiGHt : River Level Monitoring using GPS Heighting, 13th Int. Tech. Meeting of the Satellite Division of the U.S. Inst. of Navigation GPS ION-2000, Salt Lake City, Utah, 19-22 Sept, 1840-1844.

Morley T.G. (1997), Augmentation of GPS with pseudolites in a marine environment, M.Sc. Thesis, Dept. of Geomatics Engineering, University of Calgary, Canada, 144pp.

Odijk D., Marel H. van der & Song I. (2000), Precise GPS positioning by applying ionospheric corrections from an active control network, GPS Solutions, 3, 49-57.

O'Keefe K., J. Sharma, M.E. Cannon & G. Lachapelle (1999), Pseudolite-based inverted GPS concept for local area positioning, 12th Int. Tech. Meeting of the Satellite Division of the U.S. Inst. of Navigation, Nashville, Tennessee, 14-17 Sept., 1523-1530.

Pachter M. & J.B. Mckay (1998), Geometry optimization of a GPS-based navigation reference system, Navigation, 44(4), 457-470.

Parkinson, Bradford W., and Spiker, Jr., James J. (eds) (1996), Global Positioning System: Theory and Applications, Volume I. In: Progress in Astronautics and

Aeronautics, vol. 163, Paul Zarchan, Editor-in-Chief, American Insitute of Astronautics and Aeronautics, Inc., Washington, D.C.

Pratt, M., B. Burke & P. Misra (1998), Single-epoch integer ambiguity resolution with GPS-Glonass L1-L2 data, 11th Int. Tech. Meeting of the Satellite Division of the U.S. Inst. of Navigation, Nashville, Tennessee, 15-18 September, 389-398.

Rabah M. & S. Leinen (1998), Real-time crustal movement determination over long baselines, 9th Int. Symp. on Recent Crustal Movements (CRCM'98), Cairo, Egypt, 14-19 November, 75-86.

Rapoport L. (1997), General purpose kinematic/static GPS/Glonass postprocessing engine, 10th Int. Tech. Meeting of the Satellite Division of the U.S. Inst. of Navigation , 16-19 September, 1757-1772.

Raquet, J., G. Lachapelle, W. Qui, C. Pelletier, A. Nash, P. Fenton & T. Holden (1995), Development and testing of a mobile pseudolite concept for precise positioning, 8th Int. Tech. Meeting of the Satellite Division of the U.S. Inst. of Navigation GPS ION-95, Palm Springs, California, 12-15 Sept., 817-825.

Raquet J.F. (1997), Multiple user network carrier-phase ambiguity resolution, Int. Symp. on Kinematic Systems in Geodesy, Geomatics & Navigation (KIS1997), Banff, Canada, 3-6 June, 45-55.

Raquet J., Lachapelle G. & Fortes L. (1998), Use of a covariance analysis technique for predicting performance of regional area differential code and carrier-phase networks, 11th Int. Tech. Meeting of the Satellite Div. of the U.S. Institute of Navigation, Nashville, Tennessee, 15-18 September, 1345-1354.

Raquet J. & Lachapelle G. (2001), RTK positioning with multiple reference stations, GPS World, 12(4), 48-53.

Rizos, C. (1996), Principles and Practice of GPS Surveying, Monograph 17, School of Geomatic Engineering, The University of New South Wales, Sydney, Australia, 560pp.

Rizos C., Han S. and H.Y. Chen (2000). Regional-scale multiple reference stations for real-time carrier phase-based GPS positioning: a correction generation algorithm, Earth, Planets & Space, 52(10), 795-800.

Rizos, C, (2001), Precise GPS positioning: Prospects and challenges, 5th Int. Symp. on Satellite Navigation Technology & Applications, Canberra, Australia, 24-27 July, paper 37, CD-ROM proc.

Rizos, C. & Satirapod, C. (2001), GPS with SA off: How good is it? Measure & Map, 12, 19-21.

Rothacher M. & L. Mervart (1996), Bernese GPS Software,Version 4.0, Astronomical Institute, University of Berne,417pp.

Schwartz, K. P. (1978), On the application of least-squares collocation models to physical geodesy, in Approximation Methods in Geodesy, edited by H. Moritz and H. Sunkel, H. Wichmann-Verlag, Karlsruhe, Germany, 89-116.

Stansell, T.A., Jr. (1986), RTCM SC-104 Recommended Pseudolite Signal Specification, Global Positioning System, Navigation Volume III, The Insitute of Navigation, 117-134.

Schaer S., G. Beutler, M. Rothacher, E. Brockmann, A. Wiger & U. Wild (1999), The impact of the atmosphere and other systematic errors on permanent GPS networks, *Abstracts of IUGG'99*, Birmingham,UK, 19-24 July, 406.

Schaer S., Beutler G., Mervart L., Rothacher M., and U. Wild (1995), Global and regional ionosphere models using the GPS double difference phase observable,

Proc. of the IGS Workshop on Special Tropics and New Directions, Potsdam, Germany, 15-17 May, 77-92.

Shi C. (1998), Large scale GPS network adjustment & analysis theory and its application, Ph.D. Dissertation, The School of Geoscience and Engineering Surveying, Wuhan Technical University of Surveying and Mapping, 123pp (in Chinese),

Stone, M.J. & J.D. Powell (1999), Precise positioning using GPS satellites and pseudolites emphasizing open pit mining applications, 4th Int. Symp. on Satellite Navigation Technology & Applications, Brisbane, Australia, 20-23 July.

Sun H., M.E. Cannon & T.E. Melgard (1999), Real-time GPS reference network carrier phase ambiguity resolution, U.S. Institute of Navigation National Technical Meeting, San Diego, California, 25-27 January,193-199.

Teunissen, P.J.G. (1994), A new method for fast carrier phase ambiguity estimation. IEEE Position Location & Navigation Symposium PLANS94, Las Vegas, Nevada, 11-15 April, 562-573.

Teunissen P.J.G. (1987), Nonlinear inversion of geodetic and geophysical data: Diagnosing nonlinearity, in: F.K. Brunner & C. Rizos (eds.) Developments in Four-Dimensional Geoddesy, Springer-Verlag, 241-264.

Tscherning, C.C. (1974), A FORTRAN IV Program for the Determination of the Anomalous Potential Using Stepwise Least Squares Collocation. Reports of the Department of Geodetic Science No. 212, The Ohio State University, Columbus, Ohio.

Tscherning, C.C. (2001), Computation of spherical harmonic coefficients and their error estimates using least-squares collocation, Journal of Geodesy, 75(1), 12-18.

Tsujii T., C. Rizos, J. Wang, L. Dai, C. Roberts & M. Harigae (2001), A navigation/positioning service based on pseudolites installed on stratospheric airships, 5th Int. Symp. on Satellite Navigation Technology & Applications, Canberra, Australia, July 24-27.

Varner C. (2000), DGPS carrier phase networks and partial derivative algorithms, Ph.D. Thesis, University of Calgary, Dept. of Geomatics Engineering, Report No. 20129, Calgary, Canada, 160pp.

Vollath U., Bücherl A., Landau H., Pagels C. & Wager B. (2000), Multi-base RTK positioning using virtual reference stations, 13th Int. Tech. Meeting of the Satellite Div. of the U.S. Institute of Navigation, Salt Lake City, Utah, 19-22 September, 123-131.

Wang J., M.P. Stewart & M. Tsakiri (1998), A discrimination test procedure for ambiguity resolution on the fly, Journal of Geodesy, 72(11), 644-653.

Wang, J. (1998), Mathematical models for combined GPS and Glonass positioning. 11th Int. Tech. Meeting of the Satellite Division of the U.S. Inst. of Navigation, Nashville, Tennessee, 15-18 September, 1333-1344.

Wang, J., T. Tsujii, C. Rizos, L. Dai & M. Moore (2000), Integrating GPS and pseudolite signals for position and attitude determination: Theoretical analysis and experiment results, 13th Int. Tech. Meeting of the Satellite Division of the U.S. Inst. of Navigation GPS ION-2000, Salt Lake City, Utah, 19-22 Sept, 2252-2262.

Wang, J. (2000), An approach to Glonass ambiguity resolution. Journal of Geodesy, 74(5), 421-430.

Wang J,. C. Rizos, M.P. Stewart & A. Leick (2001), GPS and GLONASS integration: modelling and ambiguity resolution issues. GPS Solutions, 5(1), 55-64.

Wanninger L. (1995), Improved ambiguity resolution by regional differential modelling of the ionosphere, 8th Int. Tech. Meeting of the Satellite Division of the U.S. Inst. of Navigation, Palm Springs, California, 12-15 September, 55-62.

Wanninger L. (1997), Real-time differential GPS error modelling in regional reference station networks, Proc. IAG Symp 118, Rio de Janeiro, Brazil, 86-92.

Wanninger L. (1999), The performance of virtual reference stations in active geodetic GPS-networks under solar maximum conditions, 12th Int. Tech. Meeting of the Satellite Div. of the U.S. Institute of Navigation, Nashville, Tennessee, 14-17 September, 1419-1427.

Weiser, M. (1998), Development of a carrier and C/A-code based pseudolite system, 11th Int. Tech. Meeting of the Satellite Division of the U.S. Inst. of Navigation GPS ION-98, Nashville, Tennessee, 15-18 Sept., 1465-1475.

Wübbena G., A. Bagge, G. Seeber, V. Böder & P. Hankemeier (1996), Reducing distance dependent errors for real-time precise DGPS applications by establishing reference station networks, 9th Int. Tech. Meeting of the Satellite Division of the U.S. Inst. of Navigation, Kansas City, Missouri, 17-20 September, 1845-1852.

Zhang J. (1999), Precise estimation of residual tropospheric delays in a spatial GPS network, 12th Int. Tech. Meeting of the Satellite Division of the U.S. Inst. of Navigation, Nashville, Tennessee, 14-17 September, 1391-1400.

Zhodzishsky, M., M. Vorobiev, A. Khvalkov & J. Ashjaee (1998), Real-Time Kinematic (RTK) processing for dual-frequency GPS/Glonass. 11th Int. Tech. Meeting of the Satellite Division of the U.S. Inst. of Navigation, Nashville, Tennessee, 15-18 September, 1325-1331.

Zimmerman K.R, C.E. Cohen, D.G. Lawrence, P.Y. Montgomery, H.S. Cobb, W.C. Melton (2000), Multi-frequency pseudolites for instantaneous carrier ambiguity resolution, 13th Int. Tech. Meeting of the Satellite Division of the U.S. Inst. of Navigation GPS ION-2000, Salt Lake City, Utah, 19-22 Sept, 1024-1033.

APPENDIX

OUTLIER DETECTION ALGORITHM BASED ON CORRELATION ANALYSIS

The outlier detecion algorithm based on correlation analysis approach has been first proposed for use in the large scale GPS network adjustment (Shi, 1998), and in GNSS kinematic positioning (Dai et al., 1999). This appendix will give this approach.

A.1 Relationship Between True Errors and Residuals

The residuals can be considered as indicators of the errors and are therefore useful information to reflect outliers. In order to locate the outliers, the relationship between the true errors and residuals should be firstly analysed.

The general least-squares linearised observation equation and the criteria can be modelled as:

$$V = BX - L \tag{A-1}$$

$$V^T D^{-1} V = \text{Minimum} \tag{A-2}$$

$$L = l - BX_0 \tag{A-3}$$

where V , L and l are $n \times 1$ vectors of postfit residuals prefit residuals and measurements respectively; B is the design matrix; X and X_0 is the $t \times 1$ estimated and approximate unknown parameter vector; and D is the variance-covariance matrix of the measurements.

Based on the minimum quadratic form of the postfit residuals (A-2), the Least-Squares estimated parameter $\hat{X}$ can be derived:

$$\hat{\mathrm{X}} = (B^T D^{-1} B)^{-1} B D^{-1} \mathrm{L} \tag{A-4}$$

Substituting equation (A-4) into equation (A-1), the estimated postfit residuals can be written as:

$$V = (B(B^T D^{-1} B)^{-1} B D^{-1} - I)L \tag{A-5}$$

where I is identity matrix.

Then, the variance-covariance matrix of postfit residuals can be derived in Equation (A-6) according to the error propagation law.

$$Q_{vv} = D^{-1} - B(B^T D^{-1} B)^{-1} B \tag{A-6}$$

If X_0 is replaced by the true value vector $\widetilde{X}$ in Equation (A-1), the true error ε can be defined as:

$$\varepsilon = l - B\widetilde{X} \tag{A-7}$$

The relationship between the true errors and the postfit residuals can be derived from Equations (A-5, A-6 and A-7) as follows:

$$-V = R\ \varepsilon \tag{A-8}$$

$$R = Q_{vv}\ D^{-1} \tag{A-9}$$

where R is called the reliability matrix. In general, R is an asymmetric matrix. Nevertheless, it is symmetric when the observations are independent and have the same variance. The elements in the R matrix are usually denoted by r_{ij} .

$$R = \begin{bmatrix} r_{11} & r_{12} & \cdots & r_{1n} \\ r_{21} & r_{22} & \cdots & r_{2n} \\ \vdots & \vdots & \cdots & \vdots \\ r_{n1} & r_{n2} & \cdots & r_{nn} \end{bmatrix} \tag{A-10}$$

The R is only related to the design matrix and the variance-covariance matrix of the observations. However, there is no relationship with the observations and the corresponding errors. As it is well known that R is an idempotent matrix, hence, its rank is equal to its trace, that is:

$$Rank(R) = tr(R) = \sum_{i=1}^{n} r_{ii} = r = n - t < n \tag{A-11}$$

Equation (A-11) indicates that the sum of the main diagonal elements in the R matrix is equal to the number of the redundancy. It should be emphasised that because the R matrix is not a non-negative definite matrix for highly correlated observations. The r_{ii} (I=1,2, ..., n) is also called the observation redundancy component, which may take a negative value for some special conditions. Due to the rank deficiency of the R matrix, the true errors cannot be computed directly by inverting R using Equation (A-8). If the R_i and ε are defined as:

$$R_i = [\, r_{1i} \quad r_{2i} \quad \cdots \quad r_{ni} \,]^T \quad (i = 1,2,\cdots,n) \tag{A-12}$$

$$\varepsilon = [\, \varepsilon_1 \quad \varepsilon_2 \quad \cdots \quad \varepsilon_i \quad \cdots \quad \varepsilon_n \,]^T \tag{A-13}$$

Hence, Equation (A-8) can be written as:

$$-V = R_1 \varepsilon_1 + R_2 \varepsilon_2 + \cdots + R_n \varepsilon_n \tag{A-14}$$

Any observation error ε_i affects the residuals through the column vector R_i of the reliability matrix in the least-squares adjustment. It is observed that the R_i vector controls the influence of the true errors on the residuals. The more the component of the R_i, the more the residuals. On the other hand, the larger the true errors ε_i, the

larger the residuals. Any observation error ε_i probably contributes to all the residuals. The biggest contribution of one outlier error on the residuals is likely to occur to other residuals.

A-2 Outlier Detection Algorithm Based on Correlation Analysis

Suppose that the outliers exist in the former k observations. Equation (A-14) can be simplified because the normal errors can be neglected:

$$-V \approx R_1 \varepsilon_1 + R_2 \varepsilon_2 + \cdots + R_k \varepsilon_k \qquad \text{(A-15)}$$

Equation (A-15) shows that the residual quantities come mainly from the outliers contributions. It also shows that there is significant mathematical correlation between the vector of the residuals and the column vectors of the reliability sub-matrix relating to the outliers.

The correlation coefficient is considered critical information, which reflects the relationship between the true outliers of the observations (even correlated measurements) and the residuals.

In order to mathematically describe the quantity of this degree of correlation between outliers and residuals, two constant variables a and b are introduced so that the difference d between R_j vector and V vector can be minimised:

$$d = Min(\frac{1}{n}\sum_{i=1}^{n}(v_i - a - br_{ij})^2) \qquad \text{(A-16)}$$

where V_i (i=1,...,n) are the components of the V vector. The partial derivatives of equation (A-16) are:

$$\frac{\partial d}{\partial a} = -\frac{2}{n}\sum_{i=1}^{n}(v_i - a - br_{ij}) = 0 \qquad \text{(A-17)}$$

$$\frac{\partial d}{\partial b} = -\frac{2}{n}\sum_{i=1}^{n}(v_i - a - br_{ij})r_{ij} = 0 \tag{A-18}$$

According to Equations (A-17 and A-18), the parameters a and b can be obtained:

$$b = \frac{\sum_{i=1}^{n}(r_{ij} - \bar{r}_j)(v_i - \bar{v})}{\sum_{i=1}^{n}(r_{ij} - \bar{r}_j)^2} \tag{A-19}$$

$$a = \bar{v} - b\ \bar{r}_j \tag{A-20}$$

where $\bar{v}$ and $\bar{r}_j$ are the average values of the V and R_j vectors, respectively. Substituting equations (A-19, A-20) into equation (A-16), the difference d can be written as:

$$d = \frac{1}{n}\sum_{i=1}^{n}(v_i - \bar{v})^2(1 - \rho_{R_j,V}^2) \tag{A-21}$$

$$\rho_{R_j,V} = \frac{\sum_{i=1}^{n}(r_{ij} - \bar{r}_j)(v_i - \bar{v})}{\sum_{i=1}^{n}(r_{ij} - \bar{r}_j)^2 \sum_{i=1}^{n}(v_i - \bar{v})^2} \tag{A-22}$$

In Equation (A-21), the larger the correlation coefficient $\rho_{R_j,V}$, the less the difference d. The correlation coefficient is number in range from -1 to +1 which measures the degree to which two variables are linearly related. If there is perfect linear relationship with positive slope between the two variables, there is a correlation coefficient of 1; if there is positive correlation, whenever one variable has a high (low) value, so does the other. If there is a perfect linear relationship with negative slope between the two variables, there is a correlation coefficient of -1; if there is negative correlation, whenever one variable has a high (low) value, the other has a low (high) value. A correlation coefficient of 0 means that there is no linear relationship between the variables. If the absolute correlation coefficient value is close to 1 (or –1), there is a strong correlation

relationship between the R_j and V vectors. This also means that the contribution to the residuals comes mainly from the observation related to the R_j vector. If an outlier occurs, the observation corresponding to R_j has the largest possibility. If multiple outliers occur, they make a combined contribution to the residuals. There are also high correlation coefficients between the column vectors of the reliability matrix related to the outliers and the residuals. Based on the above analysis, outliers can be located through analysing $\rho_{R_j,V}$.

A.3 Significant Test of Correlation Coefficient

It can be assumed that the V and R_j are random variables and have a bivariate normal distribution. In order to determine whether there is a significant linear correlation between two variables (V and R_j) distribution,

The null hypothesis (no significant linear correlation) is:

$$H_0: \rho_{R_j,V} = 0 \tag{A-23}$$

and the alternative hypothesis (significant linear correlation) is:

$$H_1: \rho_{R_j,V} \neq 0 \tag{A-24}$$

According to the above hypothesis, the following statistic for the correlation coefficient test can be obtained:

$$t = \frac{\rho_{R_j,V}}{\sqrt{\frac{1-\rho_{R_j,V}}{n-2}}} \tag{A-25}$$

where t has student-t distribution with $n-2$ degrees of freedom. For a given significant level α, the critical value t_c for the t statistic can be computed.

If the absolute value of the test statistic exceeds the critical values, reject H_0: $\rho_{R_j,V} = 0$. Otherwise fail to reject H_0. If H_0 is rejected, it is conclude that there is a significant linear correlation between V and R_j. It indicates the biggest possibility that the

observation(s) relating to the significant correlation coefficient(s) should be suspected as having been contaminated by outliers. If you fail to reject H_0, then there is not sufficient evidence to conclude that there is linear correlation between V and R_j.

Publications from the

SCHOOL OF SURVEYING AND SPATIAL INFORMATION SYSTEMS
(formerly: SCHOOL OF GEOMATIC ENGINEERING)

THE UNIVERSITY OF NEW SOUTH WALES
ABN 57 195 873 179

To order, write to:
Publications Officer, School of Surveying and Spatial Information Systems
The University of New South Wales, UNSW SYDNEY NSW 2052, AUSTRALIA

NOTE: ALL ORDERS MUST BE PREPAID. CREDIT CARDS ARE ACCEPTED.
SEE BACK PAGE FOR OUR CREDIT CARD ORDER FORM.

MONOGRAPHS

Australian prices include postage by surface mail and GST.
Overseas prices include delivery by UNSW's air-lifted mail service (~2-4 weeks to Europe and North America).
Rates for air mail through Australia Post on application.

(Prices effective November 2002)

		Price Australia (incl. GST)	**Price** Overseas
M1.	R. S. Mather, "The Theory and Geodetic Use of some Common Projections", (2nd edition), 125 pp, 1978.	$ 16.50	$ 15.00
M2.	R. S. Mather, "The Analysis of the Earth's Gravity Field", 172 pp, 1971.	$ 8.80	$ 8.00
M3.	G. G. Bennett, "Tables for Prediction of Daylight Stars", 24 pp, 1974.	$ 5.50	$ 5.00
M4.	G. G. Bennett, J. G. Freislich & M. Maughan, "Star Prediction Tables for the Fixing of Position", 200 pp, 1974.	$ 8.80	$ 8.00
M8.	A. H. W. Kearsley, "Geodetic Surveying", 96 pp, 1988.	$ 13.20	$ 12.00
M11.	W. F. Caspary, "Concepts of Network and Deformation Analysis", 183 pp, 2000.	$ 27.50	$ 25.00
M12.	F. K. Brunner, "Atmospheric Effects on Geodetic Space Measurements", 110 pp, 1988.	$ 17.60	$ 16.00
M13.	B. R. Harvey, "Practical Least Squares and Statistics for Surveyors", (2nd edition, reprinted with corrections), 319 pp, 1998.	$ 33.00	$ 30.00
M14.	E. G. Masters and J. R. Pollard (Eds.), "Land Information Management", 269 pp, 1991. (Proceedings LIM Conference, July 1991).	$ 22.00	$ 20.00
M15/1	E. G. Masters and J. R. Pollard (Eds.), "Land Information Management - Geographic Information Systems - Advance Remote Sensing Vol. 1", 295 pp, 1993 (Proceedings of LIM & GIS Conference, July 1993).	$ 33.00	$ 30.00
M15/2	E. G. Masters and J. R. Pollard (Eds.), "Land Information Management - Geographic Information Systems - Advance Remote Sensing Vol. 2", 376 pp, 1993 (Proceedings of Advanced Remote Sensing Conference, July 1993).	$ 33.00	$ 30.00
M16.	A. Stolz, "An Introduction to Geodesy", 2nd extended edition, 148 pp, 2000.	$ 24.20	$ 22.00
M17.	C. Rizos, "Principles and Practice of GPS Surveying", 565 pp, 1997.	$ 46.20	$ 42.00

UNISURV REPORTS - S SERIES

(Prices effective November 2002)

Australian Prices *:	S8 - S20		$11.00
	S29 onwards	Individuals	$27.50
		Institutions	$33.00
Overseas Prices **:	S8 - S20		$10.00
	S29 onwards	Individuals	$25.00
		Institutions	$30.00

* Australian prices include postage by surface mail and GST.

** Overseas prices include delivery by UNSW's air-lifted mail service (~2-4 weeks to Europe and North America). Rates for air mail through Australia Post on application.

S17. C. Rizos, "The Role of the Gravity Field in Sea Surface Topography Studies", Unisurv S17, 299 pp, 1980.

S18. B. C. Forster, "Some Measures of Urban Residential Quality from LANDSAT Multi-Spectral Data", Unisurv S18, 223 pp, 1981.

S19. R. Coleman, "A Geodetic Basis for Recovering Ocean Dynamic Information from Satellite Altimetry", Unisurv S19, 332 pp, 1981.

S29. G. S. Chisholm, "Integration of GPS into Hydrographic Survey Operations", Unisurv S29, 190 pp, 1987.

S31. J. Soetandi, "A Model for a Cadastral Land Information System for Indonesia", Unisurv S31, 168 pp, 1988.

S33. R. D. Holloway, "The Integration of GPS Heights into the Australian Height Datum", Unisurv S33, 151 pp, 1988.

S36. A. R. Marshall, "Network Design and Optimisation in Close Range Photogrammetry", Unisurv S36, 249 pp, 1989.

S37. W. Jaroondhampinij, "A Model of Computerised Parcel-Based Land Information System for the Department of Lands, Thailand", Unisurv S37, 281 pp, 1989.

S39. C. Bosloper, "Multipath and GPS Short Periodic Components of the Time Variation of the Differential Dispersive Delay", Unisurv S39, 214 pp, 1990.

S40. J. M. Nolan, "Development of a Navigational System Utilizing the Global Positioning System in a Real Time, Differential Mode", Unisurv S40, 163 pp, 1990.

S41. R. T. Macleod, "The Resolution of Mean Sea Level Anomalies along the NSW Coastline Using the Global Positioning System", Unisurv S41, 278 pp, 1990.

S42. D. A. Kinlyside, "Densification Surveys in New South Wales - Coping with Distortions", Unisurv S42, 209 pp, 1992.

S43. A. H. W. Kearsley (ed.), Z. Ahmad, B. R. Harvey and A. Kasenda, "Contributions to Geoid Evaluations and GPS Heighting", Unisurv S43, 209 pp, 1993.

S44. P. Tregoning, "GPS Measurements in the Australian and Indonesian Regions (1989-1993)", Unisurv S44, 134 + xiii pp, 1996.

S45. W.-X. Fu, "A Study of GPS and Other Navigation Systems for High Precision Navigation and Attitude Determinations", Unisurv S45, 332 pp, 1996.

S46. P. Morgan et al, "A Zero Order GPS Network for the Australia Region", Unisurv S46, 187 + xii pp, 1996.

S47. Y. Huang, "A Digital Photogrammetry System for Industrial Monitoring", Unisurv S47, 145 + xiv pp, 1997.

S48. K. Mobbs, "Tectonic Interpretation of the Papua New Guinea Region from Repeat Satellite Measurements", Unisurv S48, 256 + xv pp, 1997.

S49. S. Han, "Carrier Phase-Based Long-Range GPS Kinematic Positioning", Unisurv S49, 185 + xi pp, 1997.

S50. M. D. Subari, "Low-cost GPS Systems for Intermediate Surveying and Mapping Accuracy Applications", Unisurv S50, 179 + xiii pp, 1997.

S51. L.-S. Lin, "Real-Time Estimation of Ionospheric Delay Using GPS Measurements", Unisurv S51, 199 + xix pp, 1997.

S53. D. B. Lemon, "The Nature and Management of Positional Relationships within a Local Government Geographic Information System", Unisurv S53, 273 + xvi pp, 1997.

S54. C. Ticehurst, "Development of Models for Monitoring the Urban Environment Using Radar Remote Sensing", Unisurv S54, 282 + xix pp, 1998.

S55. S. S. Boey, "A Model for Establishing the Legal Traceability of GPS Measurements for Cadastral Surveying in Australia", Unisurv S55, 186 + xi pp, 1999.

S56. P. Morgan and M. Pearse, "A First-Order Network for New Zealand", Unisurv S56, 134 + x pp, 1999.

S57. P. N. Tiangco, "A Multi-Parameter Radar Approach to Stand Structure and Forest Biomass Estimation", Unisurv S57, 319 + xxii pp, 2000.

S58. M. A. Syafi'i, "Object–Relational Database Management Systems (ORDBMS) for Managing Marine Spatial Data: ADCP Data Case Study", Unisurv S58, 123 + ix pp, 2000.

S59. X.-Q. Lu, "Strategies for Improving the Determination of Displacements of Sea Surface Temperature Patterns Using Consecutive AVHRR Thermal Images", Unisurv S59, 209 + xiii pp, 2000.

S60. G. Dickson, "GPS-Controlled Photography: The Design, Development and Evaluation of an Operational System Utilising Long-Range Kinematic GPS", Unisurv S60, 417 + x pp, 2000.

S61. J. Wang, "Modelling and Quality Control for Precise GPS and GLONASS Satellite Positioning", Unisurv S61, 171 + x pp, 2001.

S62. Y. Wang, "Knowledge-Based Road Extraction from Aerial Images", Unisurv S62, 178 + xi pp, 2001.

S63. L. Ge, "Development and Testing of Augmentations of Continuously-Operating GPS Networks to Improve their Spatial and Temporal Resolution", Unisurv S63, 230 + xvi pp, 2001.

S64. H.-Y. Chen, "A Study on Real-Time Medium-Range Carrier-Phase-Based GPS Multiple Reference Stations", Unisurv S64, 182 + xxiv pp, 2001.

S65. G. Y. K. Shea, "A Web-Based Approach to the Integration of Diverse Data Sources for GIS", Unisurv S65, 233 + xv pp, 2001.

S66. M. Mirbagheri, "Analysis of Interferometric SAR for Topographic Mapping", Unisurv S66, 135 + xvii pp, 2001.

S67. P. Wang, "Applying Two-Dimensional Kalman Filtering Techniques to Digital Elevation Models for Terrain Surface Modelling", Unisurv S67, 175 + xi pp, 2001.

S68. J. M. Rüeger, "Refractive Indices of Light, Infrared and Radio Waves in the Atmosphere", Unisurv S68, 92 + vi pp, 2002.

S69. C. Satirapod, "Improving the GPS Data Processing Algorithm for Precise Static Relative Positioning", Unisurv S69, 131 + viii pp, 2002.

S70. R. Mason, "Developing Australian Spatial Data Policies – Existing Practices and Future Strategies", Unisurv S70, 258 + xv pp, 2002.

S71. C. Ogaja, "A Framework in Support of Structural Monitoring by Real Time Kinematic GPS and Multisensor Data", Unisurv S71, 191 + xiii pp, 2002.

S72. L. Dai, "Augmentation of GPS with GLONASS and Pseudolite Signals for Carrier Phase Based Kinematic Positioning", Unisurv S72, 188 + viii pp, 2002.

S73. C. Roberts, "A continuous Low-Cost GPS-Based Volcano Deformation Monitoring System in Indonesia", Unisurv S73, 271 + xvi pp, 2002.